Hochschule für Angewandte Wissenschaften Hamburg
Hamburg University of Applied Sciences

Master Thesis

Felix Braunheim

Wind Farm Simulation and Validation of Analytical and CFD based Wake Models with Wind Data from Operational Wind Farms

Fakultät Technik und Informatik
Department Fahrzeugtechnik und Flugzeugbau

Faculty of Engineering and Computer Science
Department of Automotive and Aeronautical Engineering

Felix Braunheim

Wind Farm Simulation and Validation of Analytical and CFD based Wake Models with Wind Data from Operational Wind Farms

Masterarbeit eingereicht im Rahmen der Masterprüfung

im Studiengang Flugzeugbau
am Department Fahrzeugtechnik und Flugzeugbau
der Fakultät Technik und Informatik
der Hochschule für Angewandte Wissenschaften Hamburg

in Zusammenarbeit mit:
Siemens Gamesa Renewable Energy GmbH & Co. KG
SGRE ON NE&ME TE SAS
Beim Strohhause 17-31
20097 Hamburg

Erstprüfer: Prof. Dr. Peter Dalhoff
Zweitprüfer: Prof. Dr. Hartmut Zingel

Abgabedatum: 12.10.2018

Zusammenfassung

Name des Studenten

Felix Braunheim

Thema der Masterthesis

Windpark Simulation und Validierung von analytischen und CFD basierten Modellen zur Nachlaufströmungsberechnung mit Winddaten von operierenden Windparks

Stichworte

Windparks, Modelle für Nachlaufströmungen, Jensen Modell, WakeBlaster, CFD, RANSE, Windextrapolation, AEP, Leistungskurve, Vergleich von gemessener und modellierter Energieproduktion.

Kurzzusammenfassung

Windturbinen in Windparks sind oft durch Nachlaufströmungen von anderen Turbinen beeinflusst. Dadurch ergeben sich niedrigere Windgeschwindigkeiten, mehr Turbulenzen und ein reduzierten Ertrag. Für die Berechnung dieser Effekte können Modelle mit unterschiedlicher Genauigkeit genutzt werden. Diese Modelle reichen vom einfachen Jensen Modell, bis zu komplexen CFD Modellen. Die Produktion von zwei Windparks wird mit dem Jensen Modell und WakeBlaster berechnet. Anschließend werden die Ergebnisse mit mehreren Jahren Produktionsdaten von Siemens Gamesa Renewable Energy (SGRE) verglichen. Für den Vergleich wird eine Produktionsmatrix verwendet. Am Ende wird eine Aussage über die Gültigkeit der benutzten Modelle getroffen.

Name of Student

Felix Braunheim

Title of the paper

Wind Farm Simulation and Validation of Analytical and CFD based Wake Models with Wind Data from Operational Wind Farms

Keywords

Wind farms, wake models, Jensen Model, WakeBlaster, CFD, RANS equations, wind extrapolation, AEP, power curve, comparison of measured and modelled power production

Abstract

Wind turbines in wind farms regularly operate in the wake of other wind turbines and experience lower wind speeds, higher turbulences and a reduced yield. To assess the wake effects different fidelity models can be used. These range from simple ones like the Jensen Model to complex CFD models. The energy production of two wind farms is calculated applying the Jensen and WakeBlaster model. Next, the result is compared to several years of production data provided by SGRE. This data is used to create a power production matrix and compared to the modelled results. In the end a statement about the validation of the used wake models is given.

Introduction

This thesis contains chapters about general wind turbine aerodynamics, the theoretical background of wakes, wake modelling and a comparison of observed and modelled production of wind turbines. The focus lies on the influence of the wakes on the power production.

Quoted figures and tables are sometimes changed for simplification, a clearer arrangement or adaption of the nomenclature.

First of all I want to thank SGRE for providing the production data of the two wind farms. Without this data a comparison would have been impossible.

I want to thank all people from SGRE and ProPlanEn who supported me. First of all Venkatesh Jothiprakasam and Wolfgang Schlez who guided me the way with their expertise and always had time for me.

Special thanks go to Philipp Bradstock who helped me with WakeBlaster and Sascha Schmidt who investigated with me the problems of wind farm modelling.

Acknowledgement goes also to Georg Bischof and Daniel Lupianez who made it possible to write my thesis in the Siting department of SGRE.

Table of Content

List of Abbreviations

Abbreviation	Explanation
a.m.s.l.	above mean sea level
ABL	Atmospheric boundary layer
ADM	Actuator disc model
AEP	Annual energy production
BEM	Blade element momentum method
CFD	Computational fluid dynamics
json	JavaScript object notation
RANS	Reynolds-averaged Navier-Stokes
rsf	Wind resource map
SCADA	Supervisory Control and Data Acquisition
SGRE	Siemens Gamesa Renewable Energy
SRTM	Shuttle Radar Topography Mission
TI	Turbulence Intensity
TSR	Tip Speed Ratio
WAsP	Wind Atlas Analysis and Application Program
WDC	Wake decay constant
WTG	Wind turbine generator

Nomenclature

Latin Symbols

A	Cross section
a	Axial induction factor
AE	Absolute error
ALR	Adiabatic lapse rate
AT	Absolute temperature
B	Number of blades
b	Width of wake
C_P	Power coefficient
C_T	Thrust coefficient
D	Rotor diameter
D_w	Wake diameter
E	Energy
Eff	Efficiency
f	Calibration factor (0.08)
g	Acceleration of gravity
K	Constant (0.015)
k	Constant
L	Lift
ΔL	Length scale
m	Mass
$\dot{m}$	Mass flow
P	Power
p	Pressure
R	Rotor diameter
r	Distance from centre of the rotor in radial direction
s	Stratification frequency
T	Thrust
t	Time
TI	Turbulence intensity
u	Wind speed
u'	Stochastic deviations of the wind speed
$\overline{u}$	Mean wind speed
$\overline{u'v'}$	Reynolds stress
Δu	Velocity scale
Δu_∞	Speed-up factor
$(u_\infty - u_c(x))$	Velocity deficit in the centreline of the wake
v	Velocity in radial direction
w	Tangential velocity
WS	Wind speed bin
x	Distance to upstream turbine in axial direction
z	Height above ground
z_0	Roughness length

Greek Symbols

α	Shear exponent
γ	Yaw angle
δ_{ij}	Kronecker delta
κ	Wake decay constant
λ	Tip speed ratio
μ_t	Eddy viscosity
ρ	Density
σ	Standard deviation of the wind speed
Γ	Strength of root vortex
$\Delta\Gamma$	Strength of vortex
χ	Angle between wake flow and rotor axis
Ω	Angular velocity

Subscripts

0	Starting point
1	At point one
2	At point two
∞	Undisturbed
amb	Ambient
c	At centre of the wake
d	At rotor disc
i	At variable point
j	At another variable point
w	Wake

1 Wind Turbine Aerodynamics

The next chapters explain the basic principles of wind turbine aerodynamics. The content is just a rough description because a detailed introduction would go beyond the thesis` scope. Nevertheless, the following chapters provide good background knowledge.

The first part is about the general wind conditions in the atmospheric boundary layer (ABL) and how the environment influences the wind flow. The second part is about the influence of the turbine on the flow.

1.1 Characteristics of the Ambient Wind Flow

The following sub-chapters describe separately different influences on the ambient wind flow. In the reality, all factors are effective at the same time. Thus, it is difficult to extrapolate the wind flow from a known point in vertical and horizontal direction.

1.1.1 Vertical Wind Profile

Modern wind turbines operate in hub heights over 100 m and with a rotor diameter up to 150 m. This part of the atmosphere is called the ABL. This layer is the lowest part of the atmosphere and between several hundred meters and two kilometres thick. The ambient wind flow is mainly driven by the roughness of the surface and thermal effects. [1]

One of the most important characteristics of the wind flow is the wind speed because it determines how much energy a turbine can produce and how big the loads are. The wind speed decreases at lower heights because it is slowed down by the roughness of the ground. For the wind industry it is essential to know the wind speed at the turbine hub height. However, at these heights are usually no measurements available. Due to that a vertical profile is needed to extrapolate the wind speed in the vertical direction. In the following paragraphs two models for the vertical extrapolation are introduced.

The first model is a logarithmic approximation of the vertical wind profile. [1]

$$\frac{u_1}{u_2} = \frac{\ln(z_1/z_0)}{\ln(z_2/z_0)} \tag{1-1}$$

z is the height above ground and z_0 is the roughness length of the surface. Usually, the wind speed is measured at different heights and the unknown variables can be solved easily. The roughness length can also be derived when the surface is known.

Figure 1-1 shows the development of the wind speed over the height. The geostrophic wind is the wind speed above the ABL. The different trends are a result of differences in the stability of the atmosphere.

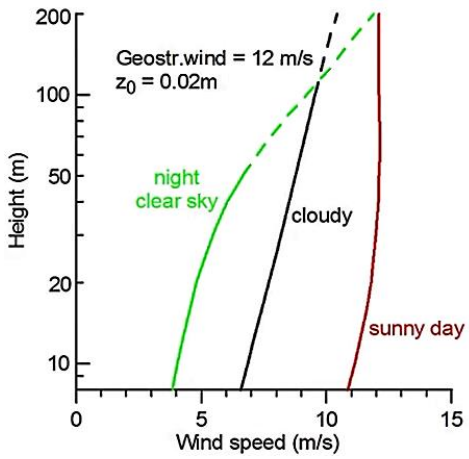

Figure 1-1: Vertical velocity profile [2]

An alternative for the calculation of the vertical profile is the power law approximation (1-2). It is an empirical approach to represent the vertical profile of the wind speed. It correlates with the real profile well for neutral atmospheric stability conditions and a smooth surface. [2]

$$\mathrm{u}(z_2) = \mathrm{u}(z_1)\left(\frac{z_2}{z_1}\right)^{\acute{\alpha}} \tag{1-2}$$

$\acute{\alpha}$ is the wind shear exponent and can be calculated if the wind speed is known at two heights. The higher the exponent the faster is the wind speed increasing with the height.

Both approaches have their limits although they are accurate enough for the aims of the wind industry. These methods are recommended from the International Electronical Commission. [3]

Another fact that should be mentioned is that the vertical profile and the shear exponent are wind speed dependent. At higher wind speed is the shear exponent lower. The shear exponent changes also with the height. [2]

1.1.2 Turbulence Intensity

The turbulence intensity (TI) is a rate for the variability of the wind speed. TI is generated by two main factors: The atmospheric stability respectively the thermal driven rise of lower air layers and the character of the ground. The surface is defined by roughness and orography. The TI is defined by formula (1-3). [1]

$$I = \frac{\sigma}{\overline{u}} \tag{1-3}$$

σ is the standard deviation of the wind speed in the average wind direction and $\overline{u}$ is the average wind speed over a certain time period. The typical averaging period in the wind industry is ten minutes. The standard sampling period is 1 Hz. This frequency was chosen because at higher frequencies the turbulence decays and at lower frequencies is a spectral gap present.

The TI decreases with the height because the surface's influence gets lower and the mean wind speed increases (figure 1-2).

The TI has a big impact on the behaviour of wakes, loads and other things like noise generation and power performance. The higher the TI the higher the fatigue loads of a turbine. The loads are more dynamic and the number of load changes is increasing. [2]

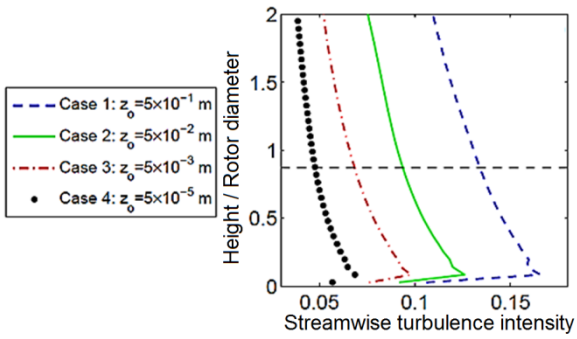

Figure 1-2: Vertical profiles of the turbulence intensity [5]

1.1.3 Atmospheric Stability

The atmosphere's stability influences the height of the ABL, the TI, as well as the vertical profile. Three stability conditions are known:

- Unstable/convective: During sunny days the air near the ground is heating and starts to rise because it is lighter than the cold air above. Through these conditions it is possible to form large eddies and the ABL is getting thicker. Additionally, these eddies increase the TI. [1]
- Neutral: This condition happens mostly in the afternoon in combination with strong winds. Strong winds are the most important case for wind turbines and this is the reason why a lot of models assume neutral stability for simplifications. It is also the average between stable and unstable. The atmosphere is neutral when the rising air is in thermal equilibrium with the air surrounding it. [1]
- Stable: When the air near the ground is colder than the air above a rise of the lower part is not possible. This indicates also that there will be no large eddies and the thermal turbulence is low compared to the part caused by the surface. This appears nearly always at night and during low winds. [1]

The vertical profile changes with the stability (figure 1-1). The wind speed is for the stable case directly at the ground lower and the shear is higher.

The atmospheric stability can be defined with the adiabatic lapse rate. It is defined as the rate of temperature decrease with height in a well-mixed and neutral atmosphere. In the ABL the adiabatic lapse rate is 1℃ per 100 m. The equation for the stability is shown below:

$$s^2 = \frac{g}{T}\left(\frac{dT}{dz} - ALR\right) \tag{1-4}$$

s is the stratification frequency, g is the acceleration of gravity, T is the absolute Temperature and ALR is the adiabatic lapse rate. For a neutral atmosphere, the equation equals zero. If the result is below null the atmosphere is unstable and above zero it is stable. [4]

A further description and some methods to calculate the stability function can be found in [5].

1.1.4 Topography

The surface of the earth causes friction on the wind and reduces the wind speed. The deceleration's size depends on the roughness length. The magnitude of the roughness length itself depends on the size and distribution of roughness elements (e.g. bushes, trees, buildings and the soil). Additionally, a higher roughness leads to a higher TI. [2]

Table 1-1 lists typical values for the roughness length. The higher and wider the elements are the higher the roughness length. Also, spreading plays an important role for a correct roughness estimation. When roughness elements are close together they have to be considered as displacement height because the wind flow is lifted over then. [2]

Table 1-1: Roughness length for typical surface characteristics [2]

Terrain surface characteristics	**Roughness length, z0 [m]**
Forest and urban areas	0.7 -1.0
Suburbs and sheltering belts	0.3-0.5
Farmland with closed appearance, many trees, bushes	0.1
Farmland with open appearance, very few buildings, trees, etc.	0.02-0.05
Mown grass and airport runway areas	0.01
Smooth snow surface	0.001
Smooth sand surface	0.0003
Water area	0.0002

Concerning water, the issue of roughness is even more complicated. The value from table 1-1 is a big simplification. The magnitude is always really small. Nevertheless, it depends on the motion of the waves, which are influenced by the wind speed. For the calculation of the vertical profile the simplification is acceptable. However, regarding the TI it is not sufficient. This thesis concerns with onshore projects so this topic is neglected. [2]

The influence on the vertical profile of the wind speed is shown in figure 1-3. The lower the roughness the higher the wind speed near the ground.

As mentioned above, dense roughness elements like forest have to be treated like a displacement height which has for turbines the same effect as a reduced hub height. The influence on the vertical profile is shown in figure 1-4. [2]

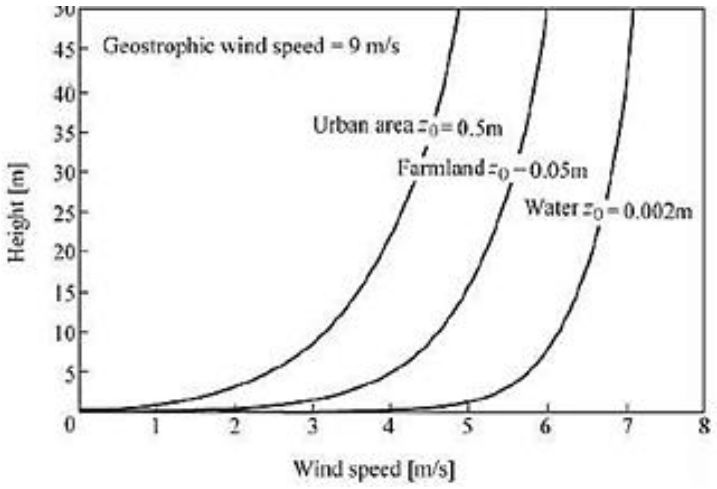

Figure 1-3: Vertical profiles for several roughness length [3]

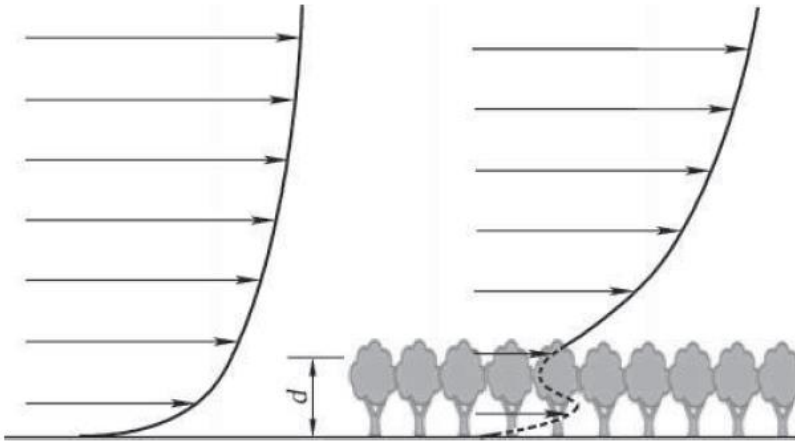

Figure 1-4: Wind profile above a dense forest [2]

An interesting phenomenon is the wind's change after a roughness alteration. The wind modifies from bottom to the top. The part that is only influenced by the new roughness is called lower layer. The upper layer is only affected by the old surface. The area between these two is called the internal boundary layer and is a mix of the two conditions (figure 1-5). [2]

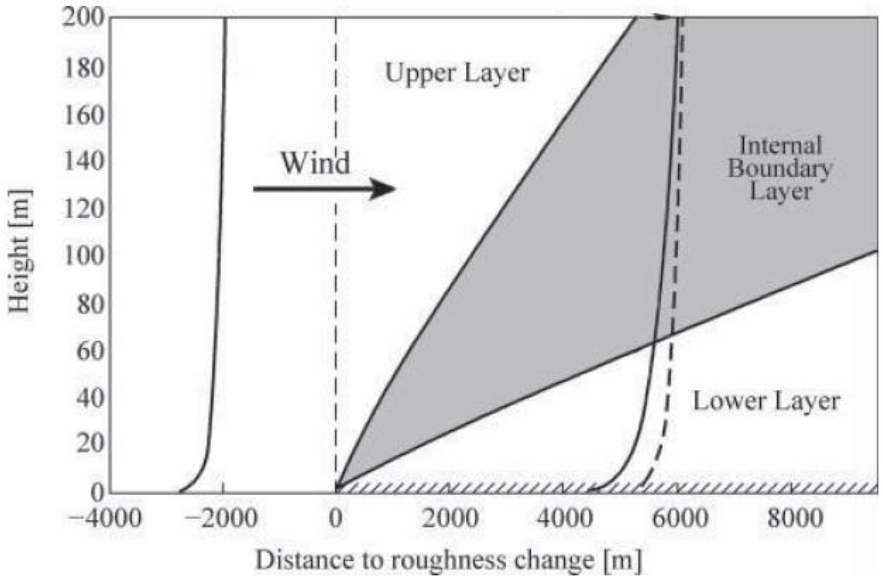

Figure 1-5: Sketch of a wind profile after a roughness change [2]

1.1.5 Orography

The best demonstration for the influence of the orography is the speed-up effect of a hill. The amout of space where the air can pass the surface is reduced by the hill. This pushes the streamlines together (figure 1-6) and with a constant air density the wind has to accelerate to fulfil the mass continuity equation (1-5). Additionally, it can be assumed from figure 1-6 that the speed-up effect is stronger near the ground than high above it. So sometimes it could be that a higher hub height does not increase the wind speed. [2]

$$\dot{m} = A_1 * \rho_1 * V_1 = A_2 * \rho_2 * V_2 \quad (1\text{-}5)$$

$\dot{m}$ is the mass flow, A is the cross section of a stream tube, ρ is the density and V is the velocity.

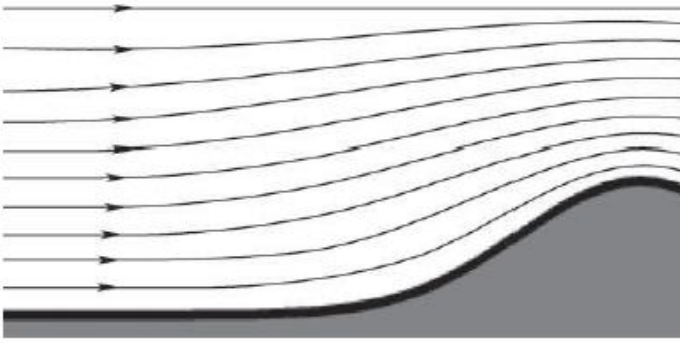

Figure 1-6: Streamlines of wind flow over an idealized hill [2]

The influence of a hill on the velocity and TI was investigated in an experiment. Two different hills were used for the experiment; one with a low slope and one with a high slope. The velocity and TI were measured at five different positions. The experimental setup is shown in figure 1-7. The distance between the positions is three rotor diameters. [6]

In a first step, the velocity and TI were measured without the turbines to catch only the influence of the hill. The progress of the velocity profile is diagrammed in figure 1-8. It can be seen that there is not only a speed-up effect at the top of the hill. Additionally, the wind is decreasing before and after the hill. The increase is stronger for the low slope hill because the wind has more time to accelerate. The decrease in front of the hill occurs through a blockage effect induced by the hill. This effect is stronger for the high slope hill and decreases when the flow is closer to the hill's top. At the lee side the speed decreases. Additionally, the flow detaches at the high slope hill. This leads to a very high TI (figure 1-9) and a greater decreasing of the flow velocity.

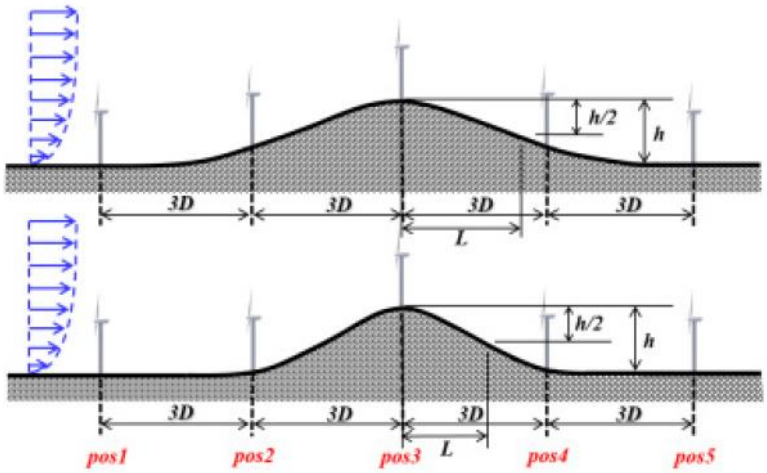

Figure 1-7: Schematic of the tested terrain model (top - low slope, bottom – high slope hill) [6]

The decrease in wind speed after the hill depends on the hill's slope. A lower slope leads to a higher wind speed. The pressure gradient is lower for a low slope and this leads to a lower deceleration. [6]

The TI's development is shown in figure 1-9. The intensity is nearly the same as for the flat surface. Only at the top of the hill it is clearly lower than for the flat case. The decrease is influenced by the increase of the wind speed. As mentioned above, the flow is detaching from the high slope hill at the lee side and the TI is getting huge. [6]

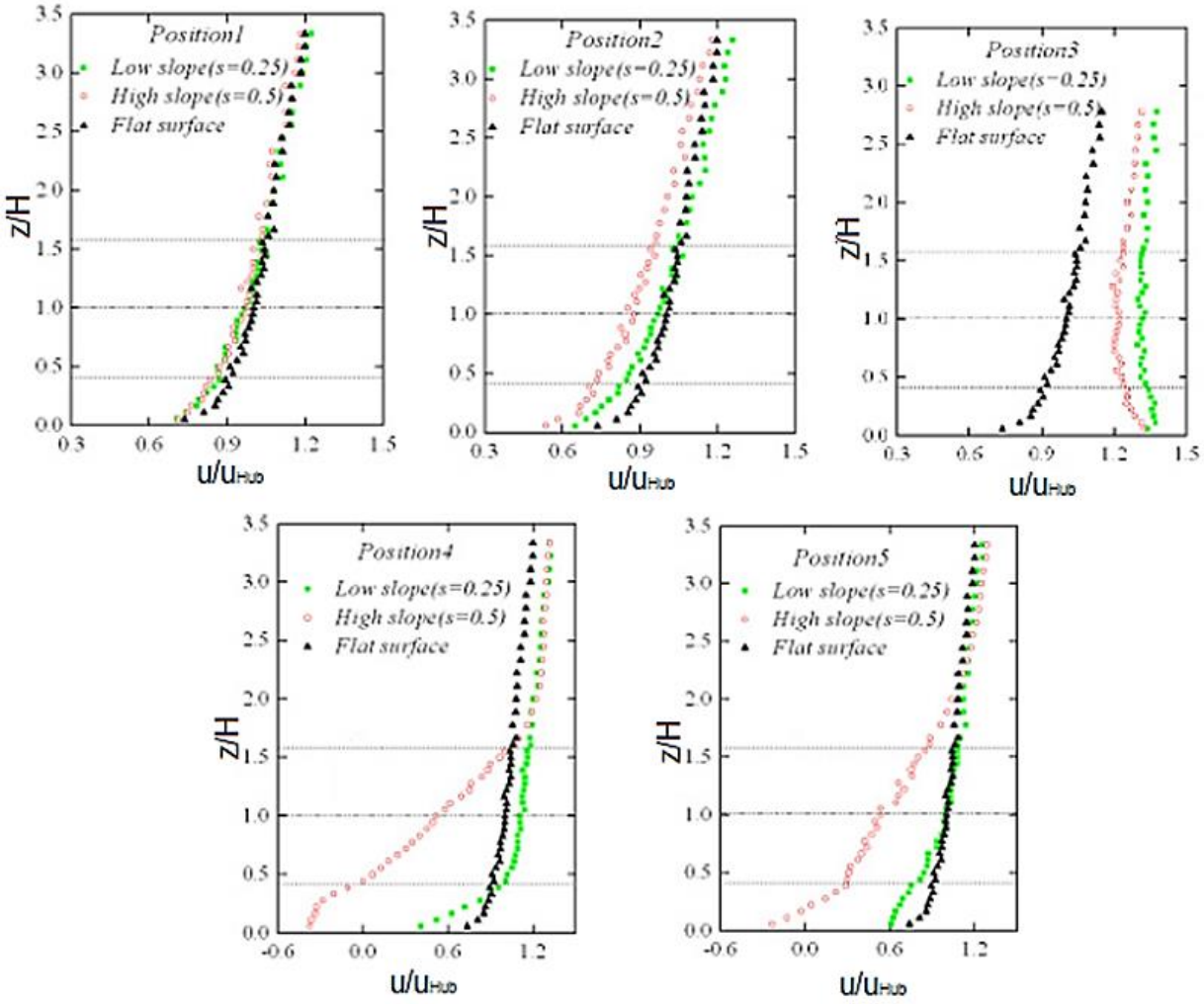

Figure 1-8: Comparison of mean stream-wise velocity profile at hilly and flat terrain [6]

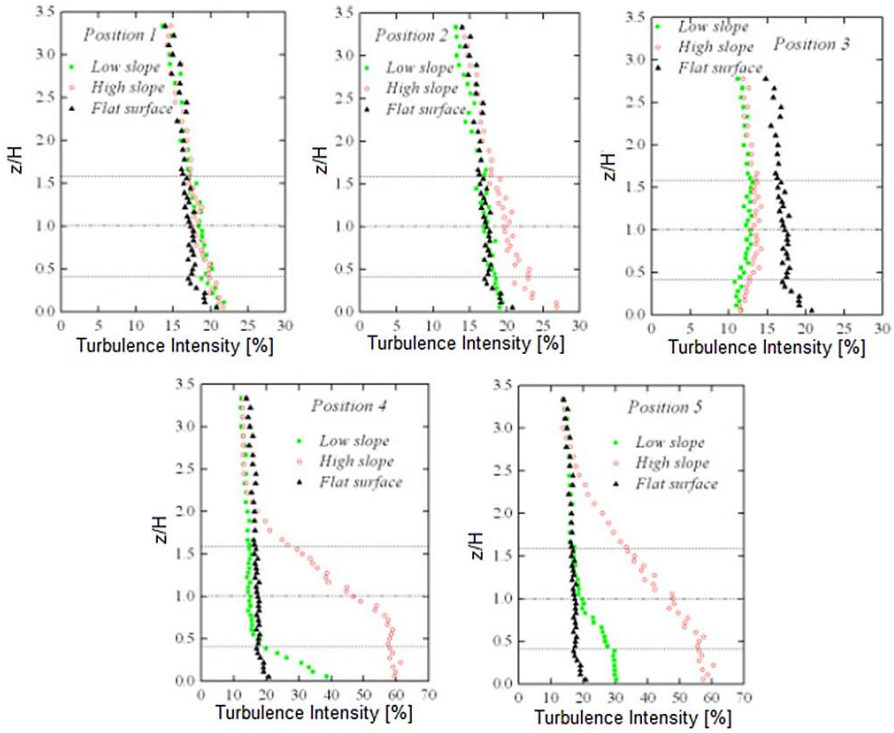

Figure 1-9: Comparison of stream-wise turbulence intensity profile at hilly and flat terrain [6]

A rule of thumb defines that flow separation occurs when the upstream slope of a hill is bigger than 22° or the slope of the lee side is bigger than 17° (figure 1-10). The wind direction changes in real cases. That is the reason why 17° is taken as limit to differentiate between complex and simple terrain. The separation of the flow occurs because the orography changes faster than the flow can follow. This is important because most of the simplified flow models are not able to calculate the separation and the results for a complex terrain would be wrong. This means, depending on the complexity of the terrain different models need to be applied to gain a valid calculation. The more complex the terrain is the more complex and time consuming the model has to be. The orography also influences the wind direction. Nevertheless, it will be neglected in this thesis. [2]

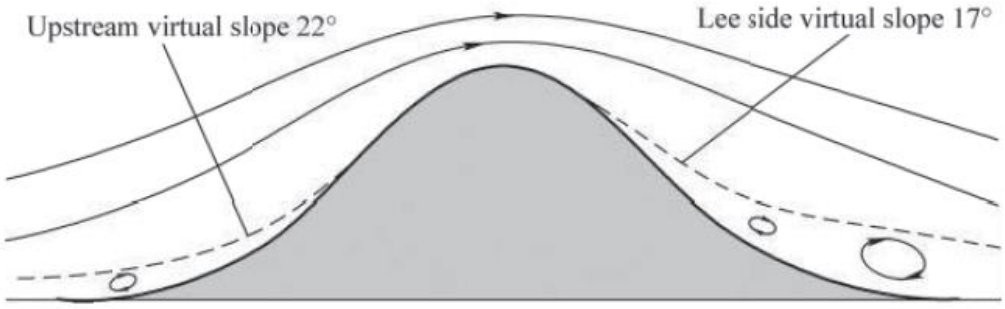

Figure 1-10: Flow separation caused by steep slopes [2]

1.2 Definition of Wake

The scope of this thesis is to validate wake models but first the wake itself is introduced.

The wake is defined as the area behind a wind turbine and characterized through lower wind speed and higher TI. The wake is often separated in near and far wake. The near wake is mostly influenced by the turbine itself while the far wake is largely affected by the ambient wind flow. [1]

Figure 1-11 shows that the air is mixing behind the wind turbine. This leads to a new shear layer. In the shear layer, the velocity deficit is reduced. The near wake range from the turbine until the two shear layers met. The length of the near wake is around one to two rotor diameters depending on the characteristics of the flow. [1]

The most important factor for the far wake is the TI. The higher the TI the faster is the recovery of the wind speed because the mixing rate between the waked and wake-free wind flow is increased. [1]

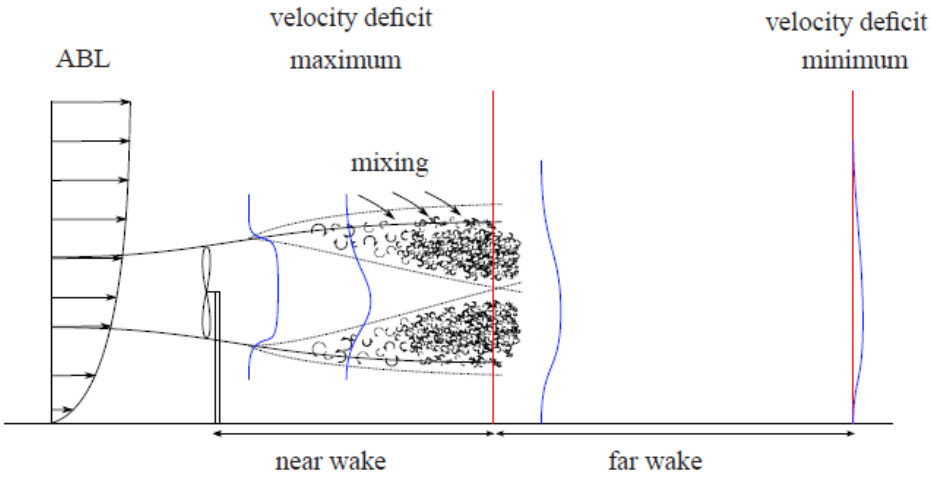

Figure 1-11: Evolution of the velocity profile in the wake [1]

1.3 How is a Turbine Generating Energy

This chapter introduce a very simple model to calculate the energy output of a turbine. Nevertheless, a short explanation of the general process is given first. Kinetic energy is extracted from the wind, converted to torque and then transformed into electric energy. A way of calculating the power production of a turbine will be explained in the following.

1.3.1 Actuator Disc Model

The classical actuator disc model (ADM) is based on one-dimensional flows and the rotor is considered as a homogenous disc. This model is used to describe elementary what is happening with the wind and will give a basic understanding of the physics. [1]

Assumptions of the ADM [1]:

- Axisymmetric flow field.
- Incompressible flow.
- Steady and homogeneous flow (no rotation).
- No viscosity (no drag and momentum diffusion).
- The wind that is passing through the disc is separated from the remaining wind by a stream tube (figure 1-12).
- The outside forces that balance the stream tube expansion and resulting radial flow components are neglected.
- The disc is infinitely thin.
- The rotor is uniformly loaded.
- No obstacles.

Figure 1-12 shows the development of pressure and wind speed before and after passing the actuator disc. The wind is slowing down because the turbine is extracting energy. The pressure is getting higher directly in front of the disc and drops right after it. The difference of pressure is the force that works on the disc. Through the lower wind speed after the turbine and the constant air density, the wake expands to fulfil the mass continuity equation (1-5). [1]

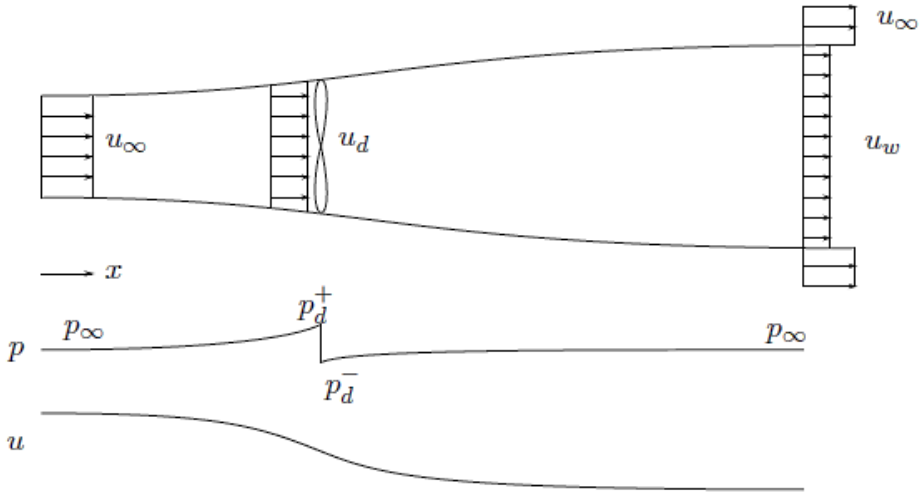

Figure 1-12: Flow through an actuator disc [1]

Bernoulli's equation cannot be used for the whole stream tube because of the pressure jump at the actuator disc. Due to the fact that the pressure jump is not accordant with the Bernoulli equation the stream tube is split into two parts. One is the upstream flow until infinite in front of the disc and one from infinite behind the disc to the downstream flow. The Bernoulli equation for the upstream part is given in (1-6). For the downstream part, the formula is equivalent. p is the pressure, the index ∞ is used for the undisturbed flow part, the d for the flow at the disc and w for the flow in the fully expanded wake. [7]

$$p_\infty + \frac{1}{2} * \rho * u_\infty^2 = p_d^+ + \frac{1}{2} * \rho * u_d^2 \tag{1-6}$$

With the Bernoulli equations for both parts, the pressure drop can be calculated (1-7).

$$(p_d^+ - p_d^-) = \frac{1}{2}(u_\infty^2 - u_w^2) * \rho \tag{1-7}$$

The formulas to calculate the energy extraction and thrust can be derived by using the equations of conversation of mass, momentum, and energy for incompressible flow. To gain more clarity the derivation will not be written down. The thrust T and the extracted energy E can be calculated with the two formulas below. M is the mass. [1]

$$T = \dot{m}(u_\infty - u_w) = (p_d^+ - p_d^-)A_d \tag{1-8}$$

$$E = \frac{1}{2}M({u_\infty}^2 - {u_w}^2) \tag{1-9}$$

The power P is just the energy divided by a time unit and also the thrust multiplied by the wind speed at the disc (1-10) this leads to (1-11). [1]

$$P = \frac{1}{2}\dot{m}({u_\infty}^2 - {u_w}^2) = \dot{m}(u_\infty - u_w)u_d \tag{1-10}$$

$$u_d = \frac{1}{2}(u_{\infty +} u_w) \tag{1-11}$$

To compare the power output of different turbines the power coefficient is specified (1-12). The coefficient is defined as the extracted energy divided by the available energy. [1]

$$C_P = \frac{P}{\frac{1}{2} * \rho * u_\infty^3 * A_d} \tag{1-12}$$

With the axial induction factor a. [1]

$$a = 1 - \frac{u_d}{u_\infty} \tag{1-13}$$

C_P becomes:

$$C_P = 4a(1-a)^2 \tag{1-14}$$

Alike to the power coefficient, the thrust coefficient can be derived by dividing the thrust through the dynamic pressure of the undisturbed flow and the rotor disc area. [1]

$$C_T = \frac{T}{\frac{1}{2} * \rho * u_\infty^2 * A_d} \tag{1-15}$$

$$C_T = 4a(1-a) \tag{1-16}$$

These two coefficients are usually measured for real turbines and are wind speed dependent.

The development of the velocity in the wake can be calculated with (1-17). The derivation is documented in [8]. x is the distance from the turbine in axial direction and D is the rotor diameter of the turbine.

$$\frac{u_i}{u_\infty} = 1 - \frac{1-\sqrt{1-C_T}}{2}\left(1 + \frac{2x/D}{\sqrt{1+4(x/D)^2}}\right) \tag{1-17}$$

The velocity of the wake for different C_T values is shown in figure 1-13. This leads to the assumption that a higher thrust coefficient increases the velocity deficit. The velocity deficit is defined as $u_\infty - u_w$ or normalized as $1 - \frac{u_w}{u_\infty}$. In addition to that, the normalized velocity is defined as $\frac{u_w}{u_\infty}$. It is also possible that the C_T value exceeds one. [1]

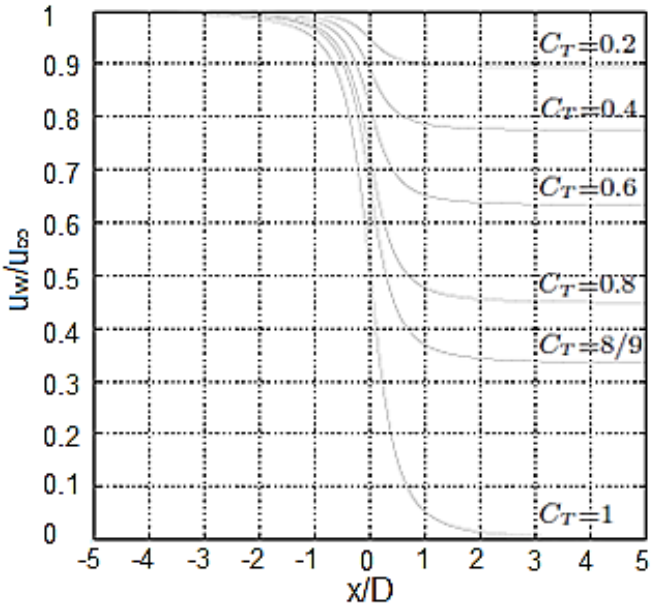

Figure 1-13: Normalized velocity of the wake for different thrust coefficients [1]

For a modern wind turbine, the thrust coefficient is high at low wind speeds and reduces with increasing wind speed. The power coefficient increases until the rated power of the turbine is reached and then decreases.

1.3.2 Betz Limit

One of the most famous restrictions of the wind industry is the Betz limit. It defines the maximum of the extractable energy. The Betz limit can be calculated with a simple derivation of the formula for the power coefficient (1-14). The maximum of this derivation is located at $a = \frac{1}{3}$. When this value is inserted into (1-14) the result is 0.59 or 59% known as the Betz Limit. [1]

For an optimal power coefficient of 0.59, the thrust coefficient equals $\frac{8}{9}$. [1]

The development of the two coefficients over the axial induction factor is pictured in figure 1-14. The theory is just valid for axial induction factors smaller than 0.5. If the factor would be bigger the downstream flow would be negative and this is not possible with the above-mentioned assumptions (1-18). [1]

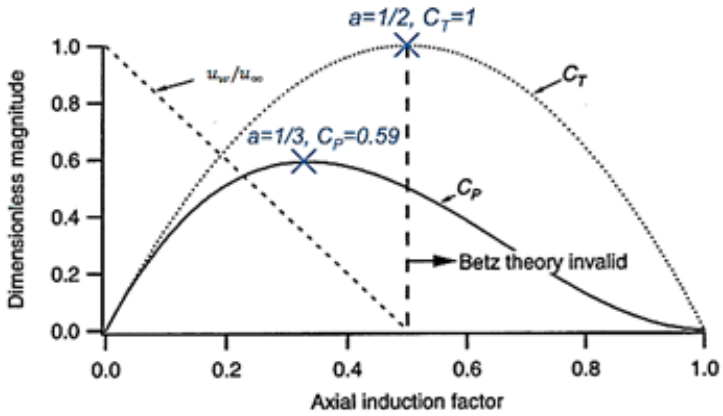

Figure 1-14: Power and thrust coefficient over the axial induction factor [11]

$$u_w = u_\infty * (1 - 2a) \tag{1-18}$$

1.4 Additional Effects

In the next chapters, some of the in the ADM neglected phenomena will be described because they are important to understand later the wake phenomenon.

1.4.1 Rotation of the Rotor

In the ADM are no blades that can rotate. Nevertheless, there are some at a wind turbine. This means the undisturbed flow velocity is not the one that is effective on the blades. The effective velocity has three different components. First, the axial one u_d, this is the velocity that was used for the ADM. The second component is the tangential velocity of the rotating blade itself and the third is the tangential velocity u_t that is caused by the torque. The influence of the rotor on the flow can be explained by Newton's third law. It declares that the force that is working on the blades is the same that is working on the flow but in the opposite direction. The blades are rotating clockwise, so the flow is rotating counter-clockwise. The different velocity parts are shown in figure 1-15. [1], [9]

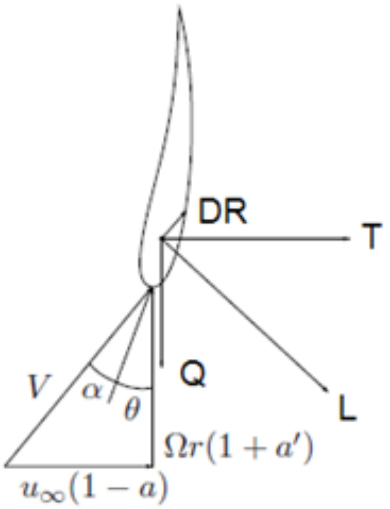

Figure 1-15: Single velocities on a turbine blade [1]

1.4.2 Vorticity

Vorticity describes the spinning motion of the flow. The basics of vorticity are described first with a simple steady wing and are then transferred to a wind turbine. The three existing vortex types on a wing are bound, starting and tip vortex (figure 1-16). The following description is only valid if the wing is generating lift. The vortices do not exist without lift. The tip vortex is induced by a difference of pressure at the wing tips which let the air spill from the high-pressure side to the low-pressure side. The wind on the top of the wing is faster than on the bottom which is creating a moment. This moment induces the bound vortex. For every bound vortex, a starting vortex far downstream exists with the same magnitude but with opposite rotation. The starting vortex is created due to the fact that the air flow below the airfoil can't reach the rear stagnation point and separates from the airfoil. [1], [10]

The dimension of the vortices can be calculated with the Kutta-Joukowski equation. For a real blade, the lift changes from the root to the tip and so the vortex does. Nevertheless, this will not be taken into account. Furthermore, the velocity is assumed uniform. [1]

$$\Delta\Gamma = \frac{L}{\rho * u_\infty} \tag{1-19}$$

Together with the tip vortices, the bound and starting vortex form a horseshoe vortex (figure 1-16). The tip vortices have the same magnitude but are working in opposite directions similar to the starting and bound vortex. According to the Helmholtz's theorems, the strength of a vortex filament is constant and all four parts of the horseshoe have the same strength. [1], [11]

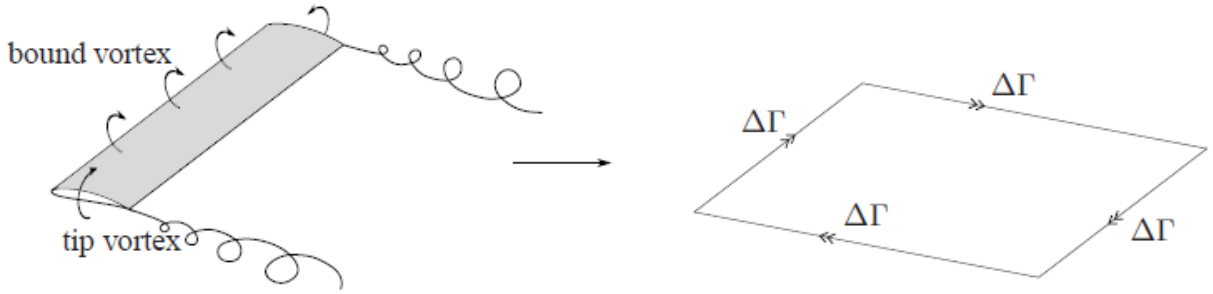

Figure 1-16: Vortex system on a steady and finite wing [1]

A blade of a wind turbine is just a rotating wing so the above-described concept can be modified and used. The vortex at the root of the blades is a little bit different than the tip vortices. Assuming that all blades end at the same point, the root vortex is the sum of all tip vortices of the blades. When all blades are equal, equation (1-20) can be used. B is the number of blades. [1]

$$\Gamma = \Delta\Gamma * B \tag{1-20}$$

The root vortex and the tip vortices (for small tip speed ratios (TSR)) generate the tangential velocity of the flow at the blades. The rotation is the opposite of the rotors one. The tip vortices are responsible for the deceleration of the flow in front of the turbine. The deceleration results from the tangential component of the tip vortices which induce an axial velocity at the blades. The tip vortices also add turbulence to the air flow. [1]

The TSR (λ) can be derived from the equation below. Ω is the angular velocity and r is the distance from the centre of the rotor in the radial direction. [1]

$$\lambda = \frac{\Omega * r}{u_\infty} \tag{1-21}$$

The vortices have their greatest magnitude at the root and the tips of the blades. The helical path of the vortices depends on the rotational speed of the blades. The higher the TSR the more parallel is the path to the rotor plane. [1]

This model is just a simplification. In the reality, the vorticity vary over the wing-span and the flow is viscous which is both neglected. However, the model gives a good impression where vorticity occurs. [1]

1.4.3 Additional Turbulence

The upstream turbines create additional turbulence or TI for the downstream turbines. This has to be added to the ambient TI. The additional TI is induced by tip vortices, turbulent boundary layers from the blade, the nacelle, the tower as well as through interaction with the undisturbed flow.

The created additional TI is non-uniform. The maximum is located at the upper tip and the minimum in the half below the nacelle. The added TI for different roughness cases from a single turbine on a flat terrain can be seen in figure 1-17. For a rough surface like in the first case, it is even possible that the TI decreases in the lower half of the rotor. The magnitude and location of the maximum depends on the inflow conditions. Higher TI levels from a rougher surface result to a larger maximum closer to the turbine. The increase of the TI in the upper part of the rotor is larger because the difference between the waked and ambient flow in this area is bigger than in the bottom part. When the distance increases the magnitude of the additional TI decreases and the distribution gets more uniform. A special case is the reduction of the TI in the lower half of the rotor. This can be explained with a reduced shear in this region because the difference between ambient and waked wind speed is lower and this leads to lower TI. [1], [12], [13]

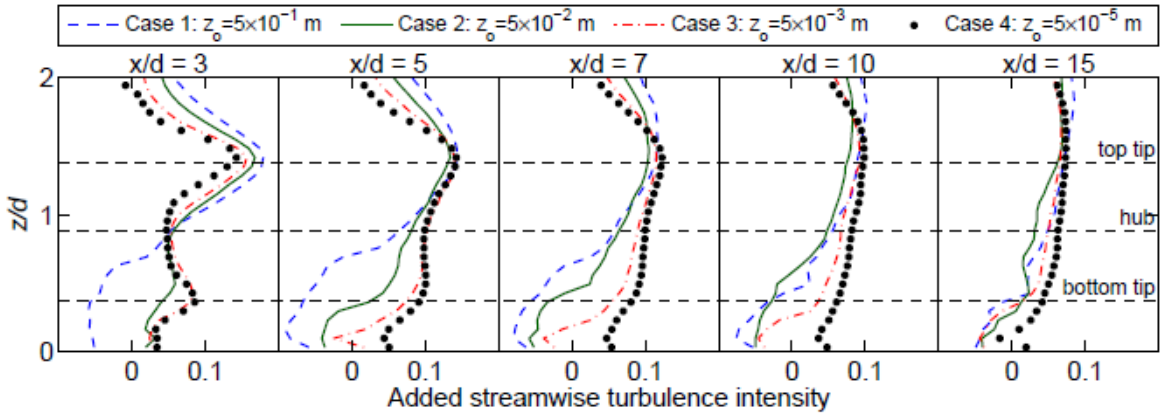

Figure 1-17: Vertical profiles of the added streamwise turbulence intensity through the hub level of the turbines installed on flat surfaces with different roughness lengths calculated with an large eddy simulation [12]

1.4.4 Velocity Profile

Towards the assumptions of the ADM, the velocity distribution behind and in front of a turbine is non-uniform. First of all the shear has to be taken into account. The incoming wind is higher at the upper part of the turbine. Also, the velocity deficit is not uniform as assumed before (figure 1-18-a). Even if a top-hat shaped profile is sometimes used for simplifications. A more realistic representation of the velocity distribution in the far wake is a Gaussian profile. This results out of the higher wind speed recovery at the border regions of the wake (figure 1-18-b). [1], [14]

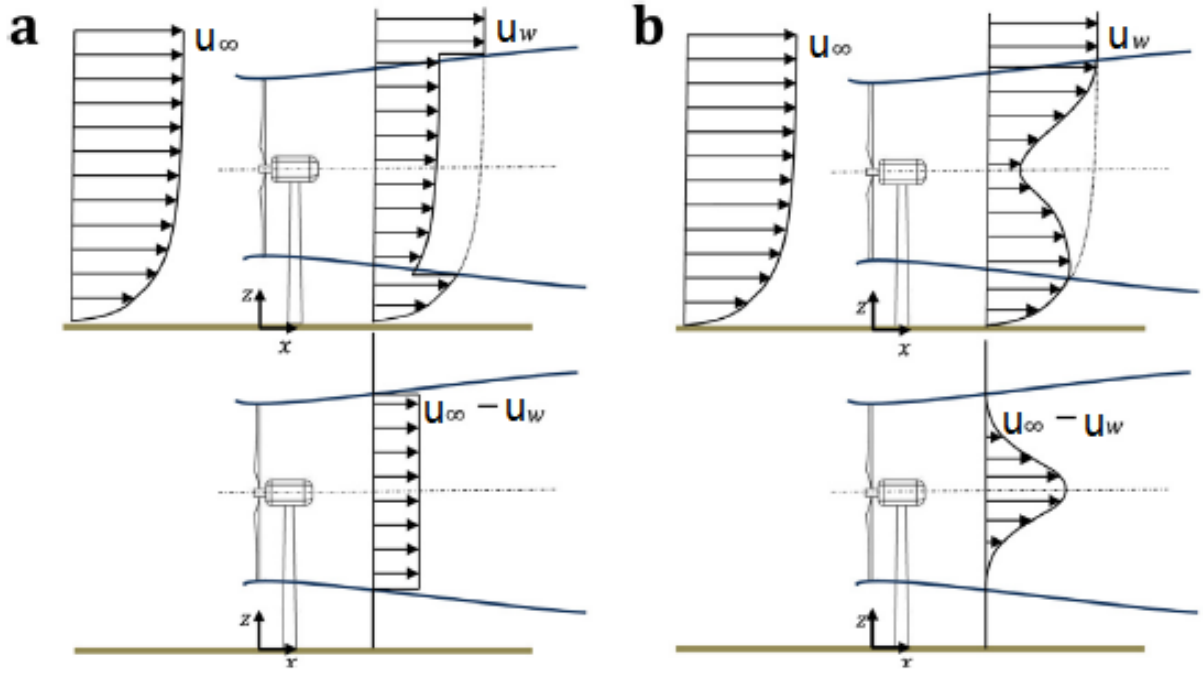

Figure 1-18: Schematic of the vertical profiles of the mean velocity (top) and the velocity deficit (bottom) downwind of a wind turbine obtained by assuming: (a) a top-hat and (b) a Gaussian distribution for the velocity deficit in the far wake [14]

2 Importance of Wakes

In this chapter, the gained knowledge of the first section is used to compile consequences for wind turbines and wind farms. In the end, the task for this master thesis will be developed.

2.1 Turbine Induced Flow Changes

The changes a turbine causes on the flow were already described in the last section. Due to their importance they will be summed up here.

The wind speed decreases significantly in the wake and the TI increases. With increasing distance, these values normalize. The velocity deficit depends on the thrust coefficient and the recovery on the TI.

2.2 Turbine in the Wake

In the following passage, the impacts of wakes on turbines are explained.

The first point is that the energy output is significantly lower than without a turbine upstream caused by the velocity deficit. The reduction depends on the distance between the turbines, the thrust coefficient and the rate of recovery.

The second point is that the fatigue loads for the waked turbine are substantially higher through the higher TI. A high TI is good for a fast recovery of the wind speed and a high energy output although bad for the fatigue loads. Through the higher loads the turbines need to be designed more robust and get more expansive or a curtailment is needed and they produce less energy.

2.3 Influence on the Layout of a Wind Farm

The consequence from the chapter above is that turbines should be separated generously for a long lifetime and high power output. A layout can be described as the distance between turbines and in which direction they are positioned to each other. The direction influences the possible closest distance and will be explained first.

2.3.1 Direction

The wind has for nearly all wind farms a prevailing direction from where it blows most of the time. Due to the fact that there is less wind from the other directions the additional loads and power losses are smaller which is used to reduce the distance between the turbines in the perpendicular direction of the prevailing one.

The direction influences also how much of a downwind turbine is in the wake (full, partial or not).

2.3.2 Distance

For the loads and power output, it would be the best solution if the distance between the turbines would be above ten rotor diameters for onshore wind farms. The problem is that the available space is restricted. Additionally, the costs concerning e.g. cable, land and measuring campaign will increase strongly with a bigger wind farm.

In reality, it is not an option to have these large distances between the turbines. Thus, a compromise is needed. An important fact that helps to solve this problem is that the wind speed reduction gets to equilibrium after several turbines.

SGRE recommends for an onshore wind farms in general a minimum distance of five rotor diameters in the prevailing wind direction and three rotor diameters in non-prevailing wind direction. These values are often not fulfilled because there is not enough space for the customer favoured number of turbines. The closer the spacing the more important is a good wake model.

2.4 Deduction of the Task

As shown above, wakes have a huge influence on the layout, loads and power output. This shows the importance of a very good model to calculate the wake. Lower uncertainties for the annual energy production (AEP) are an advantage for the customer and SGRE gets more attractive trough that.

Fast analytical and numerical models have greater uncertainties than more complex computational fluid dynamic (CFD) models. At the moment are nearly all projects calculated with the analytical Jensen Model. The currently used CFD model needs to much computational time to use it for every project. To solve this problem new wake models are tested. One of these new models is Wake Blaster developed in 2017 by ProPlanEn Ltd.

The main objective of this master thesis is to compare the performance of the Jensen Model with the WakeBlaster model. For this comparison production data from two operational wind farms are used. The focus lies on the comparison of the production of the models and the operational wind farm.

3 Theory of Wakes

The first section explained the basics of the ABL and the principles of wind turbines, the second section clarified why wakes are so important for the wind industry. This chapter describes the wake phenomenon in detail. This allows a correct interpretation of the results afterwards. The beginning is about the different influences on the near and far wake. At the end of this chapter characteristics of some special cases are explained.

3.1 Influences on the Wake

The wake is influenced by a lot of different factors which also interact with each other. Thus, it is difficult to calculate all aspects of the wake correctly and investigate single aspects. Also, the fact that the near wake is mostly affected by the turbine properties and the far wake is mainly depending on the flow characteristics complicate the calculations even more.

Firstly, the near wake is described. The explanation of the far wake follows. The focus lies on the far wake since this is the region where the downwind turbines are positioned in. Furthermore, the attention is focused on the development of the velocity deficit.

3.1.1 Near Wake

In the near wake, the disturbed flow has not exchanged with the undisturbed flow. Hence the undisturbed flow has nearly no influence on this part and it is only dependent on turbine characteristics. Some of the most important aspects are described below. [1]

A problem is that the near wake is not as good investigated as the far wake. This may come from the fact that the downwind turbines are mostly placed in the far wake. Consequently, this area is of a greater interest for the industry. Next to that, it is difficult to derive the influence of single factors, since in most of the experiments blades, airfoil parameters and wind conditions were different.

3.1.1.1 Thrust Coefficient

The thrust coefficient is the main influencing factor regarding the velocity deficit for the near and the far wake. Furthermore, it is for most of the wake models together with the rotor diameter the only turbine related variable; a higher thrust coefficient leads to a larger velocity deficit (figure 1-13). For a given turbine the coefficient depends only on the inflow wind speed and the air density. Nonetheless the density does not change for a fixed position. Resulting from this it can be assumed that the coefficient is only dependent on the wind speed (figure 3-1). This means a higher wind speed leads to a lower velocity deficit. [1]

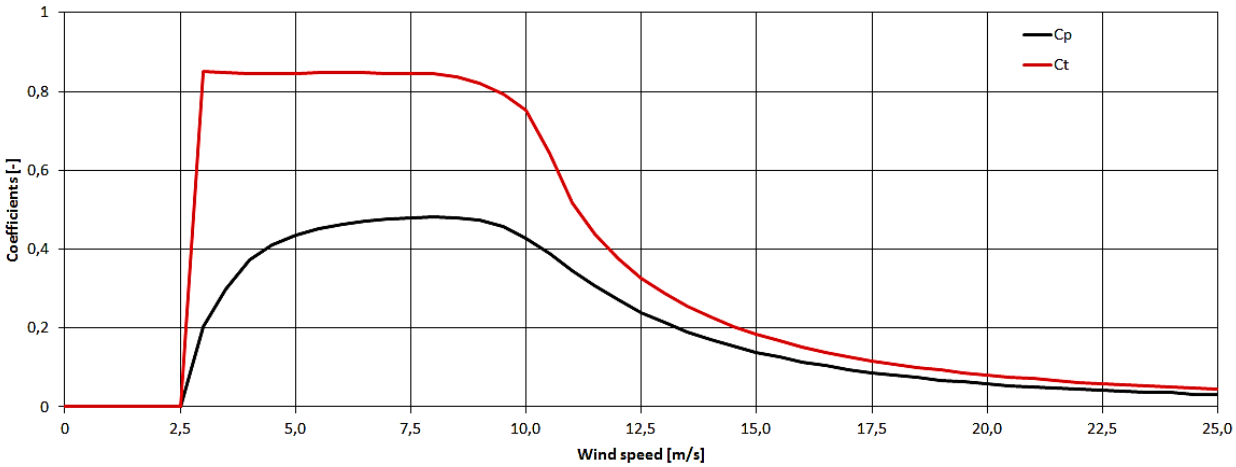

Figure 3-1: Typical thrust and power coefficient curve over the wind speed of a wind turbine

3.1.1.2 Pitch Angle

The pitch angle θ influences the angle of attack and through that the behaviour of the blades. Figure 3-2 shows the power coefficient over several pitch angles. In the research literature there was no paper found dealing with the influence on the thrust coefficient. Nonetheless, with the information from chapter 1.3.1 or figure 3-1 the content of figure 3-2 can be transferred to the thrust coefficient.

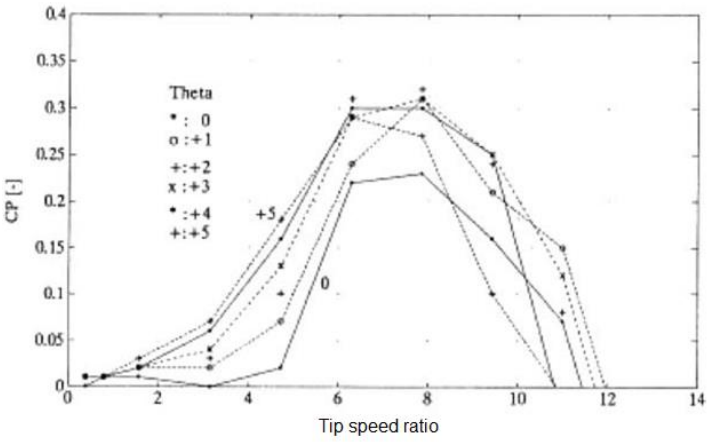

Figure 3-2: Power coefficient as a function of the tip speed ratio with tip pitch angle as a parameter [9]

A higher pitch angle leads to a higher power coefficient and the maximum appears at a lower TSR (figure 3-2). The power coefficient decreases also faster with a high pitch angle. This comes from the fact that the flow detaches earlier with a high pitch angle. [9]

Modern turbines adjust their pitch angle depending on the wind speed. A positive angle at low wind speeds for a higher production and a negative one at high wind speeds for lower loads.

3.1.1.3 Form of the Blades

As described above, the thrust coefficient is the determining factor for the velocity deficit. However, it is not constant for the whole rotor as assumed in the ADM. The thrust coefficient is changing with the span wide like the twisting of the blades and other airfoil parameters. The variable coefficients lead to a non-uniform velocity deficit in the near wake (figure 3-3). The maximum velocity deficit occurs at 0.55< r/R <0.9 which indicates that the thrust coefficient and the momentum extraction are high there. The figure shows also that the wake is expanding with increasing distance from the upwind turbine. [15]

Schümann [16] presented similar results regarding the velocity deficit and calculated additionally the TI development. The highest TI values were found for the very near wake in the blade tip regions and close to the tower. In the far wake is the TI distributed annularly. Taken into account the knowledge from chapter 1.4.2 the high values at the tips are reasonable.

A detailed description of how the airfoil values of blades can be calculated is out of the thesis' scope and will not be described.

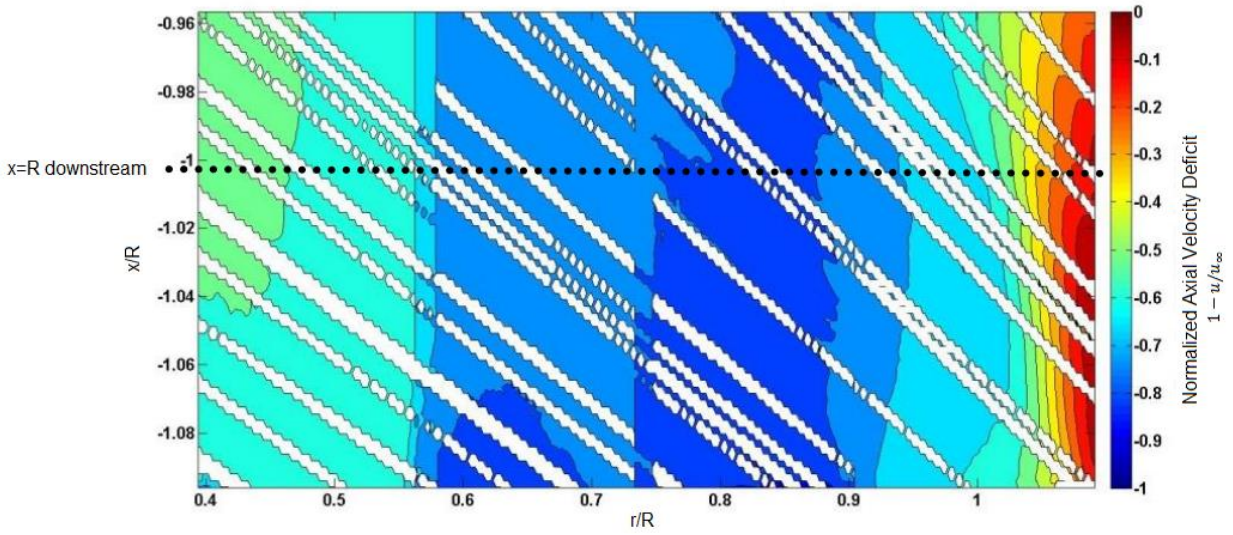

Figure 3-3: Contour of mean axial velocity deficit behind the rotor for an azimuth angle of the blade of $45°$ [15]

3.1.1.4 Tip Speed Ratio

The TSR has a significant effect on the velocity deficit (figure 3-4). The deficit is higher with a high TSR. A high TSR indicates usually low wind speeds. At lower wind speeds is the part of the energy that is extracted greater which results in a higher deficit. Lower wind speeds result also in higher thrust coefficients (figure 3-5). [9], [17]

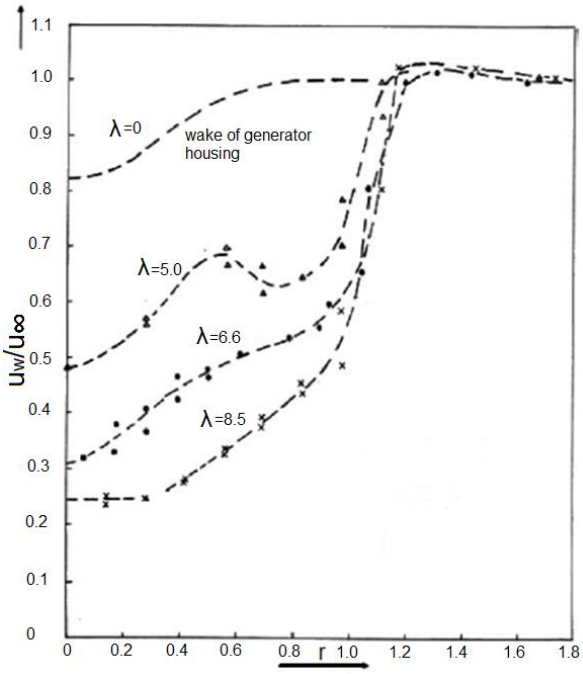

Figure 3-4: Crosswind profiles, showing velocity deficit as a function of radial distance with the tip speed ratio as a parameter for axial distance x/D = 1.67 [9]

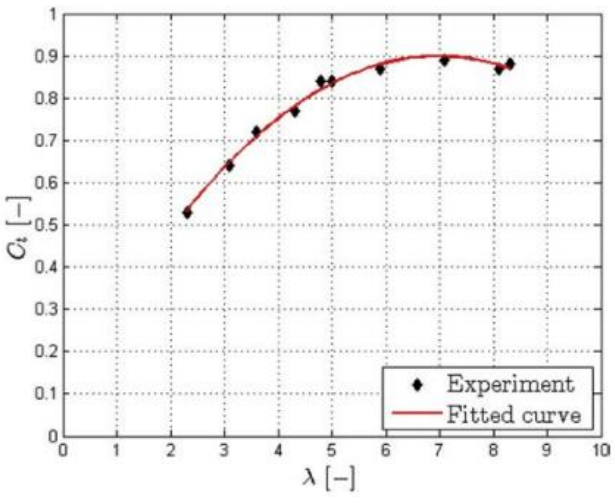

Figure 3-5: C_T-λ curve of a wind turbine model [17]

3.1.1.5 Dependency of the Phase Angle

An interesting point is the influence of the phase angle on the velocity deficit in the very near wake. The phase angle is defined as the angle between the blade at the turbine and the measurement point. The measurement point is fixed but the phase angles changes with the time because the blades are spinning. The axial velocity deficit is for r/R>0.85 phase angle dependent and for smaller values independent (figure 3-6). Already at the position x=2R is the velocity deficit completely independent of the phase angle. This finding leads to the assumption that only for the very near wake a rotor model with rotating blades like the actuator line method is needed. [15]

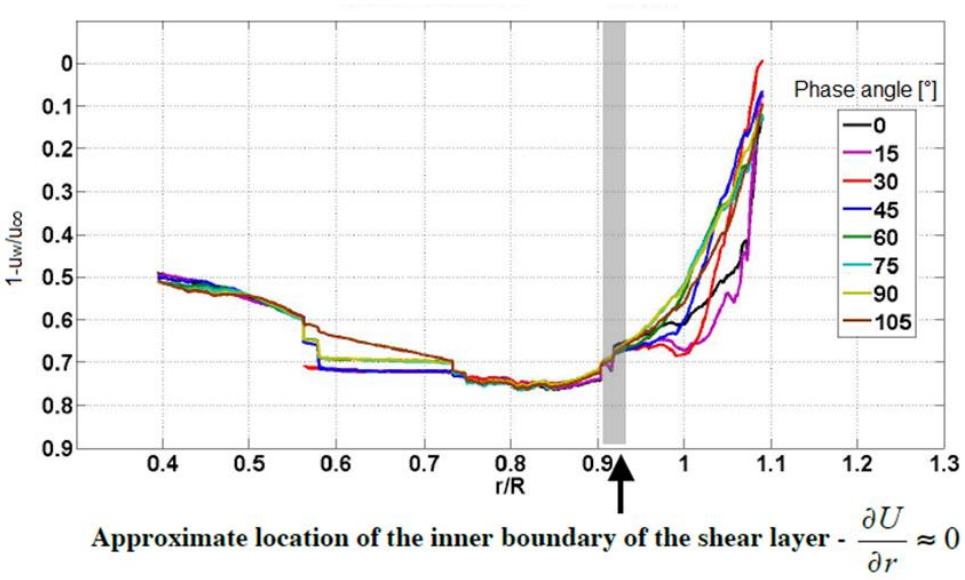

Figure 3-6: Radial profiles of the streamwise velocity deficit for eight phase angles of the blade at x=R [15]

Also, the TI is dependent on the phase angle in the very near wake and gets independent at x = 2R. Especially in the area r/R>0.85 is the dependency strong. This results out from the tip vortices. Also for r/R<0.6 is the TI dependent on the phase angle but this time the root vortices influence the flow field. [15]

3.1.1.6 Number of Blades

The commonly used variant is a horizontal rotating three-bladed wind turbine because it has some advantages over the two-bladed variant such as lower noise emission and favourable dynamic load behaviour. A benefit of the two-bladed turbine is the much lower costs due to a missing blade. [18]

At first thought, it should make a big difference if a turbine has two or three blades. Nevertheless, it seems that this is not the case. Some experiments were done with three different rotors with nearly the same thrust and power coefficient value at a certain wind speed (one three- and two two-bladed rotors). The velocity deficit is nearly the same for the two- and three-bladed rotor. Interestingly the TI level for the two-bladed variant is higher, especially at the tips. This leads to a faster recovery of the wake, especially in the near wake. [18]

The higher additional TI of the two-bladed rotor makes this variant interesting for offshore wind farms because the ambient TI is there very low. [18]

3.1.2 Far Wake

The development of the far wake depends on flow conditions like wind speed, TI and the surface. The wind speed is not explained in a single sub-chapter since it influences mainly the thrust coefficient. This relation was already explained. The same reason applies to the influence of the TI. [1]

The velocity profile of the far wake differs from the one of the near wake. The maximum of the velocity deficit is now located in the centre of the wake and the velocity increases with the radial distance. A schematic of the profile was already shown in figure 1-18.

3.1.2.1 Topography

The influence of the topography on the TI is diagrammed in figure 3-7. A higher roughness leads to higher ambient TI and to higher TI in the wake as well as to a higher shear. Also, the position of the maximum TI gets closer to the turbine with a higher roughness. [12]

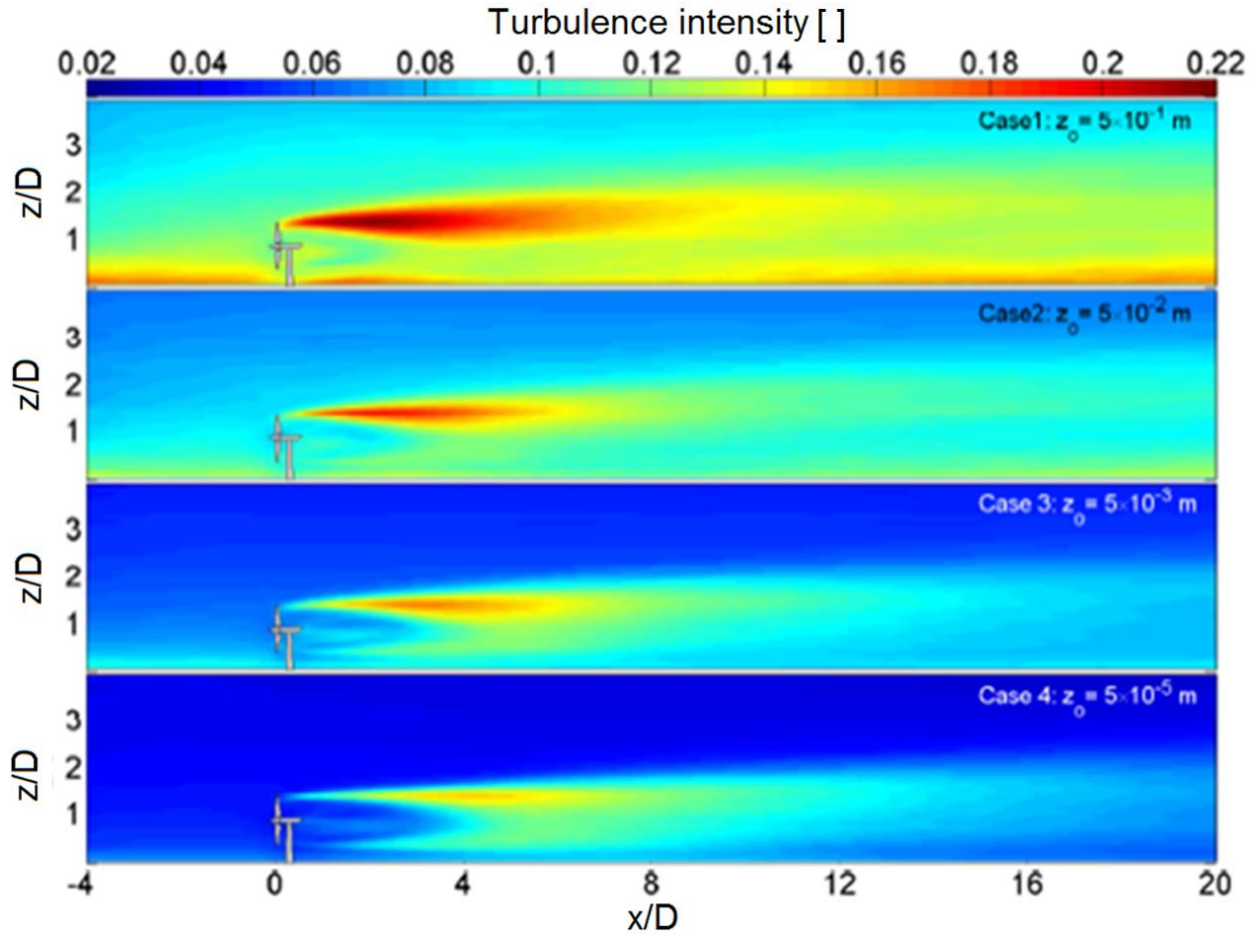

Figure 3-7: Contours of the streamwise turbulence intensity in the middle vertical plane perpendicular to the turbines installed over flat surfaces with different roughness lengths [12]

Figure 3-8 shows that the recovery of the wind speed is a lot faster when the roughness is higher. This results from the fact that the increased TI enhances the exchange with the undisturbed flow. The figure shows also that the velocity profile in the near wake is independent of the flow characteristics. [12]

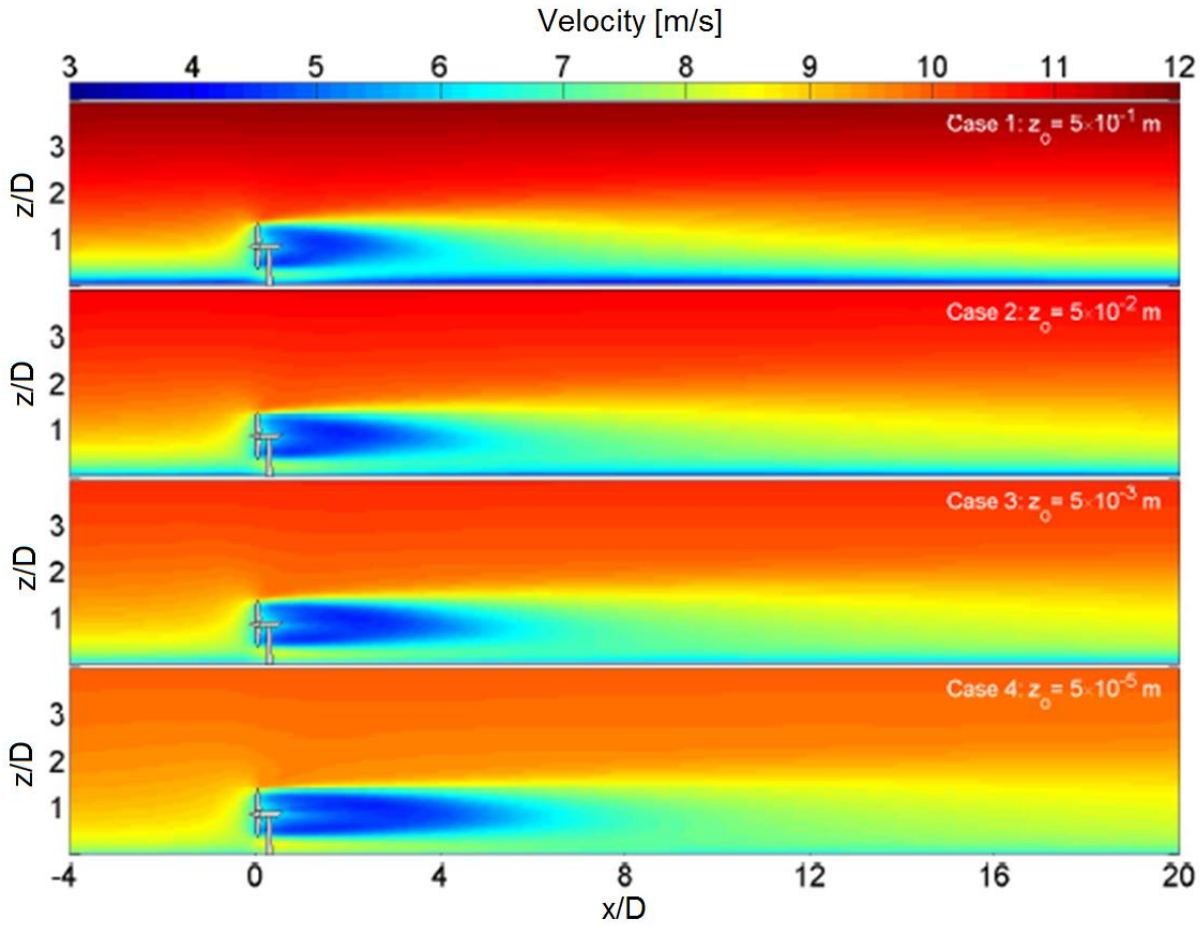

Figure 3-8: Contours of the averaged streamwise velocity in the middle vertical plane perpendicular to the turbines installed over flat surfaces with four different roughness lengths [12]

3.1.2.2 Orography

The influence of the orography on the wake is explained with the in chapter 1.1.5 introduced experiment. The difference to the content from chapter 1.1.5 is that the presented results include now the influence of the turbines at the positions. Figure 3-9 and figure 3-10 show that the velocity deficit generated by the upstream turbines is negligible for the turbine at the top of the hill (position three) and also in the zone where the flow is detached (position five of the high slope hill). The zone of the detached flow is not of interest because no turbine would be positioned there. For the turbines at the lee side of the low slope hill, the wake has a noticeable effect and also for the turbines in front of the hill. Additionally, the wake is spread more through the decrease of the hill height. This can be seen in figure 3-9 at position four and five. [6]

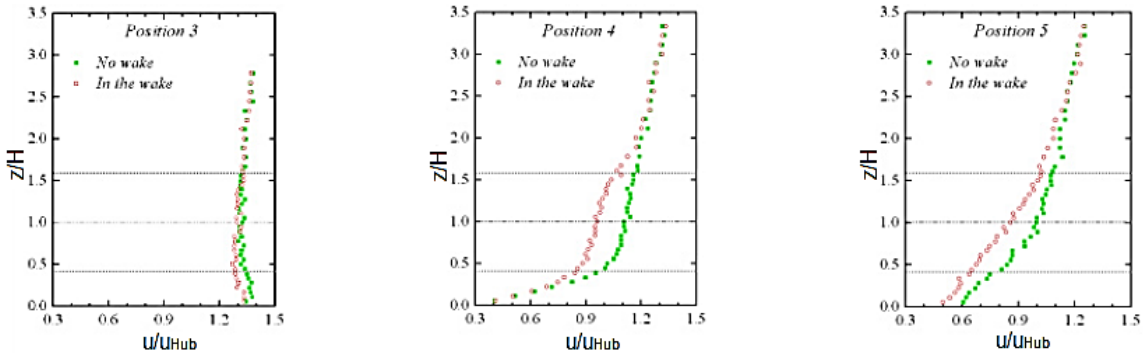

Figure 3-9: Comparison of the velocity profiles with and without wake for low slope hill [6]

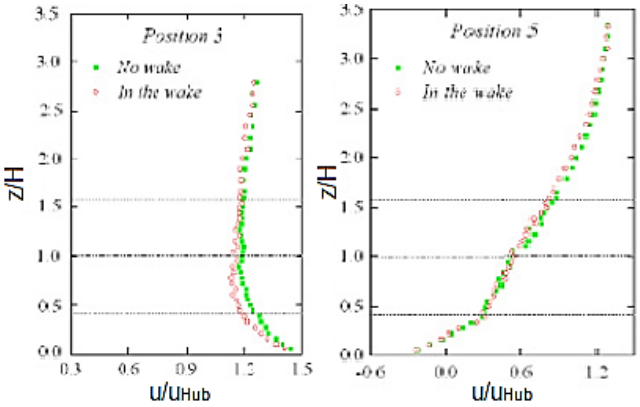

Figure 3-10: Comparison of the velocity profile with and without wake for high slope hill [6]

3.1.2.3 Atmospheric Stability

The influence of the atmospheric stability on the velocity deficit and the TI in the wake is shown in figure 3-11 and figure 3-12.

The velocity deficit in the far wake is smaller for unstable conditions because of higher TI and through that a higher mixing rate. Moreover, the velocity deficit in the near wake is nearly the same. This underlines the assumption that the main factors for the near wake are related to the turbine and not to environmental characteristics. Important is also that the wind speed recovered faster in the upper part of the wake because of the higher velocity differences between the wake-free and waked flow and the through that higher momentum flux. [19]

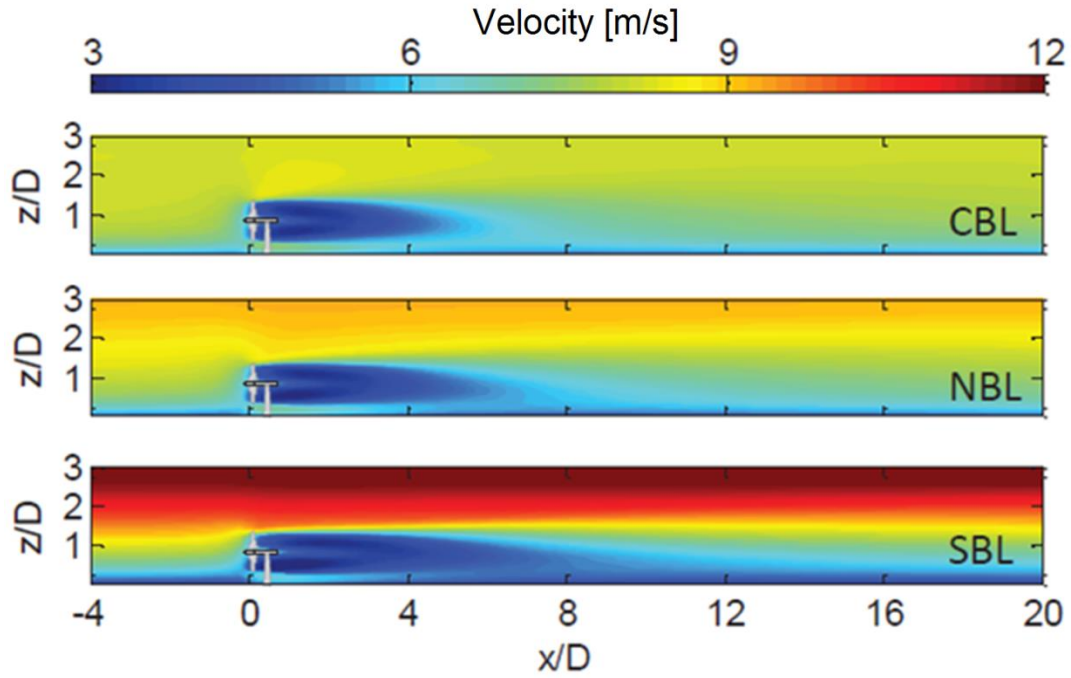

Figure 3-11: Contours of the time-averaged streamwise velocity in the middle vertical plane perpendicular to the turbine for different stability conditions (top – unstable, middle – neutral and bottom – stable)[19]

The TI is a lot higher for the unstable case. This is caused by higher ambient TI than for the neutral and stable case (figure 3-12). Also, the position and the magnitude of the maximum are dependent on the atmospheric conditions. When the ambient TI is higher the magnitude of the maximum is higher and closer to the turbine. [19]

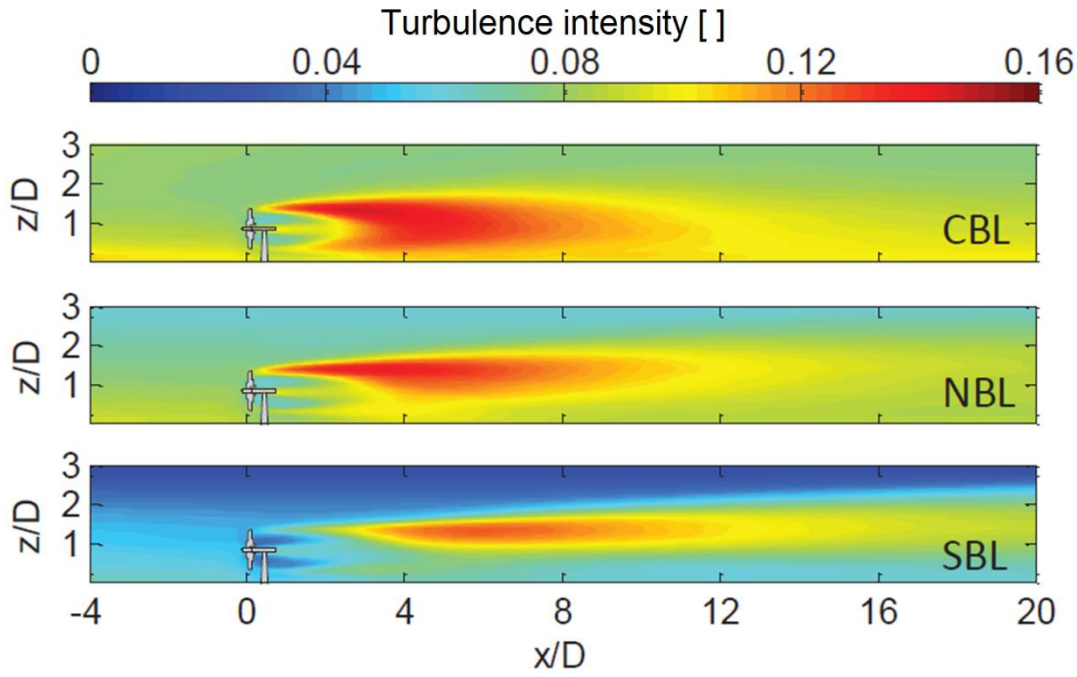

Figure 3-12: Contours of the time-averaged turbulence intensity in the middle vertical plane perpendicular to the turbines for different stability conditions (top – unstable, middle – neutral and bottom – stable) [19]

3.1.2.4 Shear

Also, the shear has an influence on the wake development although it is small compared to the one of the TI. The shear depends on the roughness and the atmospheric stability but these factors also influence the TI. Wu and Porté-Agel [12] simulated a synthetic inflow velocity field where the atmospheric stability was neutral. Three different cases were simulated. One with low roughness and the resulting low shear and low TI. One with a high roughness and high shear and TI and one with a high roughness and high shear but low TI. All cases are shown in figure 3-13. This was done to separate the impacts of shear and TI.

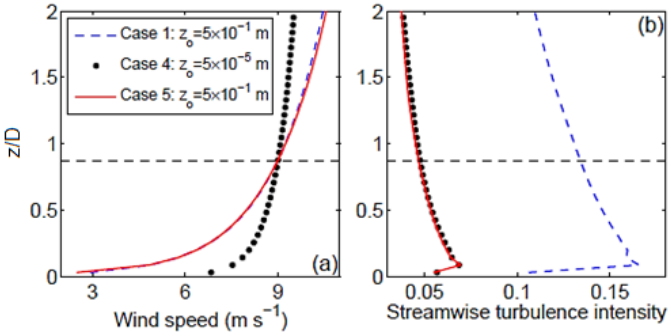

Figure 3-13: Vertical profiles of the time-averaged streamwise velocity (a) and turbulence intensity (b) [5]

The resulting vertical profiles of the velocity deficit and the TI are pictured in figure 3-14. The velocity deficit is for case four and five, which have the same ambient TI, very similar. The differences result out of the added TI which is for case five higher in the part above hub height and less in the lower part than for case four. This results from the fact that the added TI is higher when the wind speed difference between undisturbed and disturbed flow is greater, which is the case through the increased shear. In the lower part, the opposite is the case; the wind speed difference is lower which result in a lower added TI.

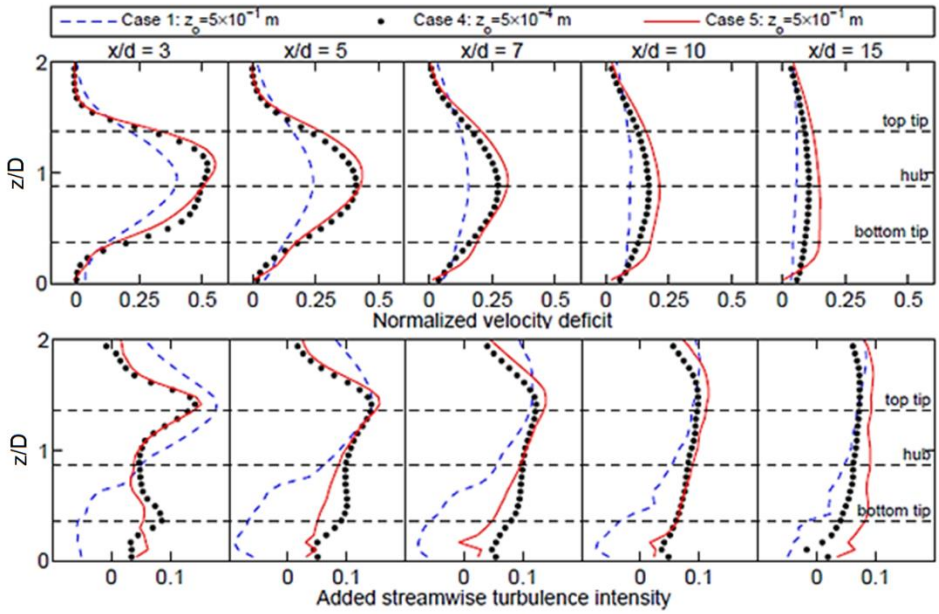

Figure 3-14: Comparison of vertical profiles of the normalized velocity deficit (top) and turbulence intensity (bottom) through the centreline of the wakes [12]

3.2 Conclusion of Wake Characteristics

A short summary of the wake characteristics will be given before some special cases are described. In the very near wake (x/R<1) is the flow phase angle dependent. At a distance of x=2R is the flow already phase angles independent.

The velocity distribution changes with the distance from the wind turbine. In the near wake is the velocity deficit maximal where the most power is extracted (normally between the mid and tip part of the blades); it depends on the blade characteristics. In the far wake, the velocity deficit is in the centre of the wake maximal and gets lower with increasing radial distance. This results through the exchange with the undisturbed flow. The exchange rate depends mostly on the TI.

3.3 Partial Wake

The partial wake is a special case with advantages and disadvantages for the downstream turbine. Partial wake means that only a part of the rotor disc of the downstream turbine is influenced by the wake effect of an upstream turbine (figure 3-15).

The advantage is that the average wind speed that is effective on the rotor is higher. One part of the flow is undisturbed which increases the energy production of the turbine. The disadvantage is that the loads are higher than in the full wake. This results out of additional moments which are induced through the different magnitudes of the wind speed (figure 3-16). [20]

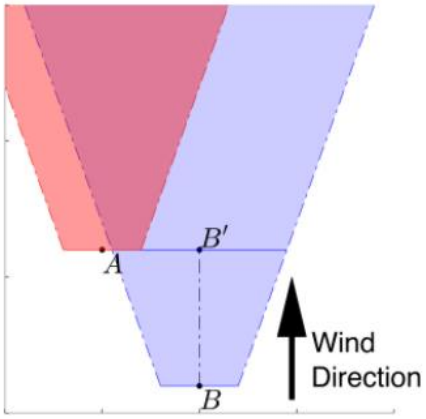

Figure 3-15: Schematic of a partial wake [21]

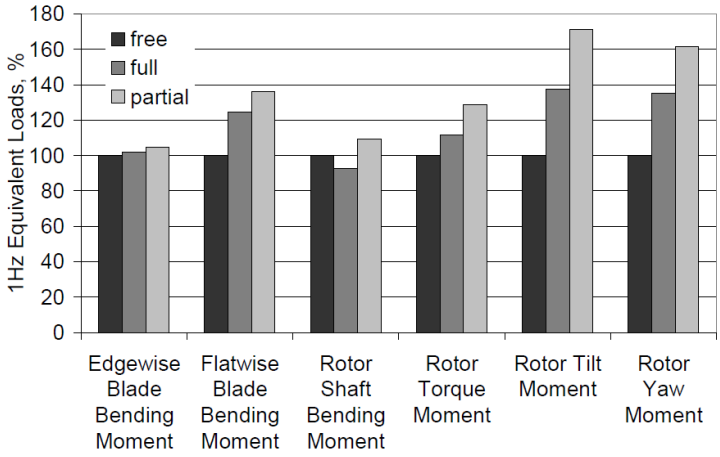

Figure 3-16: Equivalent loads for different components [20]

3.4 Addition of Wakes

Additional to the above-mentioned case of the partial wake it is also sometimes needed to sum up single wakes. This chapter describes a method to do that.

At first is the average wind speed for the rotor calculated (3-1). This is needed to calculate the production with a simple model like the ADM. [22]

The averaging has to be done for every single wake case. The next step is then to sum up all single wake case into one. A common method for this is the sum of squares principle (3-2). u_i is the velocity at the i^{th} turbine taken all wakes into account and u_{ij} is the velocity at the i^{th} turbine due to the wake of the j^{th} turbine. u_j is the wind speed at the j^{th} turbine and $u_{i\infty}$ is the undisturbed wind speed at turbine i.

$$(u_\infty - u_d)^2 = \frac{1}{A}\int_{rotor}(u_\infty - u_w)^2 dA \tag{3-1}$$

$$\left(1 - \frac{u_i}{u_{i\infty}}\right) = \sqrt{\sum_{j=1}^{i-1}\left(1 - \frac{u_{ij}}{u_j}\right)^2} \tag{3-2}$$

To make formula (3-2) clearer is a schematic shown in figure 3-17. For simplifications is the ambient wind flow for all three turbines the same. First the velocity deficit caused by turbine one is calculated, then the one from turbine two. At the end they are summed up and the root is extracted. With the known uniform velocity, the production of the turbine can be calculated. [22]

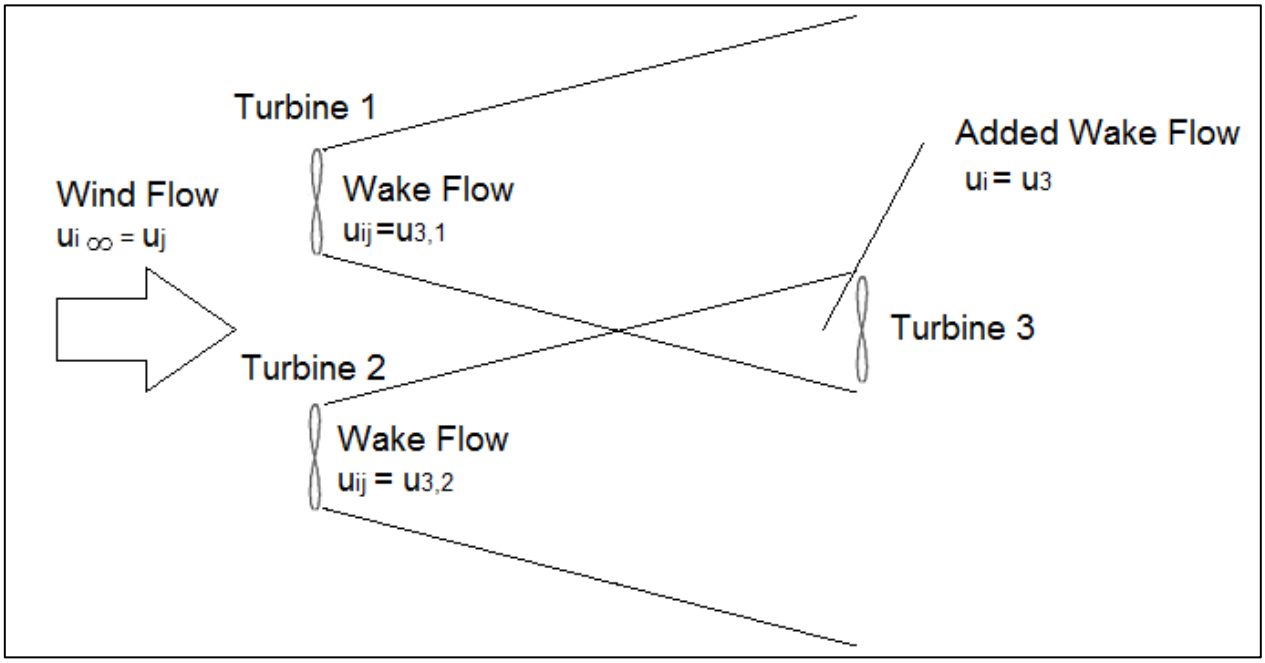

Figure 3-17: Schematic of the sum of squares method

An important fact for multiple wake cases is that after a few turbines equilibrium is achieved. Momentum extraction and recovery are of the same strength between two turbines (figure 3-18). [23]

This is possible because the turbines increase the TI and this leads to a higher recovering rate. [23]

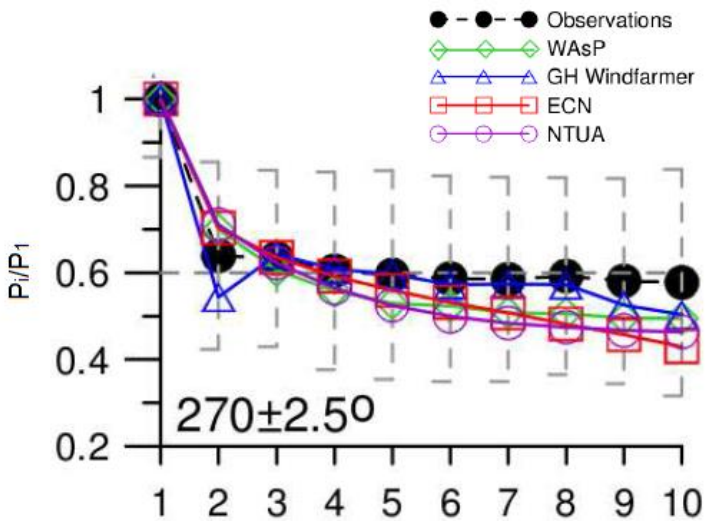

Figure 3-18: Normalised power as a function of turbine number at the Horn Rev wind farm at 8 m/s, comparison of different models and observations [25]

3.5 Meandering of the Wake

Until now it was assumed that the wake spreads continuously in the same direction as the inflow. This assumption is not always correct. Two phenomena that force the flow to change its direction will be described in this and the next chapter.

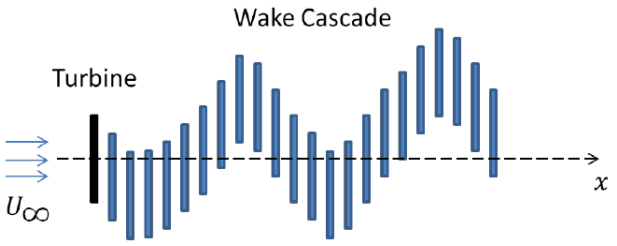

Figure 3-19: Schematic sketch of the complete meandering wake cascade from top view [26]

The term meandering describes the large-scale movement of the complete wake. It is a highly unsteady phenomenon. This is important because through this movement turbines downstream could get influenced by the wake which would otherwise be wake-free or vice versa. The meandering also reduces the velocity deficit of the flow. Furthermore, the wake meandering is present in the vertical direction. Nevertheless, it is small compared to the lateral one. [1]

The meandering accrue due to large eddies compared to the wake in the atmosphere. These eddies are more present when the atmosphere is more unstable which result in a stronger meandering effect. There are strong indicators that the meandering is caused by instability of the wake. Additionally, the meandering is also stronger when the inflow was yawned. Yaw means that the wind direction is not perpendicular to the rotor plane. The meandering effect is additionally dependent on C_T, λ, the number of blades and the pitch angle. Nevertheless, at some C_T-λ-regions, no meandering occurs. [1], [24]

The later introduced wake models neglect the meandering which means that they have all an error. However, if for example the dynamic wake meandering model is used the meandering could be taken into account. [25]

3.6 Effect of Yaw

Due to the fact that the wind direction changes with the time, it can happen that the turbine is facing the flow under a yaw angle (γ).

The angle between the wake and rotor axis (χ) is larger than the yaw angle (figure 3-20). [1]

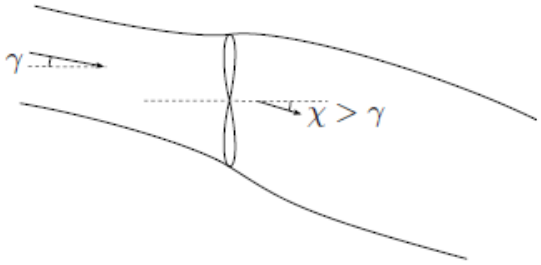

Figure 3-20: Yawed inflow with wake [1]

The influence of the yaw angle on the direction of the wake makes it possible to route the path of the wake. The bigger the yaw angle the less is the production of the turbine. However, if the downwind turbine is not or less infected by the wake the overall production could be higher. This topic is researched but not applied in practice yet. For this sort of optimization is a good prediction of wakes necessary. [26]

3.7 Effect of very large wind farms

Above a certain dimension wind farms start to influence the surrounding upper air (geostrophic wind) which has to be considered for AEP calculations. The wake models in WindPRO (like the Jensen Model) were validated for wind farms up to 75 wind turbines. If a wind farm is larger the calculation has to be adapted, WindPRO recommends increasing the roughness inside the wind farm area to imitate the effect of the large wind farm. [22]

In figure 3-21 the effect of a large wind farm on the ABL is shown. The wind speeds decreases and the TI increases even in the region above the turbines. This means that also the before assumed undisturbed flow is disturbed. [27]

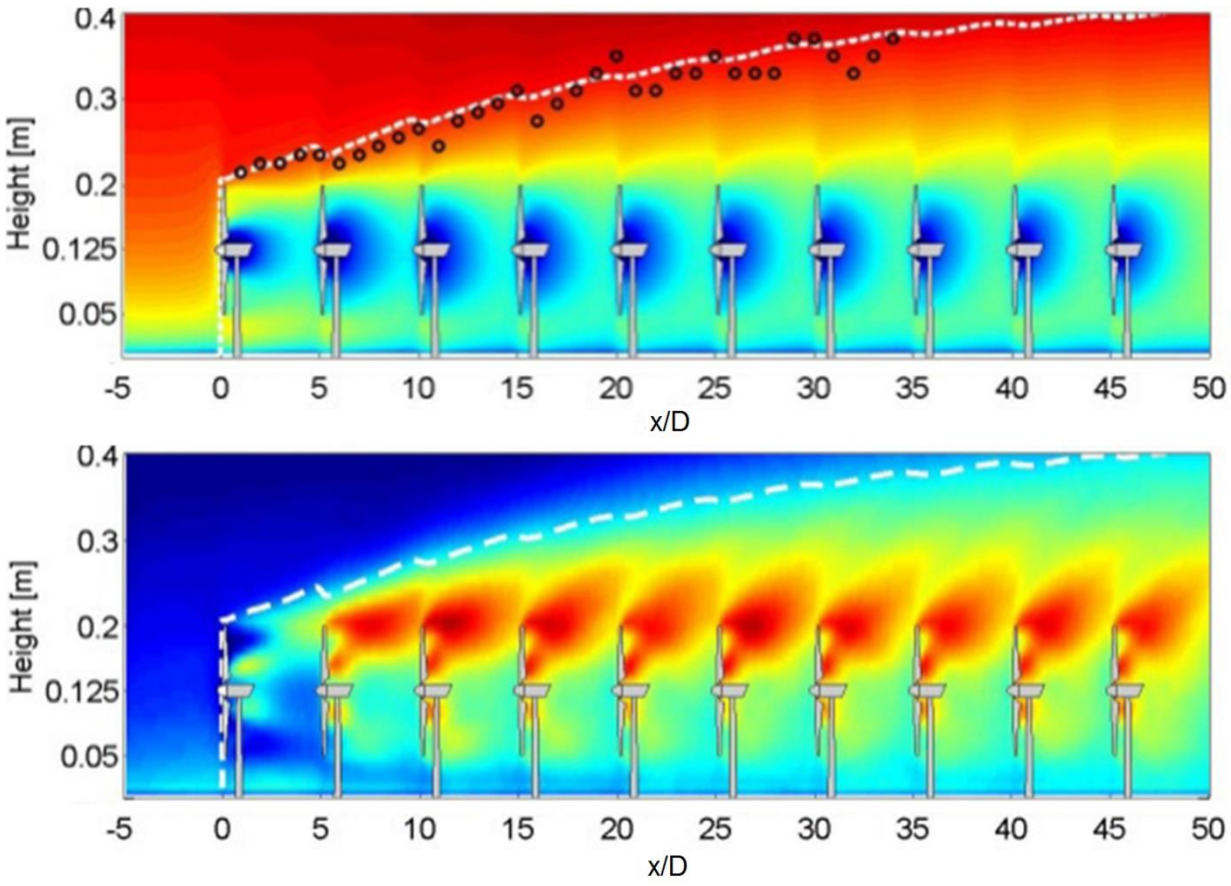

Figure 3-21: Contours of the normalized time-averaged streamwise velocity (top) and turbulence intensity (bottom) in the vertical plane at zero span (y=0) (Circles denote the edge of the measured farm wake. White dashed lines denote the edge of the simulated farm wake [27]

4 Wake Modelling

The last section described the wake phenomenon in detail. This chapter describes how the wake can be modelled. The beginning of this section is about the representation of the rotor. After that, a short explanation of the modelling of the ambient flow will be given. This is the basis for all energy estimations. In the end wake and turbulence models are introduced.

4.1 Additional Methods of Representing the Rotor

The ADM was explained in chapter 1.3.1 which is the simplest form of representing the rotor. Now some of the more advanced techniques will be presented. The representation of the rotor is essential for the estimation of the near wake. Some of the phenomena only get captured with a high resolution of the rotor. This can be seen in figure 4-1. The ADM without rotation and uniform momentum sink has the worst fit with the measurements close to the turbine (2-3 D). However, in very far wake (5 D) the difference is acceptable. The ADM with rotation uses a non-uniform momentum sink and delivers very good results. [28]

The blade element momentum (BEM) method is shortly introduced to give a better understanding of how a non-uniform momentum sink can be calculated. Further additional methods of rotor representation are the actuator line method and the full representation of the blade geometry. Both will not be explained because neither Jensen nor WakeBlaster use them.

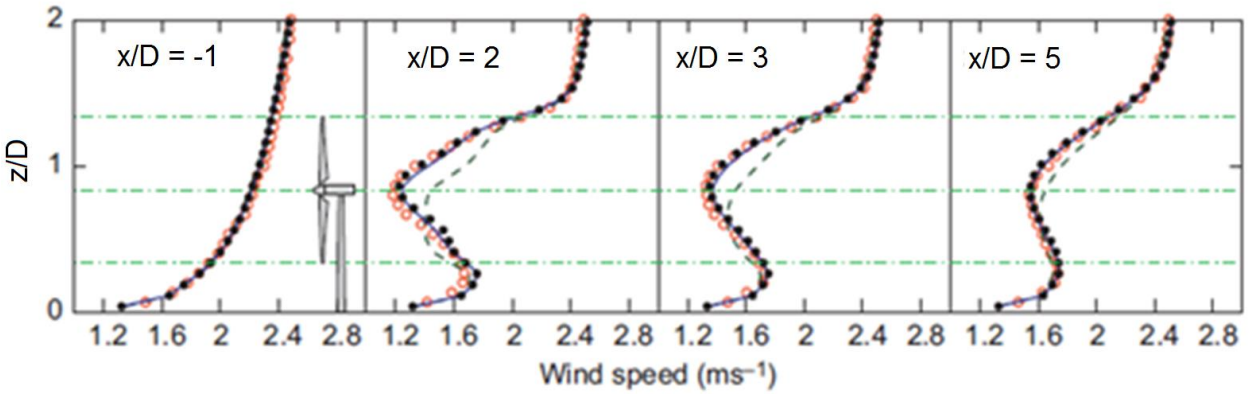

Figure 4-1: Comparison of vertical profiles of the time-averaged streamwise velocity (wind tunnel measurements - black dots, ADM-non-rotating - dashed line, ADM-rotating -solid line and actuator line method -dotted line) [28]

A very high resolution of the rotor is only needed to describe near wake phenomena in an accurate way. This is not the thesis' scope. More interesting is the development of the velocity in the far wake. Porté-Angel and Wu concluded that the resolution dependence of the mean velocity results is small if the rotor is represented with a minimum of seven points in vertical and five points in spanwise direction. [12]

The basis for the BEM is an actuator disc but this time the momentum sink is non-uniform distributed. The actuator disc is divided into infinitesimal small annular rings (figure 4-2). This makes it possible to take the aerodynamic changes from the root to the tip into account. This leads to a more realistic result. The fact that the rings are infinitesimal small allows that all variables are assumed constant for the single rings. The result for the complete disc is calculated by summing up all single annular rings. [1]

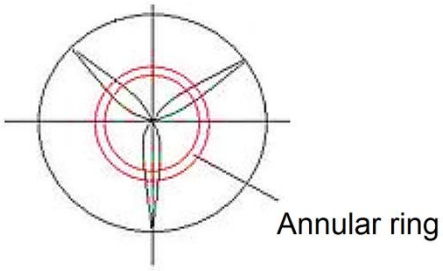

Figure 4-2: Schematic of the BEM method [29]

The main assumptions and simplifications are listed below:

- The annular rings are independent of each other. [1]
- The flow is non-turbulent and steady. [1]
- Yaw is not taken into account. [1]
- Tip losses are neglected. [1]
- Wake expansion is neglected. [1]

Additionally, the angular momentum can be taken into account. The influence of the momentum was already introduced in chapter 1.4.1. The rotor is spinning so the flow needs to rotate in the opposite direction because of the law of conservation. The introduced model is the steady variant of the BEM which is sufficient to estimate the production of a wind turbine. Although for a more accurate loads calculation the unsteady model should be used. [1]

The introduced content explains only the functional principle of the BEM. Formulas are for clarity reasons not displayed. For a deeper understanding the following sources can be used. [1], [29]

For a more realistic and accurate result are many improvements available and some of them are listed below.

- The BEM assumes a uniform force on the annular rings. This is only right if the number of blades is infinite. This is usually not the case and tip losses have to be taken into account. This is possible with Prandtl's tip loss factor. [1]
- The annular rings are assumed as independent which leads to huge errors when there is yaw misalignment. Even for this problem, some improvements were done and the results are now acceptable in comparison with measurements. [1]
- The model is only valid for non-turbulent flows. When the induction factor becomes larger than 0.4 the velocity in the wake is almost zero. The difference between the velocity in the wake and of the undisturbed flow is then so big that the shear layer becomes turbulent. For this case, Glauert developed also an empirical correction factor for the thrust coefficient. [1]

- The flow is assumed to be steady. Nevertheless, due to the dynamic nature of the wind, it is not. The most modern codes take this fact into account. [1]

Nonetheless, even with all these corrections, it will be difficult to derive results that take all influences like atmospheric stability, wind shear and neighbouring turbines into account.

4.2 Flow modelling

The modelling of the ambient flow is one of the most important aspects of the wind resource assessment. In most cases, the flow is only known at different heights of a met mast. So the flow has to be extrapolated to the turbine positions and hub heights. For this step different models are available. They will not be described in detail but the principles will be explained.

4.2.1 Wind Atlas Analysis and Application Program

The Wind Atlas Analysis and Application Program (WAsP) is a software for the extrapolation of wind climate statistics. Several models are included to describe the flow over different surfaces. To extrapolate the flow WAsP needs additional to the wind data as input an orography and topography map and information about obstacles close to the site. [30]

The models that describe the wind flow are analytical and empirical formulations like the ones that were introduced in chapter 1.1. A detailed description of the models is documented in [31]. Due to the fact that the models depend on analytical and empirical formulations, the extrapolation of the wind flow is fast and accurate as long as the terrain is simple and no flow separation occurs. [30]

4.2.2 Computational Fluid Dynamic Models

The Navier-Stokes equations are the basis for all CFD models. They include the continuity equations for mass, momentum and energy. For laminar flows, these equations can be solved. However, the computational costs are too high to solve turbulent flows. The costs are so extraordinary because the spatial resolution has to be higher than the smallest turbulent eddies and the temporal resolution has to be smaller than the smallest fluctuations. In the wind industry, all flows are more or less turbulent so the Navier-Stokes equations cannot be used. To understand this better the characteristics of turbulence are explained followed by a way to model them. [32]

4.2.2.1 Turbulence

The different aspects of the turbulence are introduced to understand how it is influencing the flow and how it can be modelled. It is difficult to define what turbulence exactly is. However, it is possible to define some of its characteristics.

- **Irregularity:** Flows with turbulent characteristics are irregular, chaotic and random. Additionally, they exist in a wide range of length-, velocity- and timescales. The large-scale motions are often described as large eddies. A certain region can be occupied by different scales of eddies. This means that smaller eddies can exist inside larger ones. The size of the smallest eddies is bordered by the viscosity and the size of the largest ones by the geometry (in our case the atmosphere). When eddies move they rotate, stretch and break up into smaller ones. The range of the different scales and the irregularity makes it difficult to simulate turbulence with a deterministic approach. Large and small eddies induce different types of velocity fluctuations. Large eddies induce fluctuation of low frequency and large amplitude. Small eddies induce fluctuations of high frequency and small amplitude. [33]
- **Diffusivity:** This characteristic was already mentioned in combination with turbulence intensity. Due to the chaotic motion in turbulent flows momentum, energy and species are transported and result in higher mixing rates than due to only molecular diffusion. The turbulent diffusion is several orders higher than the molecular one. Due to the fact that turbulence is a 3D phenomenon the mixing occurs in all dimensions. This means that there is an exchange between the streamlines when the flow is turbulent. [33]
- **Instability:** Turbulence is created due to instabilities at high Reynolds numbers. It happens when the timescale for convective transport is much smaller than for the viscous damping of a velocity fluctuation. The instability increases with a higher Reynolds number. Turbulence is a stochastic phenomenon even when the Navier-Stokes equations are deterministic. [33]
- **Three dimensional:** Turbulent structures are always three dimensional. This comes from the mechanisms like vortex stretching and vortex tilting which take place in all three dimensions. Although turbulence can be modelled in a statistical way as two dimensional. [33]

- **Dissipative:** The turbulent kinetic energy flows from the large eddies to the small ones by inviscid processes. At the smallest eddies, the kinetic energy is dissipated into heat through viscous stresses. This principle is called energy cascade. The kinetic energy enters the largest eddies by extraction of the mean flow. The energy is then transported to the smaller scales through the breaking up of large eddies. This means that turbulence fade away when no energy is added. The energy input equals the losses through the dissipation. [33]

Additional to these characteristics Kolmogorov assumed three hypotheses which are of great importance for turbulence modelling. The used nomenclature is only valid for this chapter.

- Small-scale turbulence is statistically isotropic. The reason for this is that in the downscaling process the information of direction is lost for high Reynolds numbers. It is assumed that the small scales are independent of the large scales and the mean flow (valid for $l << l_0$, figure 4-3). [33]
- For isotropic small-scale turbulence, the statistics of the motions have a universal form which is determined by the viscosity and dissipation rate (valid for $l < l_{EI}$, figure 4-3).
- For a certain range of structures, the influence of the viscosity is negligible. This means the statistic of the motions are for this range only determined by the energy dissipation rate (inertial range in figure 4-3). [33]

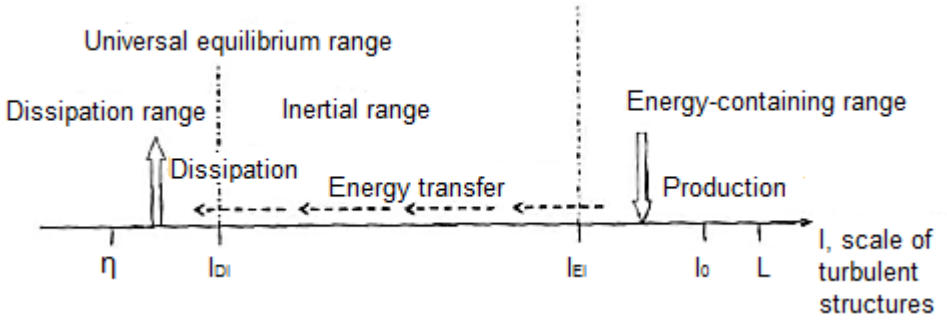

Figure 4-3: The cascade of turbulence energy on a logarithmic scale [33]

As mentioned before it is not possible for engineering applications to simulate all these effects. How the influence can be modelled instead is described in the next chapter.

4.2.3 Reynolds-Averaged Navier-Stokes Equations

The Reynolds-averaged Navier-Stokes (RANS) equations are a method to model a turbulent flow and are based on the Navier-Stokes equations. The idea is to reduce the necessary spatial and temporal resolution through averaging although without losing the influence of the turbulence on the mean flow. As a first step, the flow parameters (velocity, pressure, density and temperature) are split into time-dependent mean values and stochastic deviations (4-1). The deviations represent the turbulent fluctuations. The definition of the time-dependent mean value is shown by an example in equation (4-2). For a clearer understanding of the equations below the progress of this variable is also shown as a diagram in figure 4-4. [33], [32]

$$u = \overline{u} + u' \tag{4-1}$$

$$\overline{u} = \frac{1}{\Delta t} \int_{t_0}^{t_0+\Delta t} u dt \tag{4-2}$$

With:

$$\frac{1}{\Delta t} \int_{t_0}^{t_0+\Delta t} u' dt = 0 \tag{4-3}$$

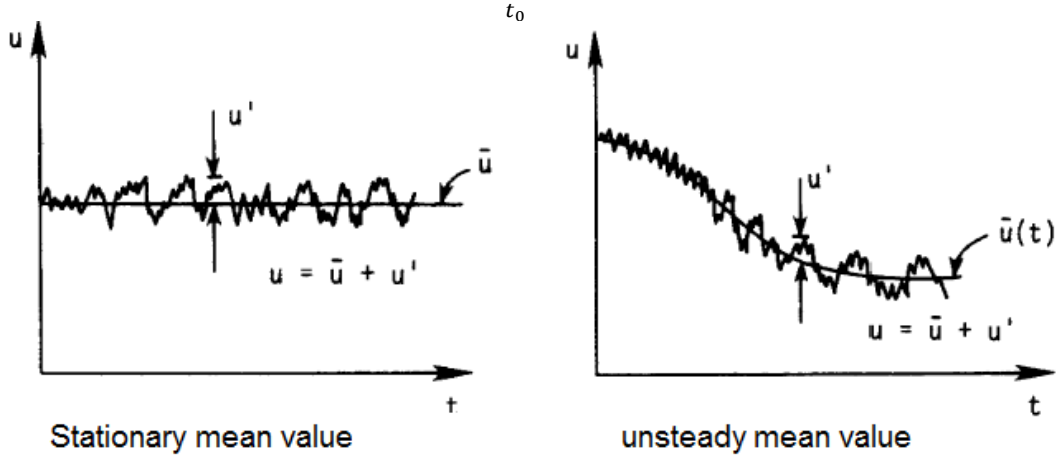

Figure 4-4: Time-dependent mean values and stochastic deviations [32]

The time step for the averaging has to be of an adequate size. If it is too big the unsteady phenomena would be sorted out through the averaging and if it is too small the calculated mean value would not be the real one. Through this averaging, an additional unknown is added to the conservation of momentum equation. It is known as Reynolds stress. To calculate them additional equations are needed, this is called closure problem. To solve this problem turbulence models are used and will be introduced later. [33]

For the use case of wake modelling, it is mostly assumed that the flow is incompressible even if it is not. In the region between the wake and the undisturbed flow is an area where the flow is compressed. Nevertheless, this will be neglected which means that the incompressible variant of the RANS equations can be used.

The derivation of the RANS equations will not be presented although the resulting formula for incompressible fluids is shown below and an interpretation will be given. The term for the body forces is omitted. The following equations are written in tensor notation to make the formulas simpler and clearer. This means that the term u_i represents the velocity in all three directions of the Cartesian coordinate system (x, y, and z). [33]

$$\rho\left(\frac{\partial\overline{u_i}}{\partial t}+\frac{\partial\overline{u_i}*\overline{u_j}}{\partial x_j}\right)=-\frac{\partial\overline{p}}{\partial x_i}+\frac{\partial}{\partial x_j}\left(\mu\frac{\partial\overline{u_i}}{\partial x_j}-\rho\overline{u'_i*u'_j}\right) \tag{4-4}$$

The equation is nearly the same as the Navier-Stokes one. The only differences are that all terms are now averaged and the additional term $\rho\overline{u'_i*u'_j}$ appears, which is the above mentioned Reynolds stress. The question is now why they appear trough the averaging.

When equation (4-1) is inserted into the Navier-Stokes equation and then the equation is integrated over a time interval and all single fluctuating terms are zero because of (4-4). This is the reason why nearly all of the fluctuating parts are removed. The only exception is the fluctuating term of momentum flux because it appears in a quadratic form which means they are not per definition zero. This is the mathematical reason why the Reynolds stress term appears and now the physical explanation. [33]

The Reynolds stress represents the momentum fluxes which are induced by the turbulent motions. These fluxes are responsible for the majority mixing in the flow. This term is called stress because it is similar to the viscous stress. It is typical that the turbulent stresses are magnitudes higher than the viscous ones. [33]

Other methods to model the turbulence are for example large or detached eddy simulations. These two are not used in this thesis and will not be introduced.

4.3 Wake Models

In the next chapters, three wake models will be explained. Firstly, the Jensen Model than the Ainslie Model and thirdly WakeBlaster will be presented. Jensen and WakeBlaster will be later used for the simulation. Ainslie is introduced because of its similarity to WakeBlaster which procedure is not published in detail. The models differ strongly in fidelity and computational costs. Figure 4-5 shows a schematic of the development of these two factors.

All introduced wake models need as input information about the turbines like rotor diameter, C_{T}-curve, etc. Moreover, the ambient flow field is needed as input. This is caused by the simplification that the ambient flow and the wake are calculated independently from each other. This simplification makes it possible that all the introduced models are very fast.

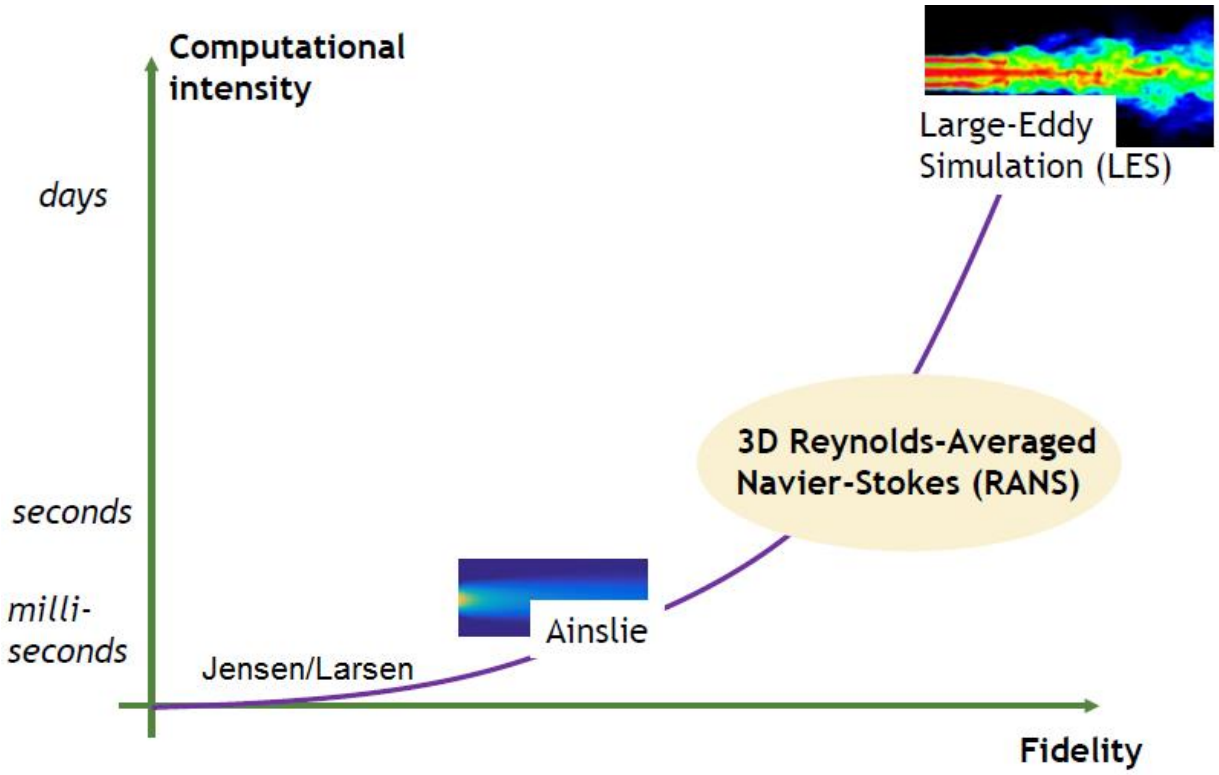

Figure 4-5: Comparison of the different wake models regarding fidelity and computational intensity [34]

4.3.1 Jensen Model

This model is one of the oldest wake models and it is still the popular workhorse of the wind industry. The model assumes a uniform hat-shaped velocity profile and a linear expansion of the wake. A schematic of the model is shown in figure 4-6. The presented variant is the one that is used in WindPRO. The Jensen Model is an analytical wake model and uses simple analytical expressions to describe the wake and needs very low computational resources. [22]

The diameter of the wake can be calculated with formula (4-5). [22]

$$D_w = D + 2 * \kappa * x \tag{4-5}$$

The wind speed of the fully developed wake (far wake) can be derived by formula (4-6). [22]

$$u_w = u_\infty \left[\frac{1 - \sqrt{1 - C_T}}{(1 + 2 * \kappa * x/D)^2} \right] \tag{4-6}$$

κ is the wake decay constant (WDC), it depends on the TI. The recommended standard values for the WDC are 0.075 for onshore and 0.04 for offshore wind farms but can be adjusted to the site conditions. [22]

The velocity development calculated with the Jensen Model is shown in figure 4-7. The diagrammed flow does not look like the real flow field. Nevertheless, though the fact that for power calculation an averaged velocity is used the Jensen Model provide acceptable results.

The Jensen Model will be the competitor of WakeBlaster in the later following comparison of the results. SGRE has wide experience with the Jensen Model because it is used for all energy calculations for sites with simple terrain, which makes it to a good benchmark.

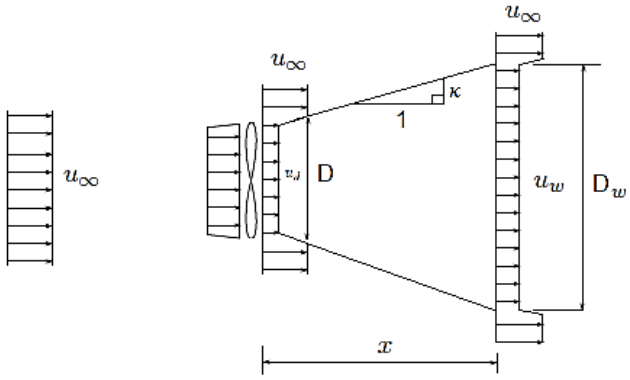

Figure 4-6: Schematic of the Jensen Model [36]

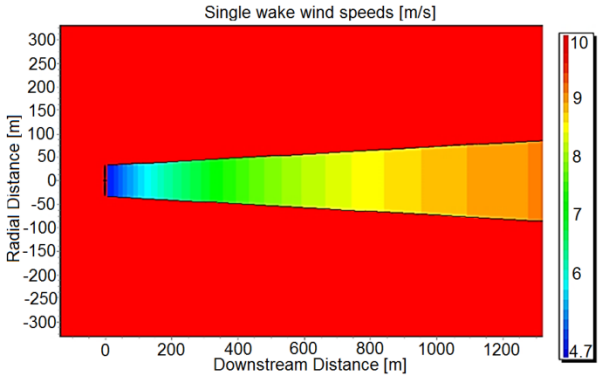

Figure 4-7: Velocity development in the wake of a single turbine with the Jensen Model [22]

4.3.2 Ainslie Model

The Ainslie or eddy viscosity model is a numerical model and is based on the RANS equations. The flow is assumed axisymmetric, stationary, fully turbulent, and incompressible with zero circumferential velocity. Through the axisymmetric assumption, the flow can be described as two-dimensional and in cylindrical coordinates. External forces, viscous terms and pressure gradients are neglected. A schematic of the model is shown in figure 4-8. Also, the Reynolds stress needs to be solved for the Ainslie model. This is done with a turbulence model, which is very similar to the one from WakeBlaster. [22]

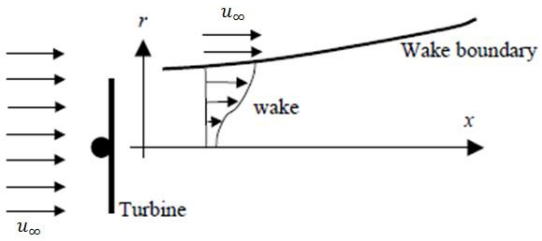

Figure 4-8: Schematic of the Ainslie wake model [22]

All formulas were taken out of the WindPRO implementation of the Ainslie model which is experimental. [22]

$$\overline{u}\frac{\partial\overline{u}}{\partial x}+\overline{v}\frac{\partial\overline{u}}{\partial r}=-\frac{1}{r}\frac{\partial\left(r\overline{u'v'}\right)}{\partial r} \tag{4-7}$$

The model is combined with the continuity equation shown below. [22]

$$\frac{1}{r}\frac{\partial(r\overline{v})}{\partial r}+\frac{\partial\overline{u}}{\partial x}=0 \tag{4-8}$$

The Reynolds stress is modelled with the eddy viscosity μ_t: [22]

$$-\overline{u'v'}=\mu_t(x)\frac{\partial\overline{u}}{\partial r} \tag{4-9}$$

The eddy viscosity is split into an ambient and a wake part. The last one is generated through the shear in the wake. [35]

$$\mu_t(x)=\mu_{amb}+\mu_w(x) \tag{4-10}$$

The ambient part depends on the ambient TI which includes the influence of the atmospheric stability and can be calculated with the formula below. k is a constant. [22]

$$\mu_{amb}=\frac{k*TI_{amb}*u_\infty*z}{2.4} \tag{4-11}$$

Ainslie [36] suggested that the wake part of the eddy viscosity is described with a length (ΔL) and velocity scale (Δu). These two are proportional to the width of the wake and velocity deficit. [22]

$$\mu_w(x)=\Delta L(x)*\Delta u(x) \tag{4-12}$$

$$\mu_w(x)=K*b\left(u_\infty-u_c(x)\right) \tag{4-13}$$

b is the width of the wake and can be calculated with (4-14). K is a constant with the value 0.015 and $(u_\infty - u_c(x))$ is the velocity deficit at the centreline of the wake.

$$b = \sqrt{\frac{3.56 * C_T}{4(u_\infty * u_c)[2 - (u_\infty - u_c)]}} \tag{4-14}$$

The eddy viscosity depends only on the distance of the rotor and not on the radial distance. Additionally, the calculation of the eddy viscosity is independent of the shear exponent. Nevertheless, the physical phenomenon depends on the shear. This simplification leads to a fast model because the shear depends on the ambient and wake flow. Otherwise a separate calculation of ambient wind field and wake flow would not be possible. [22]

The Ainslie model assumes that the pressure is constant in the wake. This is wrong in the near wake (compare chapter 1.3.1). The solution for this discrepancy is that the near wake is not modelled and the flow is initialized two diameters behind the turbine with the following equations. [22]

The velocity profile is assumed Gaussian and described with:

$$1 - \frac{u}{u_\infty} = (u_\infty - u_c) exp\left[-3.56\left(\frac{r}{b}\right)^2\right] \tag{4-15}$$

The velocity deficit for the initialisation at the centreline is defined as:

$$(u_\infty - u_c) = C_T - 0.05 - (16 * C_T - 0.5)\frac{TI_{amb}}{10} \tag{4-16}$$

An example of the velocity development is diagrammed in figure 4-9. In the near wake are the velocities constant.

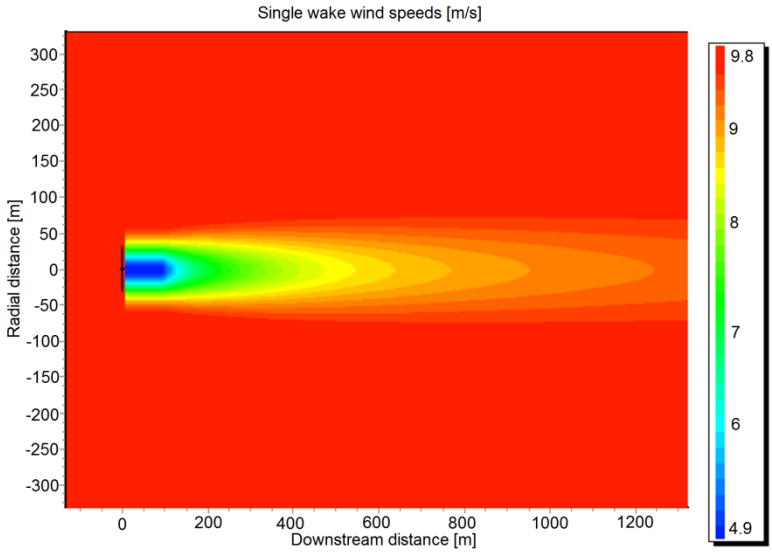

Figure 4-9: Ainslie wake model [22]

Other sources suggest a modifiable near wake length. Vermeulen recommends a near wake length that depends on ambient TI, rotor-generated TI and shear generated TI [37]. This is out of the thesis' scope and will not be introduced.

4.3.3 WakeBlaster

WakeBlaster is the last wake model that will be introduced and the most complex one. Furthermore, it is the newest model. The developer ProPlanEn does not want to share the complete calculation process. Thus, not all equations can be shown and mostly only assumptions and principles can be explained.

WakeBlaster uses a RANS equations solver for mass and momentum in 3D with some simplifying assumptions and is neglecting the energy equation. A key advantage is that the 3D RANS equations should be better suited for multiple wake scenarios. In general is WakeBlaster similar to the Ainslie model. [38]

The assumptions for the RANS equations solver are:

- The flow is stationary. [38]
- Thin shear layer approximation. [38]
- Pressure terms are neglected. [38]
- Flow is incompressible. [38]
- Reynolds stress is solved with eddy viscosity closure. [38]

Like Ainslie WakeBlaster uses the eddy viscosity to solve the Reynolds stresses (4-17). The eddy viscosity is the key term for the mixing of the wind flow and influenced by the TI. [38]

$$u\frac{\partial u}{\partial x} + v\frac{\partial u}{\partial y} + w\frac{\partial u}{\partial z} + \frac{\partial \overline{u'v'}}{\partial y} + \frac{\partial \overline{u'w'}}{\partial z} = 0 \tag{4-17}$$

$$u\frac{\partial u}{\partial x} + v\frac{\partial u}{\partial y} + w\frac{\partial u}{\partial z} - \mu_t\frac{\partial^2 u}{\partial y^2} - \mu_t\frac{\partial^2 u}{\partial z^2} = 0 \tag{4-18}$$

A point that reduces the complexity and increases the speed of the calculation is that ambient wind field and the wake effect are calculated independently from each other. The ambient wind speed is in WakeBlaster calculated via a combination of an input values (e.g. wind speed, direction and TI) and a wind resource file (rsf). These rsf files contain information about the ambient mean wind speed at a certain height over a certain area. With these files, it is possible to calculate a speed-up effect from point to reference point, like from a met mast with input values to a wind turbine. These files can be calculated with several wind flow models like WAsP. The only disadvantage is that with these file the speed-up effect is treated wind speed

independent. The ambient TI is treated in the same way. The principle is shown in equation (4-19). Δu_∞ represents the speed-up effect. [39]

$$TI_{amb} = \frac{\sigma}{u_\infty * \Delta u_\infty} \tag{4-19}$$

The near wake (two rotor diameters) is not calculated like in the Ainslie model because of the negligence of the pressure terms which is not correct for the near wake. [39]

The rotor of the turbines is represented with an advanced actuator disc model. “Advanced” means that the extraction of momentum is non-uniform. WakeBlaster resolves the rotor area with 100 points for the non-uniform extraction. This resolution is higher than the in chapter 4.1 mentioned minimum resolution to avoid resolution dependence for the mean wind speed. The used representation of the rotor is similar to the introduced BEM method. The sink of the momentum is induced axisymmetric. However, through the 3D shape of the RANS equations and the different shears the symmetry is dissolved downstream of the turbine. [34]

The grid of the model depends on the layout of the wind farm. The model is always rectangular and three rotor diameter high. Additional to the dimension of the wind farm the model includes a three rotor diameter buffer zone. The standard spatial resolution of the grid is 0.1 rotor diameters and can be changed. The grid is fixed to the ground which is defined by the elevation of the turbines. [39]

The flow is only calculated downwind via a flow plane. This means the turbines only influence the wind behind them and blockage effects are neglected. This type of calculation makes an iterative calculation scheme unnecessary. The direction of propagation of the plane is always the same as the ambient wind direction. How the calculation looks like is shown in figure 4-10. The boundary conditions are Dirichlet so the values at the borders of the plane are fixed. [38]

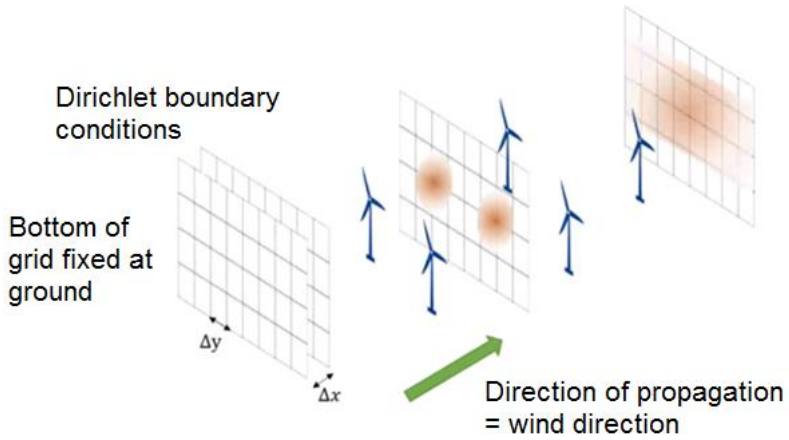

Figure 4-10: Calculation scheme of WakeBlaster [38]

Additional to the calculation of wakes, WakeBlaster is capable of power curve (PC) adjustments. The PC can be corrected to TI or air density. Also, yaw misalignment can be taken into account. Another advantage is that it is possible to calculate with WakeBlaster time dependent in contrast to the other wake models which only use statistical mean values. [34]

The outputs for every turbine are TI, rotor equivalent wind speed, turbine power, unwaked power, wake speed factor and air density. Unwaked power is the power the turbine would produce if there are no wakes. The wake speed factor is the waked rotor wind speed divided by the wake-free rotor wind speed. Figure 4-11 shows the velocity development calculated with WakeBlaster. Also, the flow plane can be seen. [40]

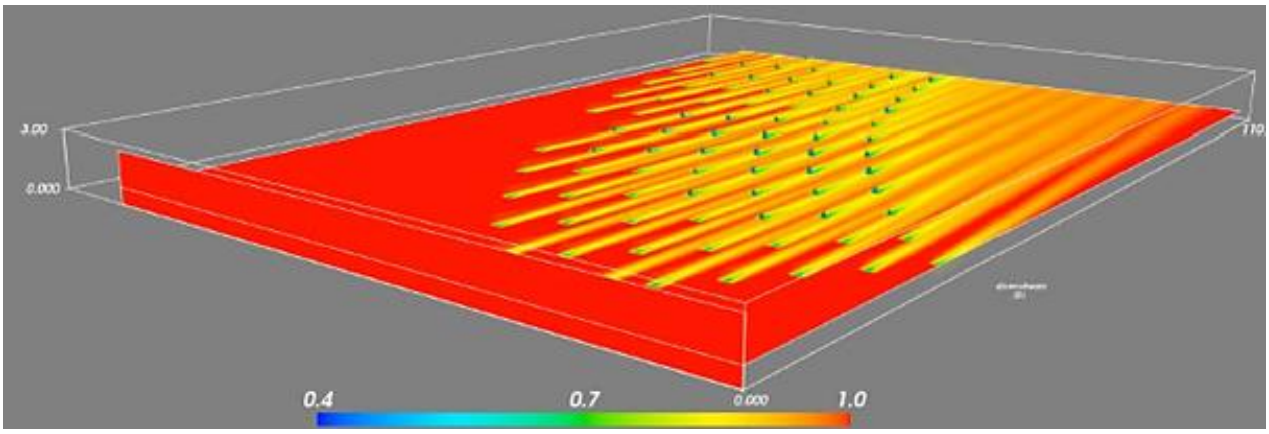

Figure 4-11: Normalized velocity development calculated with WakeBlaster for a wind farm [34]

4.4 Turbulence Models

There are two types of turbulence models which are relevant for the wake calculation. One type is used to calculate the Reynolds stress and the other one is used to calculate additional TI. Both types of turbulence models rely on empirical assumptions which mean that their results do not have the same quality for different use cases. To underline this are in the end several common turbulence models compared.

An important point is that all these models do not simulate the turbulence they calculate the TI or model just the influence on the flow.

The models for the additional TI will not be explained because the thesis' scope is a comparison between WakeBlaster and Jensen and not WakeBlaster and different TI models. If there is interest in these models they are documented in [22]. The TI model of WakeBlaster is introduced because it is necessary so solve the RANS equations and Reynolds stress.

Before the turbulence model for WakeBlaster is introduced the Boussinesq hypothesis is explained, which is the basis for most of the common turbulence models.

4.4.1 Boussinesq Hypothesis

The Boussinesq hypothesis assumes that the turbulence is isotropic and the Reynolds stress is proportional to the mean velocity gradients. The assumption that the turbulence is isotropic reduces the unknowns of the Reynolds stress tensor from six to one because they are now all of the same magnitude. Assuming that the Reynolds stress is proportional to the mean velocity gradients like the viscous stresses leads to the eddy viscosity approach. This results in the following equation where δ_{ij} is the Kronecker delta. [32], [33]

$$-\rho * \overline{u'_i * u'_j} = \mu_t \left(\frac{\partial \overline{u_i}}{x_j} + \frac{\partial \overline{u_j}}{x_i} \right) - \frac{2}{3} \delta_{ij} * \rho * \frac{\overline{u_i' * u_i'}}{2} \tag{4-20}$$

$$\delta_{ij} = \begin{matrix} 1 \; if \; i = j \\ 0 \; if \; i \neq j \end{matrix} \tag{4-21}$$

The eddy viscosity μ_t can vary by time and place and is higher when the turbulence is higher. The turbulent fluid can now be interpreted as pseudo-laminar fluid with an increased viscosity which leads to a higher diffusion of the flow properties. Other characteristics of the turbulence are lost. Nevertheless, the mixing of the flow or recovering of the wind speed in a wake can be modelled with this approach. [33]

The mentioned assumptions are not valid for all use cases because the Reynolds stress does not have to be proportional to the velocity gradients. For simple flows with straight boundary layers or wakes they are valid. However, for flows with strong curvatures or fast velocity changes they are not. [33]

How the eddy viscosity is calculated depends on the turbulence model. The WakeBlaster model will be explained in the next chapter.

4.4.2 WakeBlaster Turbulence Model

The WakeBlaster turbulence model solves the eddy viscosity on basis of a simple equation which is similar to the approach from the Ainslie Model. The velocity and length scale are already known from the Ainslie Model. f is a calibration factor and the default value is around 0.08. The turbulence model is assuming a logarithmic profile for the ambient wind speed. This is reasonable for simple terrain but in complex area this can lead to problems (figure 4-12).

$$\mu_t = f * \Delta u * \Delta L \tag{4-22}$$

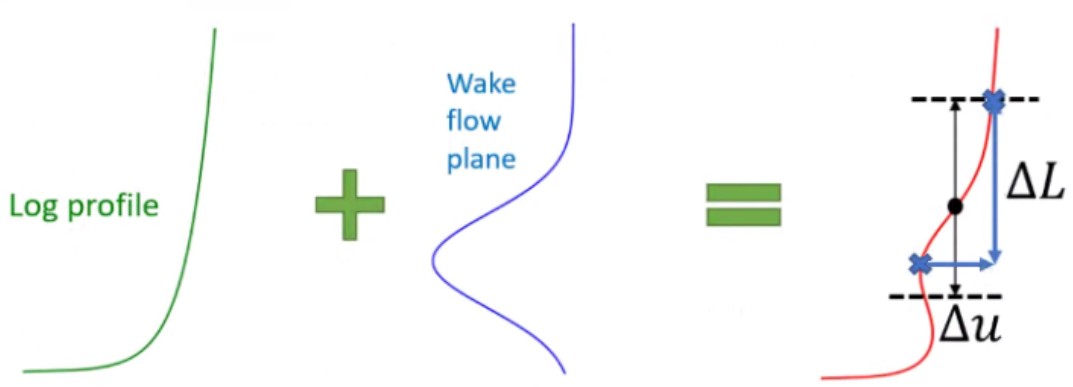

Figure 4-12: Schematic of WakeBlaster's turbulence model [38]

A more detailed explanation is not possible because ProPlanEn didn't publish more content although it is planned to do this at the WindEurope Conference in September 2018. Nonetheless, this is too late to implement it in this thesis.

To give the reader an impression which common and already published turbulence models can be used in the wind industry a comparison is shown now. For the comparison of the models, the results from a study of Stergiannis [41] are used (figure 4-13). The study simulated wakes with 3D RANS equations with different turbulence models and with different models for the rotor (ADM and full representation of the rotor). It seems that wake predictions with RANS equations are very sensitive to the turbulence model especially if an ADM is used. The following turbulence models were used in the study:

- Standard k-ε
- Realizable k-ε
- RNG k-ε
- Wilcox k-ω
- Menter k-ω SST

For the simulation with the ADM, all turbulence models underestimate the velocity deficit except the RNG k-ε one which shows good accordance with the measurements in the far wake. The simulations with the full rotor representation delivered good results for the near wake. Nevertheless, overestimate the velocity deficit in the far wake which is related to the underestimation of TI by the full rotor representation. [41]

The derivation of the different turbulence models and their formulas will not be part of this thesis because the wake models do not use them.

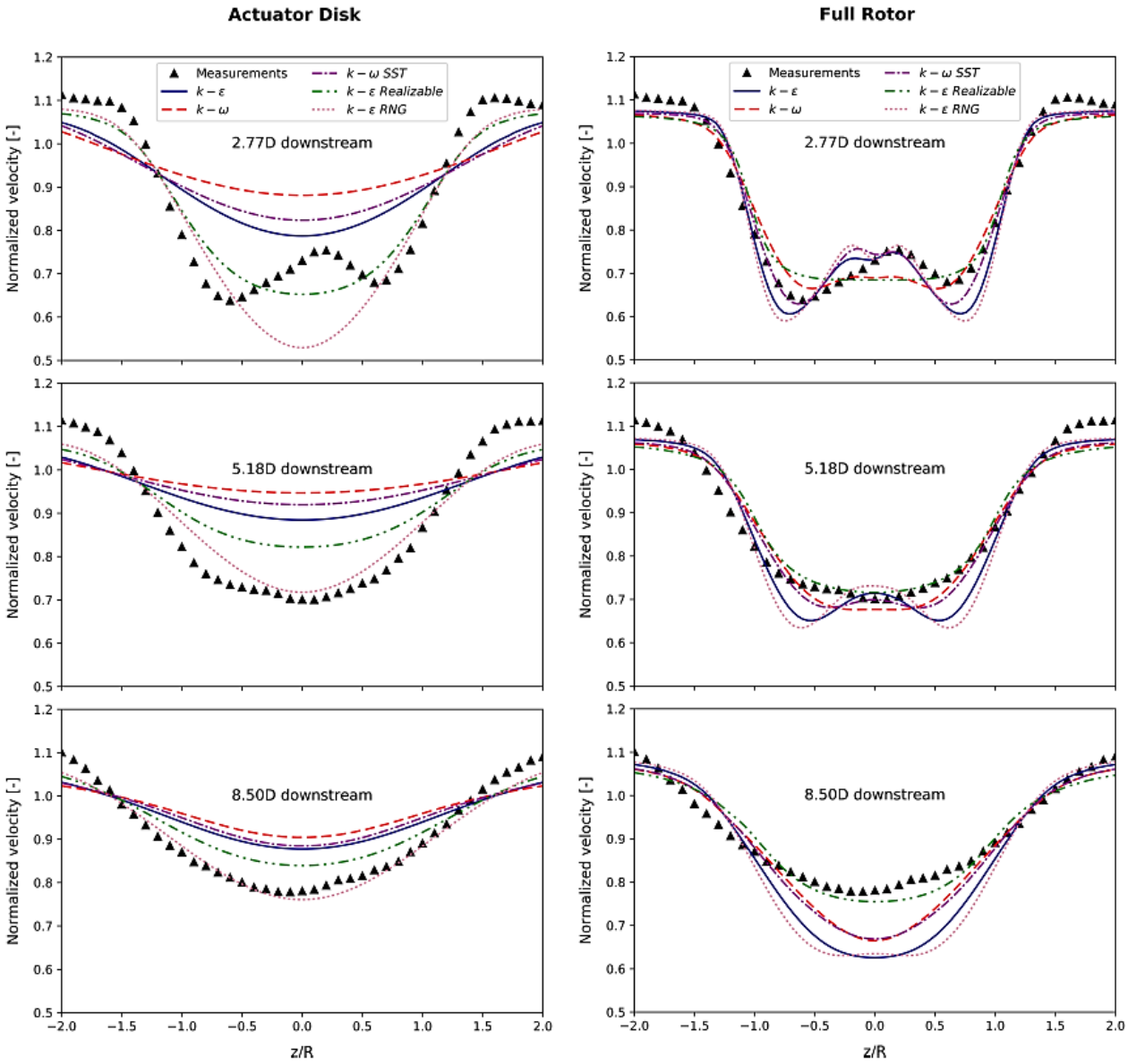

Figure 4-13: Results of ADM (left) and full rotor (right) simulations, comparing several turbulence models against measurements for different downstream distances [41]

5 Simulation of Wakes

This chapter describes all necessary information to set up the wake models correctly. Including for example the site description and used method. Next to that the supervisory control and data acquisition (SCADA) system will be described. This system delivers the data of the wind farms.

5.1 Supervisory Control and Data Acquisition System

The SCADA system delivers on the one hand measured wind data like the wind speed and on the other hand production data of the turbines. The wind data can be measured with a meteorological met mast that is placed nearby the wind farm or with nacelle anemometers. Both methods provide a ten-minute averaged time series.

However, when using nacelle anemometers the measurement errors are higher. Because of these measurement errors, the consistency of the nacelle anemometers needs to be verified with other nearby measurements. [42]

SGRE developed a method that calculates from the different nacelle anemometers an ambient wind speed. The method is confidential and cannot be shared. The same method is also used to remove the influence of the turbines from the met mast measurements.

Nevertheless, the signal that is used for the wind speed is another one. This signal is called in the SCADA data Winavail. The wind speed from this signal is reconstructed based on a single turbine without considering any others in the wind farm. The wind speed is calculated with a power to wind function which uses the PC. Additional inputs for the calculation are different control parameters and the nacelle anemometry. If the turbine is off only the nacelle anemometer is used. This signal includes some uncertainties. These uncertainties will be investigated with a measurement campaign for the Mount Lucas wind farm. [42]

The production data of the turbines is also delivered as a ten-minute averaged time series and contains signals from several sensors. [43]

The SCADA data needs to be filtered before it can be used for this thesis. All periods that contain unavailable or curtailed turbines were disabled because it is much more difficult to set up a model when the operating state of the turbines is variable. These disabled periods were identified by using status indicator fields, pitch angle and speed-torque control characteristics that are also delivered by the SCADA system. The filtering was done by ProPlanEn because of its experience and the lack of resources in SGRE. [42], [44]

5.2 Description of the Sites

Two sites were investigated for this thesis. Mount Lucas in Ireland and Gasiri in South Korea. These two were chosen because the terrain is simple which reduces the uncertainties of the ambient wind flow calculation. Addtionally both have no problems with icing or similar difficulties. Furthermore, the two sites have a completely different spacing which is excellent for the assessment of the wake models. The structure of the description is oriented on the turbine suitability reports SGRE creates for its customers.

5.2.1 Mount Lucas

At the Mount Lucas site, SGRE erected 28 SWT-3.0-101 at 99.5 m hub height with a rated power of 3.0 MW and a rotor diameter of 101 m. Further site information is listed in table 5-1. SCADA data is available from May 2014 to April 2018. [45]

Table 5-1: Site information Mount Lucas

Issue	Information
Site Name	Mount Lucas (Ireland)
Coordinate System and Datum	Irish Grid-IRELAND65
Site Coordinates	250974 E, 255028 N
Nearest City	Daingean, Dublin
Site Elevation (range)	70 m to 80 m AMSL
Target Installed Capacity	84 MW
Turbine Type(s)	SWT-3.0-101
Hub Height(s)	99.5 m
Number of Turbines	28

5.2.1.1 Topography, Orography and Obstacles

The surface roughness is characterized by open farm- and grassland. Nonetheless some forest is close to the site. No site visit was done therefore the height of the trees could only be guessed with Google Earth and Street pictures. The terrain is simple and flat so the ambient wind can be extrapolated with WAsP. No relevant obstacles were identified. [46]

5.2.1.2 Preconstruction Wind Data

Before the wind farm was erected data was received from a met mast. The wind data was provided by the customer Bord Na Mona Energy Ltd. The configuration of this mast is specified in table 5-2. The mast induced a blockage effect on all anemometers except the top one. However, the booms were all oriented into the prevailing wind direction and the effect is negligible. Figure 5-1 and figure 5-2 show the wind rose and the Weibull distribution of the top height of the met mast. Important for wake development is also the TI which is diagrammed in figure 5-3. It contains the mean TI of all sectors and the one for the prevailing wind direction.

The raw data has been screened and erroneous data has been removed. To remove the seasonal bias the reference period was adapted. A long term correction was for the thesis` purpose not necessary.

Table 5-2: Mount Lucas met mast configuration [47]

Mast name	Easting	Northing	Measurement heights [m]	Measurement period	Reference period
ML_MetMast	249208	224400	10.5, 30.2, 50.2, 69.8, 71.3	10.05.2006 - 01.08.2012	01.06.2006 - 31.05.2012

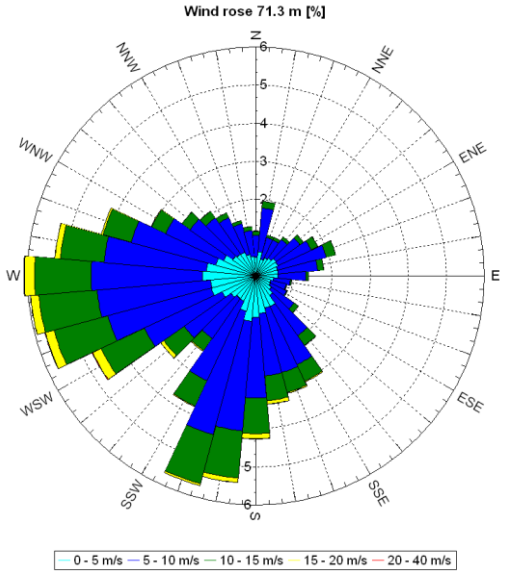

Figure 5-1: Wind rose of ML_MetMast at 71.3 m

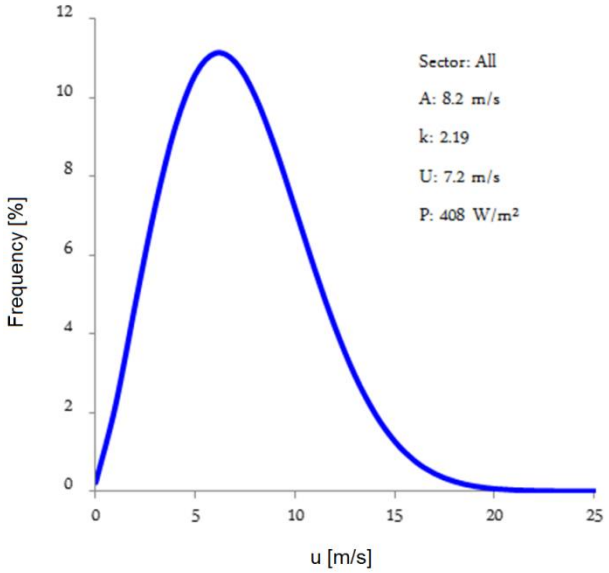

Figure 5-2: Weibull distribution of ML_MetMast at 71.3 m

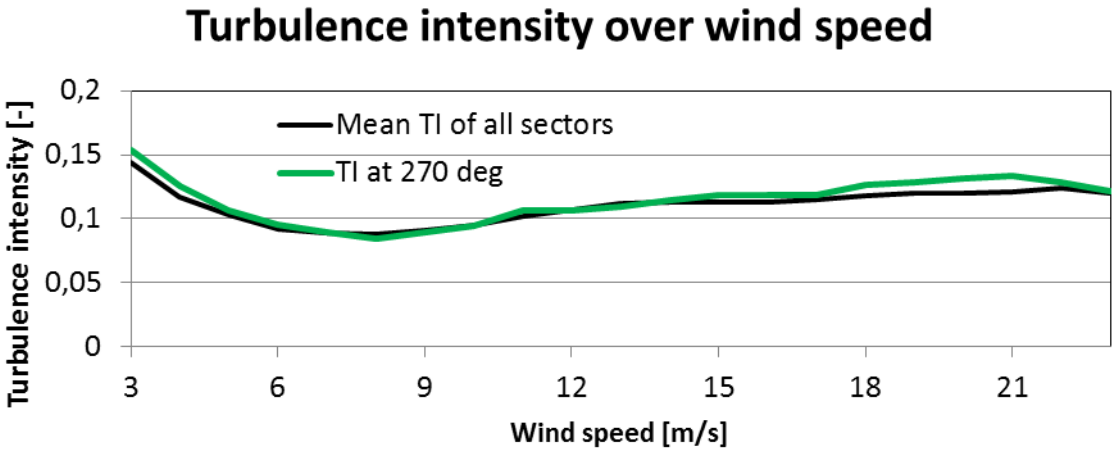

Figure 5-3: Turbulence intensity of ML_MetMast over wind speed at 99.5 m (extrapolated to hub height)

The TI plot from figure 5-3 shows an interesting phenomenon. Till 9 m/s the curve behaves typically but then it increases again. The definition of the TI (1-3) should lead to lower values at higher wind speeds. To explain the rise the stability is taken into account. Figure 5-4 shows the development of the frequencies over the wind speed. The plot is created with mesoscale data

with hourly resolution and an SGRE internal tool. For stability calculations are a wind speed and temperature sensor at two heights necessary. This was not given for the local measurements so the mesoscale data has to be used. This introduces some uncertainties because of the hourly time series but for rough stability analysis it should be suitable.

At low wind speeds are the unstable stability classes dominating which explains the high TI values at these wind speeds. At medium wind speeds (4-7 m/s) is the atmosphere more stable. This leads to low TI values. At higher wind speeds the neutral stability class is dominating so the TI rises again.

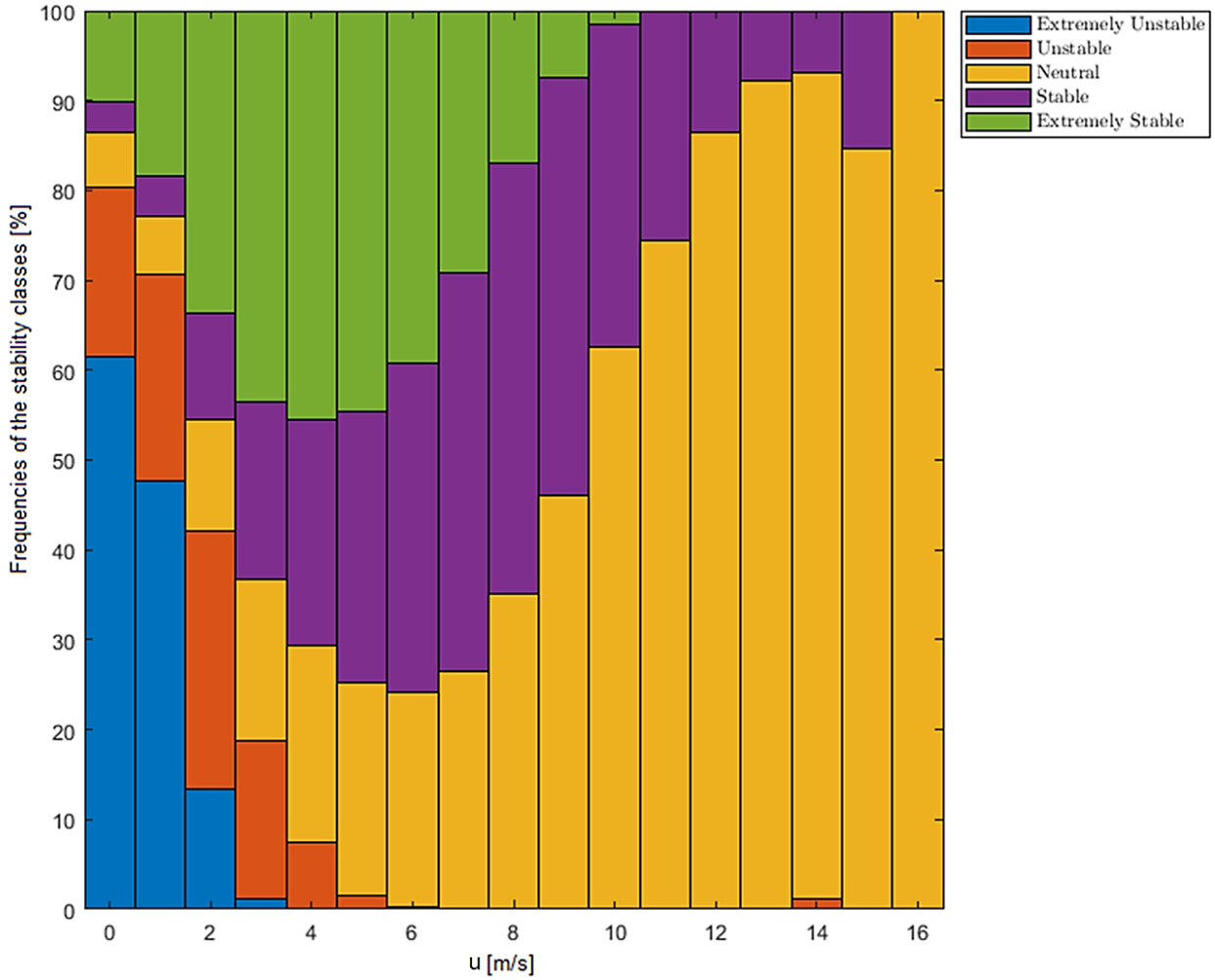

Figure 5-4: Frequencies of the stability classes over wind speed for the Mount Lucas wind farm

The preconstruction data is later used to derive the shear and sector wise TI values because the measurement period is long enough and can be assumed as representative. Additionally, these measurements are not influenced by the turbines. Other sources for the TI could be the SCADA mast or an estimation with the topography map. The approach with the topography map would assume that the stability is neutral which is only at high wind speeds true and that the TI is wind

speed independent. The SCADA mast would be the best option if it wasn't influenced by the turbines because it contains data from the actual period. Both mast options assume that the TI at the mast position is representative for the whole wind farm. For this terrain, the assumption is acceptable.

Figure 5-5 shows an rsf map of the mean wind speed at turbine hub height. The map was calculated with the measurement data of the met mast and WAsP 11. The ambient wind flow is nearly for all turbines equal. This is in agreement with mast data, orography and topography.

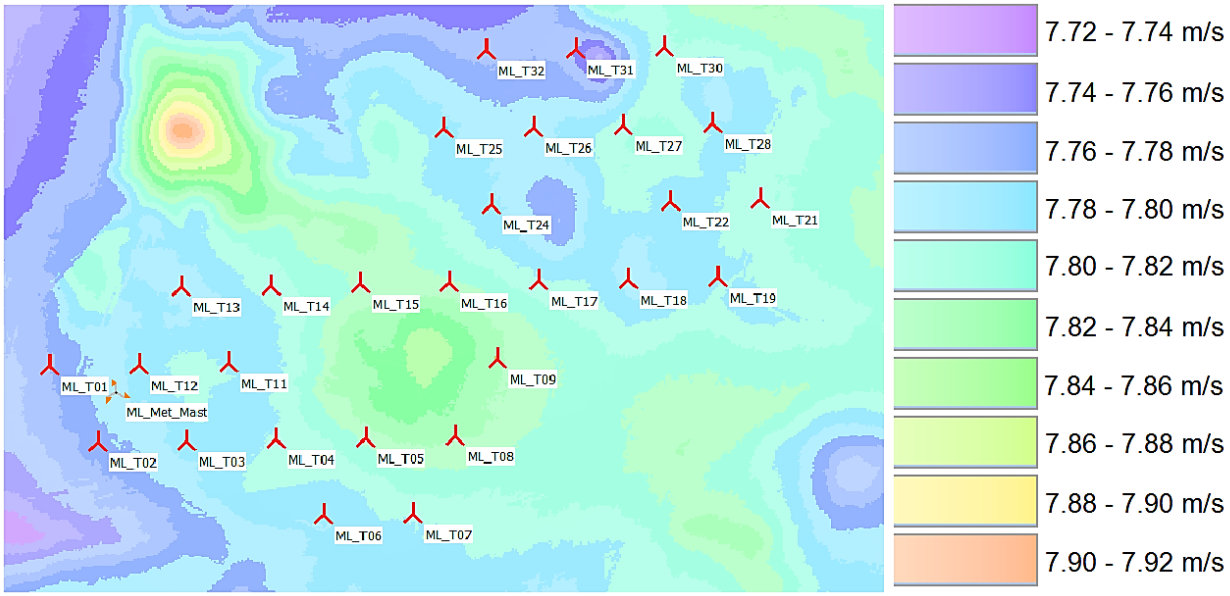

Figure 5-5: Resource map of the ambient mean wind speed at turbine hub height of the Mount Lucas wind farm

5.2.1.3 Layout

The layout of the wind farm and met mast position are shown in figure 5-6. Further information like coordinates and detailed turbine information is listed in table A-1. [45], [46]

There are no neighbouring turbines close to the wind farm which could influence the results. [46]

The layout is interesting for the testing of WakeBlaster because there are some multiple wake cases. The multiple wakes are an even more complex phenomenon than a single wake because of the merging.

Figure 5-6: Layout of the Mount Lucas wind farm (circle radius is 4.5 rotor diameters) [46]

5.2.1.4 Spacing

The distance between the turbines is for the prevailing and the non-prevailing wind direction nearly uniform which is very untypical. In addition to that is the spacing with 4.9 rotor diameters very coarse. Table B-1 shows the minimum distances and the direction.

5.2.1.5 Wind Sector Management

The Mount Lucas turbines need curtailment because the grid capacity is limited to 80 MW [48]. This curtailment only steps in when nearly all turbines produce close to rated power. This happens when the wind speed is high. For the comparison of the models and the production data only non-curtailed periods will be used which means that no comparison at high wind speeds is possible. This is a disappointment but high wind speeds are mostly not very interesting for wake calculations because the production is nearly unaffected through wake effects.

5.2.2 Gasiri

At the Gasiri site, SGRE erected 10 turbines with a rated power of 3.0 MW and 13 turbines from other manufactures are placed in the north east of the wind farm. The site is located on an island called Jejudo. Further information is listed in table 5-3. SCADA data is available from December 2014 to April 2018. [49], [50]

Table 5-3: Site information Gasiri [49]

Issue	**Information**		
Site Name	Gasiri (South Korea)		
Coordinate System and Datum	UTM (north)-WGS84 Zone: 52		
Site Coordinates	288843 E, 3696069 N		
Nearest City	Jeju, Jejudo		
Site Elevation (range)	254 m to 280 m AMSL		
Target Installed Capacity	30 MW		
Turbine Type(s)	SWT-3.0-101	SWT-3.0-101	SWT-3.0-108
Hub Height(s)	79.5 m	74.5	79.5
Number of Turbines	4	1	5

5.2.2.1 Topography, Orography and Obstacles

The terrain inside the wind farm is flat and simple but around the area are some small hills and a mountain is located western. The slopes are lower than 17 deg and no flow separation is expected so WAsP can be used. The coastline of the island takes course around ten kilometres in the east and south of the wind farm. [50]

The roughness is more complex than for Mount Lucas because the farmland has a lot of bushes and trees and is interrupted by some villages and an airport in the north-west. An advantage is that no forest is located close to the site which reduces the uncertainties in the ambient wind extrapolation. [50]

5.2.2.2 Preconstruction Wind Data

Before the wind farm was erected wind data was received from two met masts. The data was provided by the customer SK D&D Ltd. The configuration of the masts is specified in table 5-4. No installation reports for the masts were provided from the customer so no further information can be given about the installation and equipment. [51]

The M1 met mast was not taken into account for the site assessment because it was heavily influenced by the wakes of existing wind turbines in the eastern and southern direction [49]. Furthermore, the mast is also influenced by a 450 m high hill 1.4 km in norther eastern direction which is the prevailing wind direction [50]. Additionally, the height difference of the measurements is just 2 m and introduces a big uncertainty for the shear calculation. [51]

The measurement of M2 does only contain eleven months which could result in a small seasonal bias. However, it is acceptable. The raw data has been screened and erroneous data has been removed. The prevailing wind direction is north-north-east (figure 5-7). The Weibull distribution is shown in figure 5-8.

The TI development over the wind speed is diagrammed in figure 5-9. It shows the mean TI for all sectors and the one for the prevailing wind direction.

Table 5-4: Gasiri met mast configuration [51]

Mast Name	Eastern [m]	Northern [m]	Measurement Heights [m]	Measurement period	Reference period
M1	290079	3697216	70, 68	15.05.2012 – 18.05.2013	-
M2	288636	3696172	83, 79, 60, 40	12.12.2012 - 06.11.2013	12.12.2012 - 06.11.2013

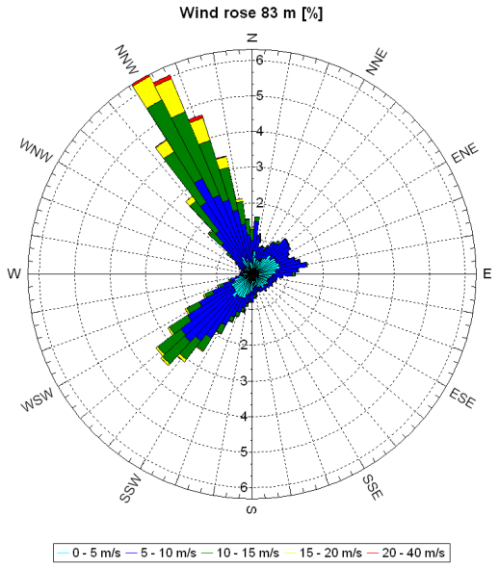

Figure 5-7: Wind rose of M2 at 83 m

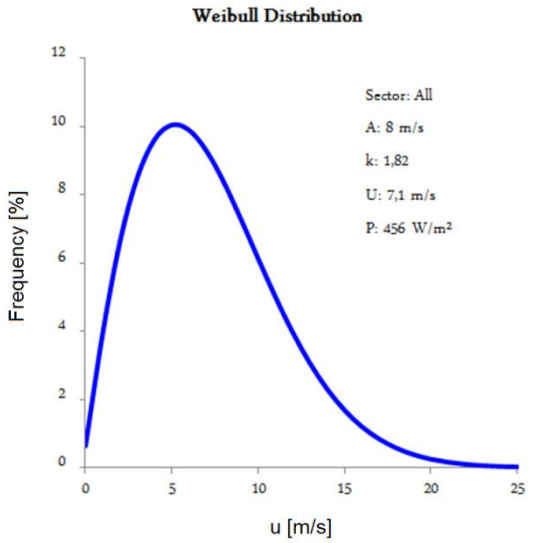

Figure 5-8: Weibull distribution of M2 at 83 m

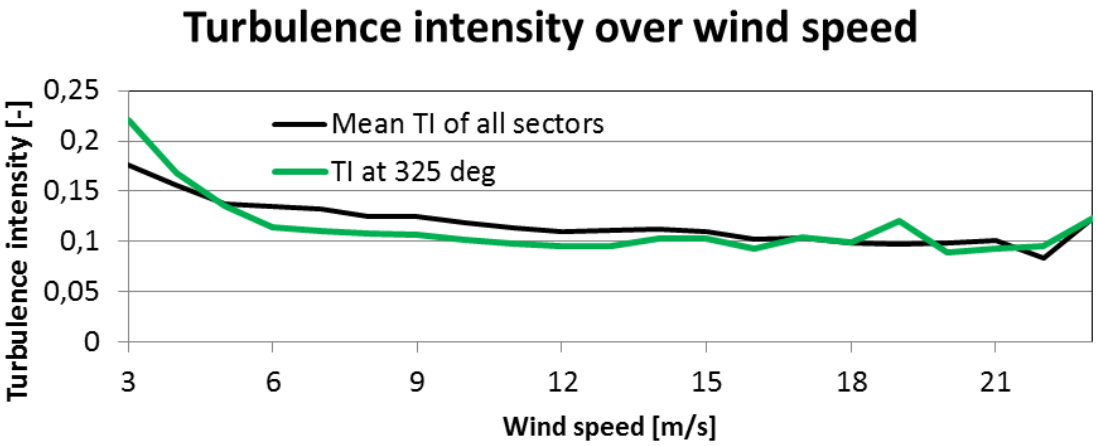

Figure 5-9: Turbulence intensity of M2

The development of the TI for Gasiri is more typical, with increasing wind speed is the TI decreasing. Opposite to that is the trend of the stability untypical. At low wind speeds the stability is dominated by extreme stable or unstable cases. With increasing wind speed is also the frequency of the neutral atmosphere rising. Nevertheless, at 12 m/s is a drop visible. The stable atmosphere is at 12 and 13 m/s absolute dominating. This is unexpected because the usual case is that the atmosphere is neutral at high wind speeds. A further investigation is out of the thesis` scope and the result will not be questioned further.

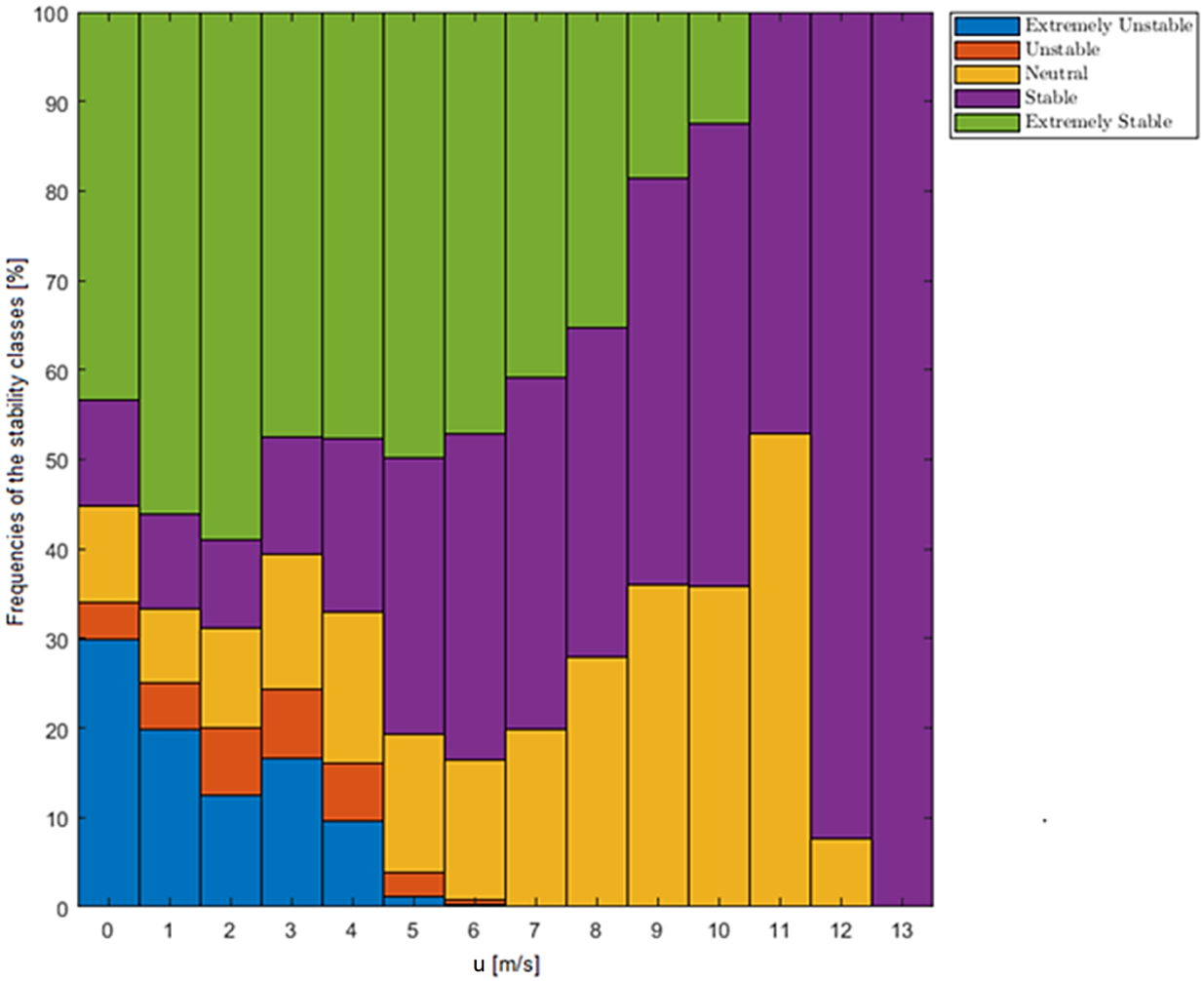

Figure 5-10: Frequencies of the stability classes over wind speed for the Gasiri wind farm

Figure 5-11 shows an rsf map of the mean wind speed at 79.5 m above the ground. The ambient flow is nearly constant for all turbines. This is in agreement with mast data, orography and topography.

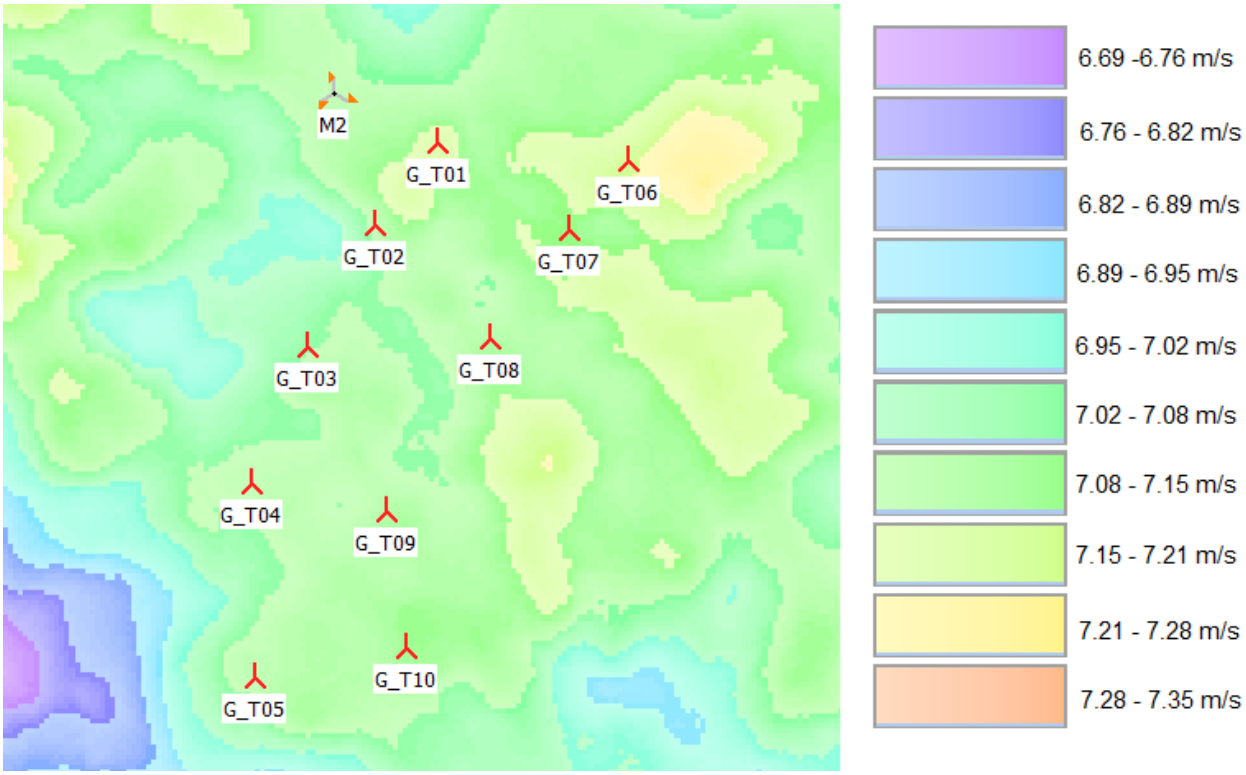

Figure 5-11: Resource map of the ambient mean wind speed at turbine 79.5 m of the Gasiri wind farm

5.2.2.3 Layout

Additionally, to the ten planned turbines 13 already existing turbines, ten rotor diameters northeastern from the site, are taken into account. The details of the SGRE and existing turbines are listed in table A-2 and table A-3. [49]

The SGRE turbines are equipped with a Power Boost function which allows producing more energy than the rated power at high wind speeds.

All turbines and the met mast are shown in figure 5-12. The wind farm is a very special case because the spacing is very close and a second wind farm is influencing the wind flow.

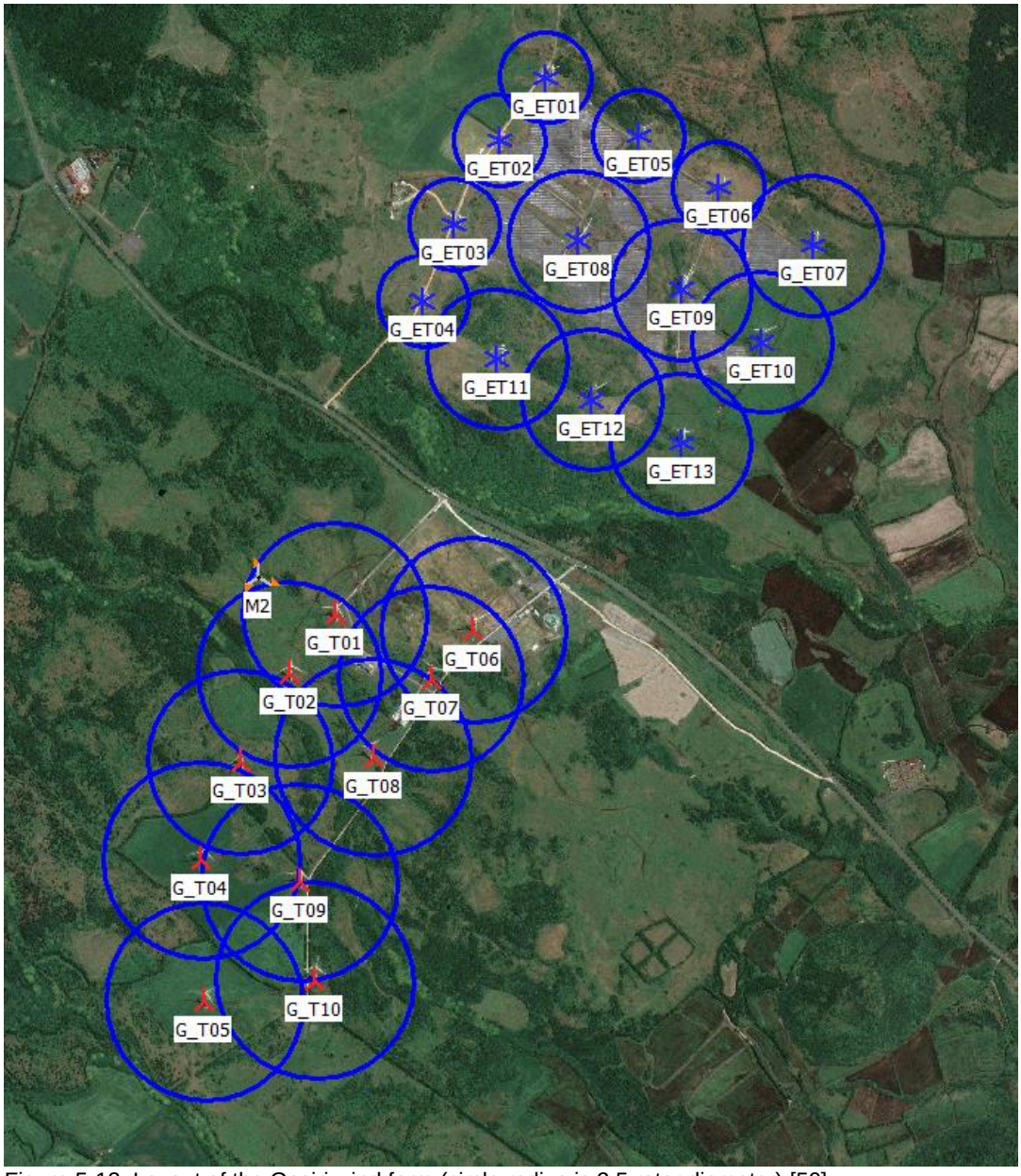

Figure 5-12: Layout of the Gasiri wind farm (circle radius is 2.5 rotor diameter) [50]

5.2.2.4 Spacing

The spacing for the Gasiri wind farm is really dense. The minimum spacing in the prevailing and non-prevailing wind direction is approximately the half of the SGRE recommendations. This makes curtailments necessary to reduce the loads. The spacing of the single turbines is listed in table B-2.

The distance between the turbines G_T06 and G_T07 is smaller than two rotor diameter. As already mentioned WakeBlaster starts the calculation only after two rotor diameter which is a problem for this wind farm.

5.2.2.5 Wind Sector Management

The below listed curtailment is necessary to not overload the turbines. For the wake calculations is it an advantage that G_T07 is always curtailed when it would influence G_T06 or would be influenced by G_T06. This solves the problem that otherwise WakeBlaster would not be able to calculate this case.

Table 5-5: Curtailment of the Gasiri wind farm [52]

Turbine Id	Eastern	Northern	Start wind speed [m/s]	End wind speed [m/s]	Start sector angle [°]	End sector angle [°]	Note(s)
G_T01	288843	3696069	15	32	185	255	Shut down
G_T02	288713	3695907	15	32	5	75	Shut down
G_T07	289101	3695890	0	32	5	80	Shut down
			0	32	185	260	Shut down
G_T09	288724	3695336	8	32	255	310	Shut down
G_T10	288758	3695065	8	32	325	20	Shut down

5.3 Method

This chapter describes the method that is used to compare the observed and simulated data.

The analysis of the simulation and production data can be done in two ways. The more accurate and data intensive approach is the analysis with a time series. This means that every single time step is analysed with a full simulation. A year has 52560 ten minute time intervals which result in a very huge dataset, even for short time periods. The advantage of this method is that all inputs for the models are as precise as possible which leads to the most realistic results. Nevertheless, the disadvantage is that some scenarios will be calculated several times. This approach will not be used because of its data intensive characteristics.

The second approach is to split the data into bins for wind speed and direction. This reduces the number of needed simulations a lot and leads to a clearer view of the data. However, through the binning the accuracy is reduced. The decrease depends on the size of the bins. The binned approach is the chosen one and will now be defined in more detail. [42], [44]

The result of the binned approach is a so called power matrix where the production for all single turbines is listed for all wind directions and wind speeds like shown in table 5-6. The bins are always valid for a certain range of values ($\text{bin value} \pm \frac{\text{Steps between bins}}{2}$).

Table 5-6: Schematic of a power matrix

Turbine	Wind speed	Wind direction 1	Wind direction 2	Wind direction 3
T01	WS1	Power T01 1, 1	Power T01 1, 2	Power T01 1, 3
T01	WS2	Power T01 2, 1	Power T01 2, 2	Power T01 2, 3
T02	WS1	Power T02 1, 1	Power T02 1, 2	Power T02 1, 3
T02	WS2	Power T02 2, 1	Power T02 2, 2	Power T02 2, 3

This matrix exists in three variants; one with the WakeBlaster results, one with the ones from the Jensen Model and one from the observed data. The ways the matrices of the models and the observed one are filled differ. To fill the matrices of the models the power is calculated at the value of the bin and the result is only one value per bin. The bins of the observed matrix contain more than one value which makes it necessary to calculate out of this several values one for the comparison. For this thesis, it was assumed that the values are distributed equally over the bins and that the PC is a continuous function. These assumptions allow to use the mean value of all values in one bin. These assumptions are also responsible for the deviations from the time series approach.

5.4 Settings and Inputs for the Models

The following chapters describe how the models were set up. The wind farms were already described in detail. How these sites can be implemented in the models is documented in the user guides, [40] and [53]. The content of this chapter are the ambient wind conditions that are used to fill the power matrix, the PC and the settings of the models that differ from the default.

5.4.1 Wind Flow Input Data

For the binned approach a compromise between accuracy and simplification has to be done for the bin sizes. The in table 5-7 listed input values were used for the simulation. The steps are from ProPlanEn recommended. ProPlanEn is experienced with this type of analysis and already did this for some other sites. [42]

The wind speed starts at 3 m/s because below this value no power is produced. At Mount Lucas ends the wind speed already at 15 m/s because of the grid curtailment. This makes a comparison at high wind speeds impossible.

Table 5-7: Simulation input data

Input data	Start values	End values	Steps
Wind speed	3 m/s (WakeBlaster)	15 m/s (Mount Lucas) 25 m/s (Gasiri)	1 m/s
Wind direction	0 deg	355 deg	5 deg
TI	6 %	20 %	2 %
Shear	Mean shear value from representative met mast		
Air density	from a meteorological station close to the wind farm		

The Jensen Model needs only wind speed and direction as input. In contrast to that WakeBlaster takes also the shear and TI into account. To reduce the number of simulations and data only the average shear value for the site is used. This reduces the accuracy of the results a little bit. However, it is still acceptable. The air density is needed to get a correct power calculation.

It would be possible to trim both models by changing the settings to get closer to the observed data but this is not the aim of this thesis. The settings of the models are chosen because of the known conditions of the wind farms before they were built. This represents the use cases of the two models better them trimming then with observed data.

5.4.2 Power Curve

Next to the ambient wind conditions, the PC is the most essential input to calculate the power matrix. The curve links wind speed and power. The PC is site specific and depends for example on the air density, TI and shear. For these simulations the site specific PC was derived with the SGRE WTG (wind turbine generator) tool. This tool is able to adapt the PC regarding the air density and TI. Nevertheless, even with these adjustments it is possible that there are differences between theoretical and practical curve. The most accurate PC could be derived with a PC measurement campaign which needs many resources such as time which is not available. So the deviations trough the PC has to be accepted.

A higher TI value increases the power output close to the cut-in wind speed but decreases the output in the transition region to rated power (figure 5-13). This influence will be only taken into account in WakeBlaster. The Jensen Model does not calculate the TI and does not correct the PC. [54]

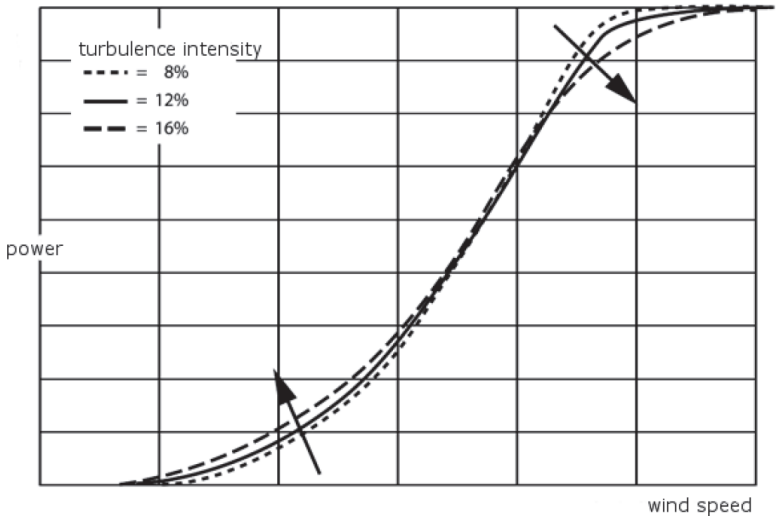

Figure 5-13: Influence of TI on a power curve [55]

5.4.3 Jensen Model

The settings of the Jensen Model differ from the one SGRE uses in their standard siting process. The reason is that the input is different than for a normal siting project and that also the needed output changed. The wanted output is the production data for every single turbine and matrix bin. The normal procedure would only lead to a single result for the whole wind farm. To achieve this output the time varying approach is used. The extrapolation of the ambient wind is done with an rsf file like in WakeBlaster to exclude deviations between the models caused by the extrapolation. The rsf file can be calculated with WindPRO or WAsP [53]. This chapter will only describe the options that were changed from the default settings.

WindPRO has two different implementations of the Jensen Model. For the calculations the variant from 2005 will be used because it is better implemented and delivers slightly better results. The turbine induced TI will not be calculated because it does not influence the Jensen Model. [22]

The WDC is changed from the standard value of 0.075 for onshore projects to a TI and sectorial dependent value. WindPRO is able to calculate this value with the TI table from a representative met mast. Furthermore the calculation of mirror wakes is excluded. Mirror wakes are wakes that hit the ground and will be reflected back like a light in a mirror. This can lead to unrealistic results and is excluded for this reason.

To get the results of the virtual time series the option “Use time series from Meteo object” has to be used and the meteo object with the time series has to be chosen. A meteo object contains information about the wind conditions at a certain point. A usual meteo object is a met mast.

Important for the correct output is that all SGRE turbines are selected in the “output specifications” otherwise it differs from the needed format.

5.4.4 WakeBlaster

This chapter describes the changes from the default settings. The input format for WakeBlaster and a user guide are documented in [40]. WakeBlaster can be used with Matlab or Python but the process was developed for Matlab because more engineers in SGRE are familiar with it.

WakeBlaster is able to calculate the rotor equivalent wind speed for each turbine but this feature is not used because of two reasons. The first argument is that the SGRE PC ’s are valid for the wind speed at hub height. Secondly the differences between the wind speed at hub height and the calculated rotor equivalent wind speed are a lot higher than they should be. To use the wind speed at hub height the simulation configuration file is changed. A full description of the settings is documented in [56]. All other settings stay in default.

To set up WakeBlaster it is also necessary to feed it with data of the wind farm, including the wind conditions and how the ambient wind is extrapolated. Further explanation can be found in the Matlab code or the Excel sheet that is used to transform the data from WindPRO to the WakeBlaster format.

5.5 Process

After clarifying the settings of the models and the method, the complete process of deriving results is now described. A process chart is shown in figure 5-14.

The process starts with a standard SGRE siting WindPRO project. This file contains all the necessary information about the turbines (type, coordinates, elevation, etc.), the terrain (orography and topography) and the wind data.

The next step is to check the data quality. Due to the fact this thesis is part of a research project, the demanded accuracy is much higher than for standard projects. Therefor it is required to refine the orography and topography maps. Aditionally, it is essential to check the turbine details regarding power curve revision or position. It can happen that the turbines are built at a different position then assumed in the WindPRO file or that the PC is updated.

The last step before the calculation can start is to choose a reference point. The simulations are initialized at this point and height. The wind speed and direction at this point are also used to sort the measured data into the bins of the power matrix.

From now on, until the results are compared, the process is different for the two models. Firstly the Jensen process is described and then the one for WakeBlaster. All necessary Excel sheets contain detailed user guides.

The first step for the Jensen Model is to create an artificial time series for the power matrix calculation. This is done with the help of the Excel sheet “Time Series”. The result is a ten minute time series that contains all cases for the power matrix. The next step is then to import the time series into the WindPRO project. This is described in detail in [53] and will not be further explained. Nevertheless, it is essential to choose the right height for the time series. This height has to be the same as for the reference point.

Now, the production is calculated with the time varying park model. The settings for the Jensen Model were already described. Further information about this variant of the park model can be found in [53].

It is now needed to copy the time varying results to the “02_Matrix” Excel sheet. This sheet converts the format of the WindPRO output into the power matrix. The resulting matrix is then copied into the “03_Results” sheet.

After presenting the process of the Jensen Model, the description of the WakeBlaster process can start. The first step is to use the Excel “Transfer Script” which converts the WindPRO format

into the format WakeBlaster needs. The script is able to transform data of turbines, met masts and measurements (for the case that the time series approach is tested).

The next step is then to copy the transformed information into several JavaScript object notation (.json) files. The easiest way to do this is to copy the needed data into Notepad++ and save it as .json. In addition to these files, it is needed to provide for each turbine type a WTG file. These files contain power and thrust curve, rotor diameter, hub height and the air density the two curves are valid for. The WTG file can be extracted from WindPRO or created with the SGRE WTG tool.

The last step before starting the simulation is to adapt the standard Matlab code to the new project. A detailed description is available in the code and the parameters that are needed to change are listed in table C-1.

After running the simulation and checking the results for plausibility they need to be copied into the “01_Combine_TI_Matrices” Excel sheet. The results of WakeBlaster differ when the TI is changed. That is the reason why it is necessary to calculate the wakes at different TI settings. This Excel sheet combines the results of the different TI levels with the turbulence table from the measured preconstruction data. The resulting matrix from this step is then copied into the “03_Results” sheet.

The information from the SCADA data that was analysed by ProPlanEn is also inserted in the “03_Results” sheet. This sheet contains now the observed values and the results from both models. Now, the comparison can start. The sheet allows a comparison for single turbines at different wind speeds as well as for the production and wake losses for the whole wind farm and the AEP.

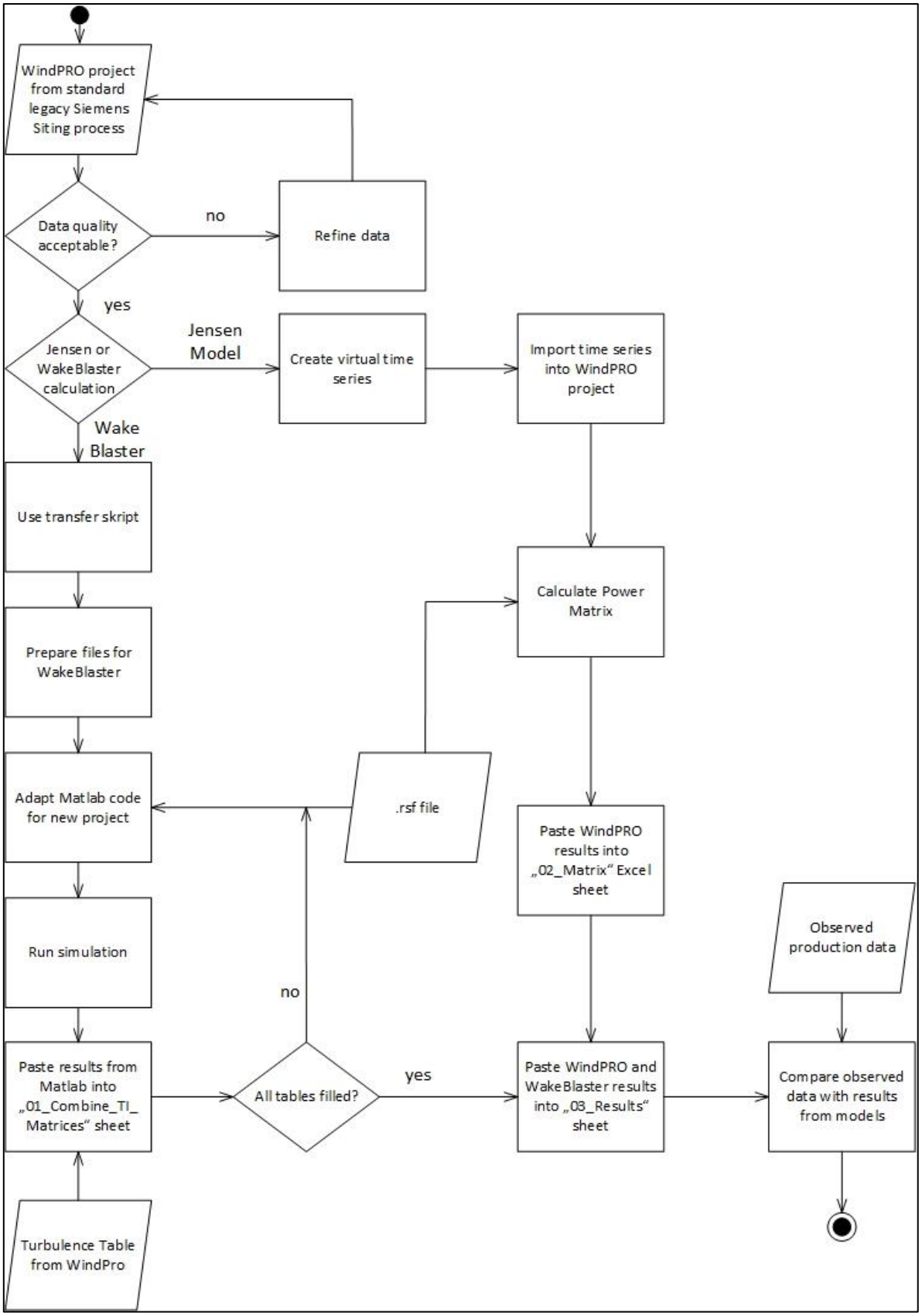

Figure 5-14: Process diagram for simulation of the wind farms

6 Comparison of the Results

This chapter compares the results that were produced with the process described in the last chapter. At the beginning of this chapter a general introduction of the results is given. This is followed by a detailed analysis of both wind farms. The comparison will be split into two sub-chapters, one for each wind farm.

In the task description a comparison of AEP, TI, etc. was mentioned. The comparison of TI values is not possible because the Jensen Model does not calculate TI values and the binned observed data is not acceptable for a TI comparison. The AEP will be calculated from the power matrices and the measured wind distribution. The produced power is compared for the whole wind farm and for single turbines. Additionally, the absolute error of the two models is analysed.

Another interesting point would be the wind speed reduction which both models calculate but also for this is the data not feasible because of the binning. A comparison based on wind speed reduction would be great because it would eliminate the deviations resulting from the PC.

Before the wake model comparison is done it will be checked how good the estimation of the production in the wake-free sectors is. This is necessary to know where the deviations come from. If the deviations are too high a calibration factor will be used to decrease them. Only with small deviations in the wake-free sectors an analysis of the wake models is possible.

The calibration factor will be applied to the wind speed of the artificial time series. The calibration is reasonable because the thesis` scope is to analyse the wake models and not the complete siting process. The calibration factor is defined with the AEP of the Jensen Model. The aim is to match the overall observed AEP with the Jensen’s one. This is a fast and practical solution but will distort the AEP results. A better solution would be to compare just the wake-free sectors for an AEP calculation and achieve with this number a calibration factor. However, this needs more resources than available.

The wake models will be compared at different wind speeds. Nonetheless, most of the examples will be done for 8 m/s because it is the commonly used value in the literature. Moreover, at this wind speed are the wake effects significant, the production is high and for this wind speed are enough data points available.

All not in this chapter shown plots are available in appendix D and E.

6.1 Mount Lucas

The first site that is analysed is Mount Lucas. The comparison starts with a general check of the wake-free sectors goes on with the whole wind farm, AEP calculation and sectorial wake losses and end with a detailed analysis of the single turbines.

The grid limit of the wind farm makes it impossible to analyse high wind speeds for Mount Lucas but these are not interesting for wake effects so this restriction is acceptable.

6.1.1 Wake-Free Sector Analysis

The first step is to check how well the production in the wake-free sectors is matched. This is done because the base for the wake models is the ambient wind speed extrapolation and the PC. If one of them deviates from the reality it is nearly impossible to differentiate between errors of the wake models and other sources. The wake models have no influence on the production in the wake-free sectors and the deviations of the non-wake related aspects are clearly visible.

To analyse these aspects three turbines at three different wind speeds are presented. Three turbines are used to get an overall overview and to avoid a wrong conclusion based on location dependent anomalies. The different wind speeds are used for the same reason. It is important that the wake-free production is valid for the whole wind speed range. Especially, because the calculated speed-up effects are wind speed independent.

For the analysis plots are used that show the mean value (black line), standard deviation (orange bars) and number of data samples of the matrix bin (grey bars) of the observed data and the modelled production (WakeBlaster–green line, Jensen–purple line).

The production of turbine ML_T02 at 8 m/s is shown in figure 6-1. The wake-free sector starts at around 120 deg and ends at 300 deg. It can be clearly seen that the models are for this sector nearly identical, the only deviation comes from the fact that the TI changes with the sectors and WakeBlaster adjust the PC for that and WindPRO not. From 170 to 300 deg is the modelled production nearly constant and the observed is changing just a little bit. For all these sectors are the models overestimating the production. This can have two reasons one that the ambient wind extrapolation is overestimating the wind speed or that the PC values are too high. At 120 to 170 deg is the overserved production changing a lot while the modelled is nearly constant. This could indicate that the ambient wind extrapolation is not very precise at the turbine position.

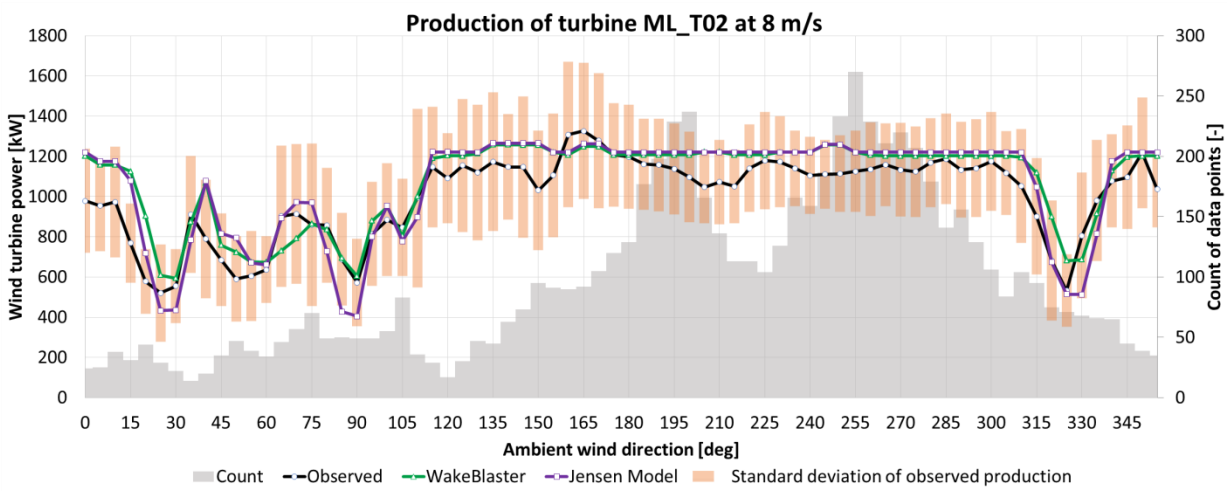

Figure 6-1: Production of turbine ML_T02 at 8 m/s

The next example is ML_T13 with a wake-free sector from 255 to 45 deg (figure 6-2). This time equals the wind speed 10 m/s. The trend from 255 to 360 deg is good but the production is clearly overestimated. For 0 to 45 deg is the fit bad. This could result out of the lower amount of data or missing details from the orography or topography map.

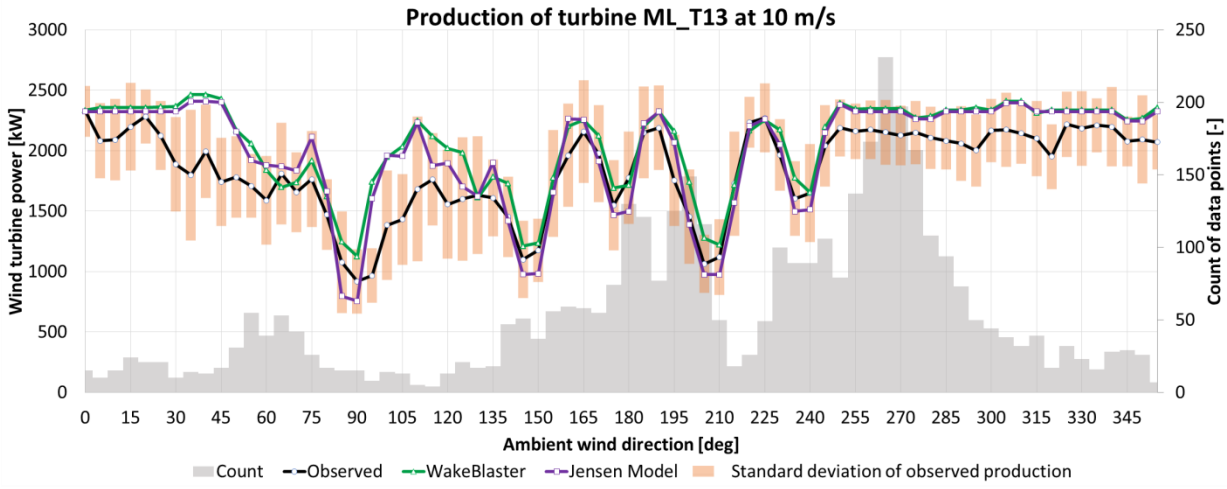

Figure 6-2: Production of turbine ML_T13 at 10 m/s

The last example is turbine ML_T30 at 5 m/s (figure 6-3). The wake-free sector ranges from 285 to 120 deg. Also here, are the models following the trend of the observed data but overestimating the production again.

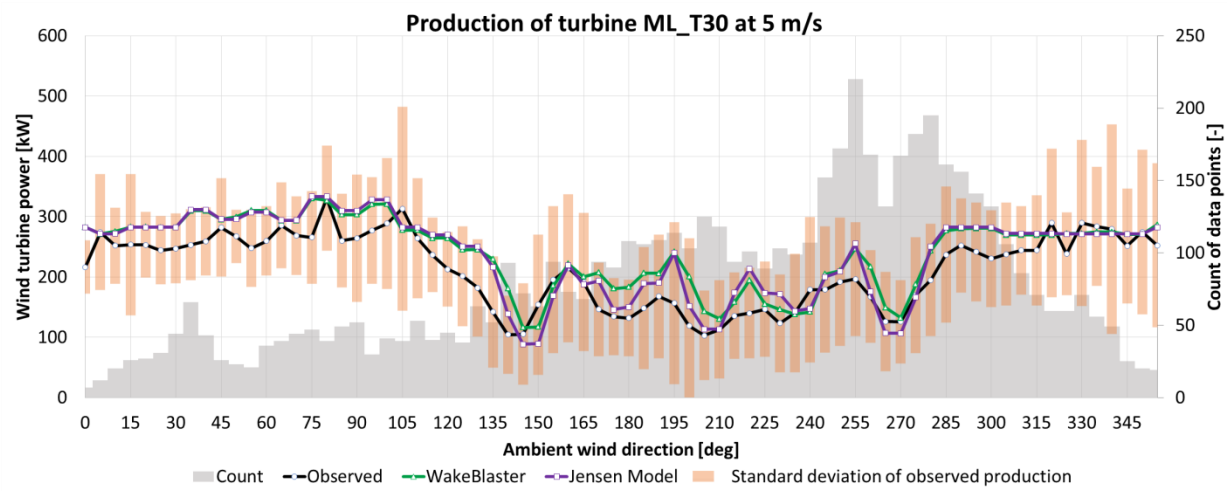

Figure 6-3: Production of turbine ML_T30 at 5 m/s

The wake-free sectors were checked for more than the three examples above and showed for all examples the same characteristics. The production is overestimated for all turbines and wind speeds. For this reason the waked sectors are not analysed and a calibration factor will be used. The AEP of the Jensen Model is used to define the value of this factor. The factor equals 0.9635. Important is to remember that already a small reduction of the wind speed will decrease the production a lot. In the next chapters are only calibrated results shown.

The wake-free sectors are for the calibrated plots not analysed again but it can be clearly seen that the fit is a lot better.

6.1.2 Wind Farm Production

After the wake-free sector analysis is completed the next step is to compare the production of the whole wind farm. This is done at 5, 8 and 10 m/s.

The trend over the wind direction should be for all wind speeds the same. Taken the layout into account the wake effects for 90 and 270 deg should be the highest. Nevertheless, also for 30, 150, 210 and 330 deg they should be significant. All of them can be clearly identified at the examples (figure 6-4, figure 6-5 and figure 6-6). As predicted is the lowest production located at 90 deg. Also the decreases at 30, 150, 270 and 330 deg are well diagrammed.

Both wake models follow the general trend very well except for some special cases (e.g. at 355 deg at 8 m/s). The deviations of WakeBlaster are mostly smaller than for the Jensen Model, especially when multiple wakes are the dominant phenomenon (e.g. 90 or 270 deg). This makes sense because of the 3D characteristics of WakeBlaster's RANS equations this should be a strength of it. Additionally, the predicted production of WakeBlaster is in general higher than the one of the Jensen Model.

WakeBlaster seems also to predict the transition from more to less waked sectors and vice versa better.

The deviations at 5 m/s are much higher than for the two higher wind speeds. This is reasonable because at this low wind speed already small errors lead to high deviations.

Interesting is also that the deviations for WakeBlaster at 90 deg increase a lot from 8 to 10 m/s. A reason for this could be that the number of data points is lower at 10 m/s then at 8 m/s.

The general fit of the wake models seems to be wind speed independent. This assumption is based on the plots below. The models over- or underestimation is nearly constant for all wind speeds.

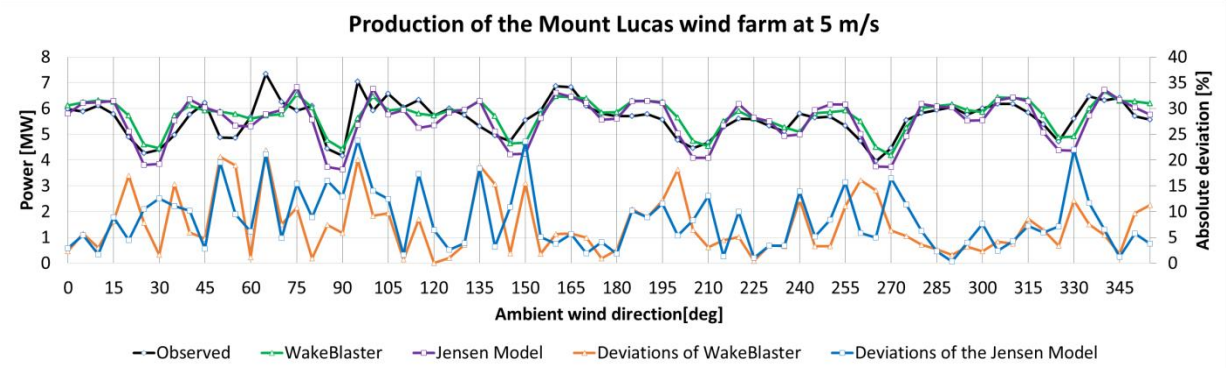

Figure 6-4: Production of the Mount Lucas wind farm at 5 m/s

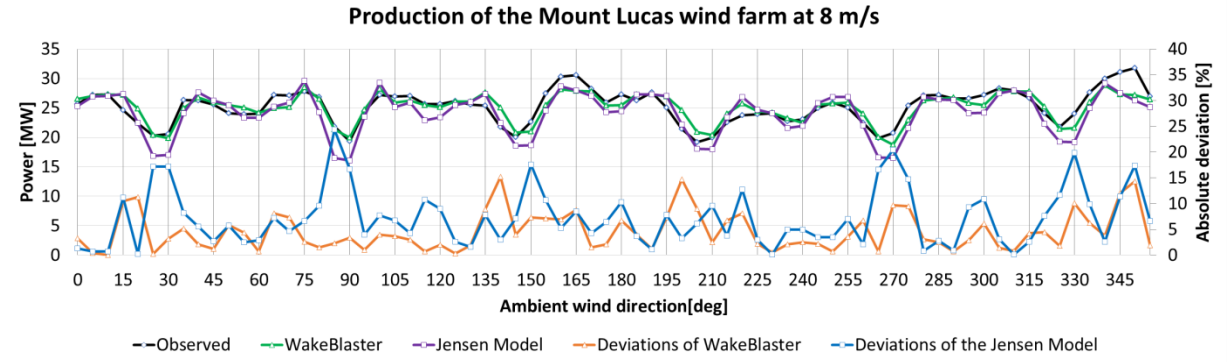

Figure 6-5: Production of the Mount Lucas wind farm at 8 m/s

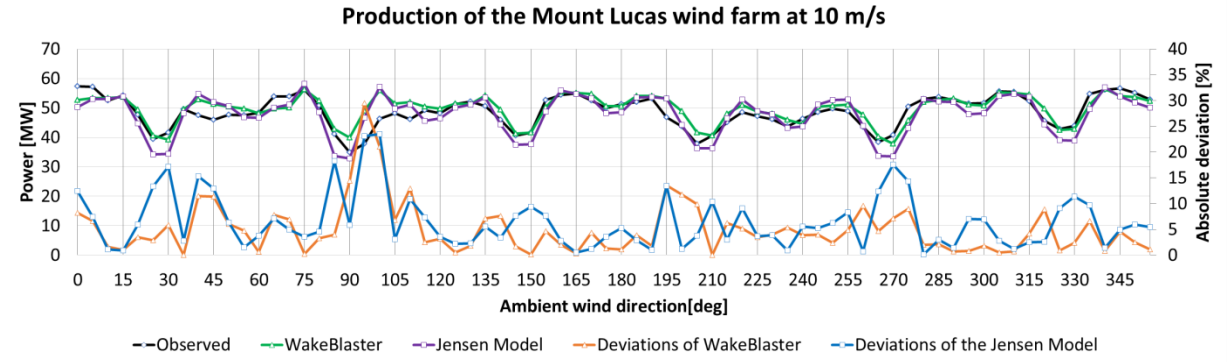

Figure 6-6: Production of the Mount Lucas wind farm at 10 m/s

The last three figures showed the production of the wind farm which is needed to validate the models and get an understanding of the wake situation. However the value that is important for the customer is the AEP prediction which will be introduced next.

6.1.3 AEP Calculation

Before some numbers are presented a short excurse is needed to explain how the AEP can be calculated from the power matrix. In the literature, several ways for the AEP calculation are discussed. For this thesis the 1-6-1 pattern is used. The AEP is a combination of the power matrix and the wind distribution.

Before the 1-6-1 pattern is explained a short look back at the available data is given. On one side is the power matrix which defines the produced power for all wind speeds at 1 m/s steps and on the other is the wind distribution which is also sorted into the bins of the power matrix but as counts not produced power so it is a count matrix. Opposite to the power matrix of the models the values for the count matrix are distributed over the whole bin size. To take this into account is the power integrated over the single bins.

The assumptions that are used with the 1-6-1 pattern are that the points of the count matrix are equally distributed over the bins and that the PC is a continuous function. They are the same that are used for the power matrix approach. [39]

These two assumptions allow a simple integration. To get then from the integrated power to the yield is the wind distribution used. The first step is to know the power at the beginning and end of the bins. For this the equations (6-1) and (6-2) are used. This is possible because the function can be assumed as linear. The wind speed is declared as WS. [39]

$$P(WS-0.5)=\frac{P(WS-1)+P(WS)}{2} \tag{6-1}$$

$$P(WS+0.5)=\frac{P(WS+1)+P(WS)}{2} \tag{6-2}$$

The bin is now split into two parts and with the assumption from above they look like below.

$$LeftYield=Probability(WS)*\frac{P(WS-0.5)+P(WS)}{2} \tag{6-3}$$

$$RightYield=Probability(WS)*\frac{P(WS+0.5)+P(WS)}{2} \tag{6-4}$$

Sum the two above up and insert (6-1) and (6-2) leads to (6-5).

$$Yield=Probability(WS)*\frac{P(WS(-1)+P(WS)*6+P(WS+1)}{8} \tag{6-5}$$

For the resulting formula all values are known and the AEP per bin can be estimated. The bins are then summed up and multiplied by 8766 hours (hours of a year) to get the AEP of a complete year. [39]

The result of the calculation is shown in table 6-1. The Jensen Model is very close to the observed AEP which validates the calibration of the wind speeds. WakeBlaster is also close to the observed production. The AEP value is not used to assess the models because with the calibration this would be unfair.

Interesting is that the values of the models are closer together than expected. The deviations of the Jensen Model were higher than the one from WakeBlaster. This should lead to differences regarding the AEP. It seems that the Jensen Model is for the overall windfarm competitive even when for single turbines and wind conditions it is not.

As already known are the wind speeds calibrated to the Jensen AEP. So the Jensen Model is clearly closer to the observed AEP value. To take this calibration into account an additional power matrix is created. This matrix includes the absolute error for every bin (6-6). This new matrix is used to calculate an absolute error AEP. It shows that WakeBlaster's results are closer to the observed production. Opposite to that is the Jensen Model just closer to the AEP through a mix of under- and overestimation. The difference between WakeBlaster and Jensen is small but would be greater if the wind speeds would be calibrated to the AEP of WakeBlaster.

$$AE = |Observed\ Production - Modelled\ Production| \tag{6-6}$$

Table 6-1: AEP of the Mount Lucas wind farm

	Observed	Jensen Model	WakeBlaster
AEP [GWh]	172.59	174.12	180.43
Deviation [%]	-	-0.89	-4.54
Absolute Error [GWh]	-	17.15	15.25

6.1.4 Sectorial Wake Losses

Next to the production and AEP of the wind farm it is also important to understand the wake situation. To do this the wake and efficiency losses are shown per sector. The wake losses are calculated with equation (6-7) and the efficiency with equation (6-8). To derive the annual wake losses per sector the wind distribution together with the 1-6-1 scheme from the AEP calculation is taken into account. The wake-free power values are taken from the WakeBlaster calculation. The Jensen Model does not calculate it and in the SCADA data it is not provided. The wake-free power values include the deviations from the ambient wind extrapolation and PC. With the calibration and for this simple terrain they should be acceptable small.

$$Wake\ Losses = Unwaked\ Power - Waked\ Power \tag{6-7}$$

$$Eff = \frac{Unwaked\ Power - Waked\ Power}{Unwaked\ Power} \tag{6-8}$$

To understand the annual sectorial wake losses (figure 6-8) better is the wind rose of the observed data plotted (figure 6-7).

The prevailing wind direction is clearly west and south-south-west. This is also visible in the wake losses. The wake losses in these sectors are the highest. Interesting is that the wake losses decrease massively when the wind direction changes to west-north-west even when the frequency is not much lower.

High wake losses are also diagrammed in the sector of 150 and 200 deg. Together with the efficiency plots (figure 6-9 and figure 6-10) this will be investigated further.

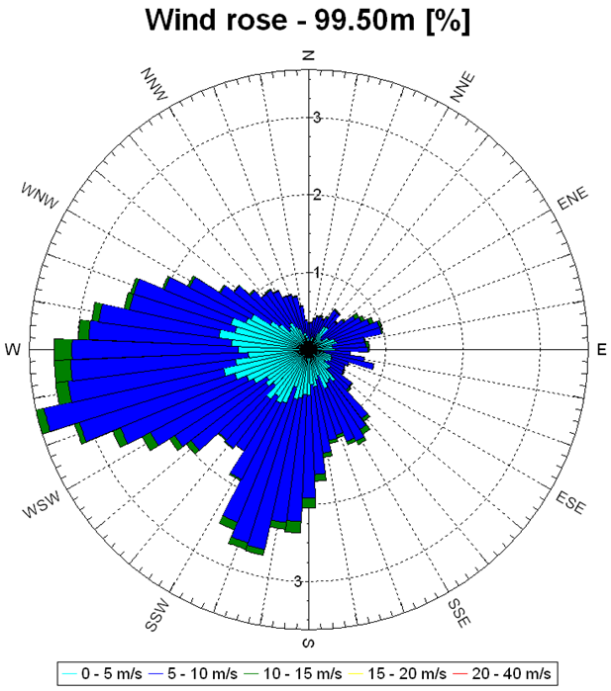

Figure 6-7: Wind rose of the SCADA mast of the Mount Lucas wind farm

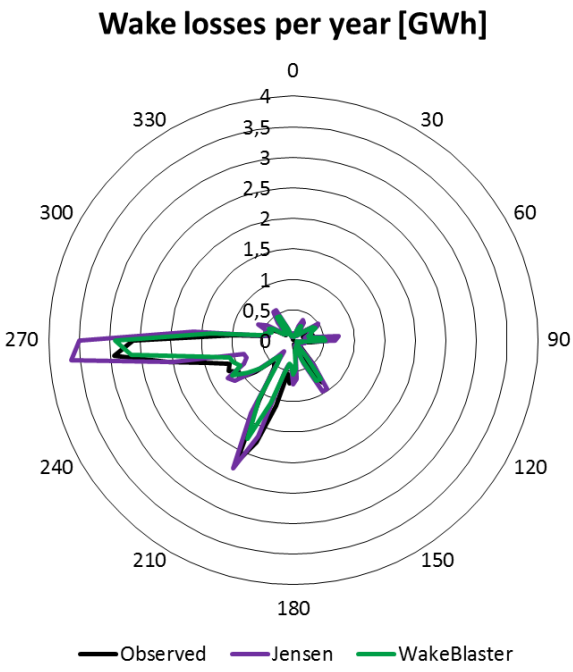

Figure 6-8: Sectorial wake losses per year for the Mount Lucas wind farm

The first efficiency diagram (figure 6-9) shows the percentage that is lost due to wakes at 8 m/s. WakeBlaster is in general fitting the observed graph very well. Opposite to that is the Jensen Model most of the time overestimating the wake losses.

Curious are the values at 160 and 355 deg. The observed data shows negative efficiency losses for these sectors. These are by definition impossible. Nevertheless, they indicate that for these sectors the ambient wind speed is underestimated. The plots for the turbines ML_T08 (figure D-8) and ML_T18 (figure D-16) underline this assumption.

The regular layout of the wind farm is also displayed in this chart. Every 60 deg are the efficiency losses high. Experienced Siting engineers get a feeling for layouts and wake losses but with this chart it is possible to get a real feedback.

Figure 6-10 shows the observed efficiency losses for different wind speeds. It is curious that the efficiency losses are nearly wind speed independent for this wind farm. This phenomenon needs to be investigated further because before it was assumed that higher wind speeds lead to lower wake losses. First the trust curve will be evaluated. A typical thrust curve was shown in figure 3-1. The thrust coefficient is nearly constant until 8 m/s. Also that the TI is decreasing from 5 to 8 m/s is a reason for constant efficiency losses (figure 5-9). These two reasons explain why the graphs for 5 and 8 m/s are so similar. Nevertheless, a reason for the missing difference to 10 m/s is still absent. From 8 to 10 m/s is the TI increasing again and the thrust coefficient is decreasing. Both should lead to lower efficiency losses but aren't.

An explanation for nearly equal efficiency losses could be that between wind speed and recovery is an equilibrium reached (figure 3-18). The equilibrium would reduce the differences between the different wind speeds. This is still not a complete explanation but a starting point. For a complete explanation more data than provided is needed. However, this should be investigated further in the future.

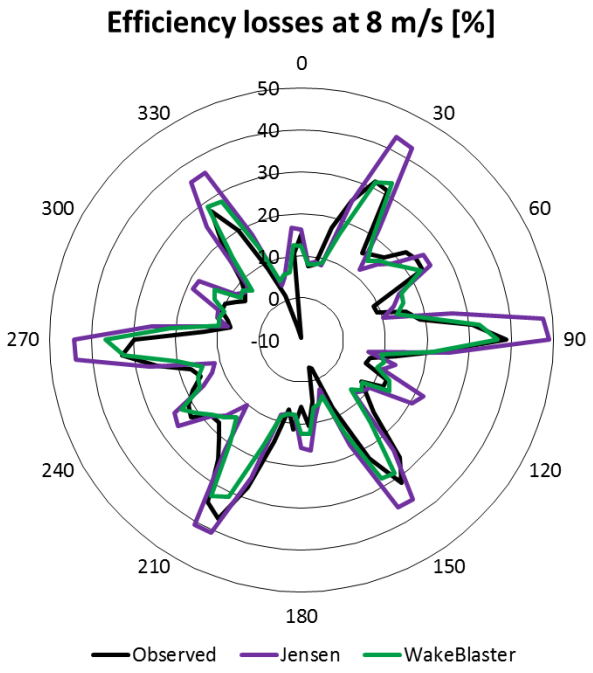

Figure 6-9: Sectorial efficiency losses of the Mount Lucas wind farm at 8 m/s

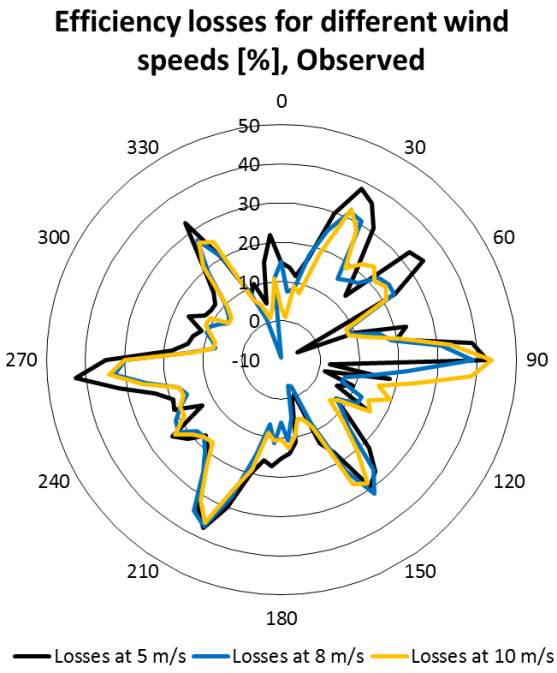

Figure 6-10: Observed sectorial efficiency losses for different wind speeds at the Mount Lucas wind farm

6.1.5 Single Turbine Production

After analysing the whole wind farm, the next step is to look into the details. The aim is to investigate at which wake cases the deviations are huge or small and for which cases one model is superior.

The new introduced turbines ML_T11 and ML_T27 are waked from nearly all sectors. Both turbines are placed in the centre of several other ones but in different parts of the wind farm. Ml_T11 is single waked from 25, 90, 205, 235 and 330 deg. The wake from 90 deg is induced over 10 rotor diameter away from the turbine. All other single wakes are induced with a spacing of five rotor diameter. Multiple wakes arise from 60 to 85 deg, 120 to 150 deg and 270 deg. The production of ML_11 is diagrammed at 5 and 8 m/s (figure 6-11 and figure 6-12) to show that the models are valid for different wind speeds. The trend of the two diagrams of ML_T11 is very similar, only the production values are higher at 8 m/s.

In general both models estimate the production well. Nonetheless, WakeBlaster is especially at the multiple wake cases closer to the observed data. At single wakes is it not that clear. At 25 deg are both models equidistant from the observed data. WakeBlaster is overestimating and the Jensen Model is underestimating the production. The wake from 90 deg is predicted well from WakeBlaster while the Jensen Model is underestimating the production. Opposite to that is the Jensen Model estimating the production at 205 deg nearly perfect while WakeBlaster is overestimating it. At 235 deg the opposite is visible. WakeBlaster is close and Jensen is underestimating. The last single wake at 330 deg is again from WakeBlaster estimated better.

Both models are at 5 m/s at 95 deg far away from the observed data. This could be caused by a data error. The standard deviation (orange bars) for this bin is extremely high. This indicates that something strange is happening here. However, without a deep look into the data it is not possible to solve this anomaly.

Both models at both wind speeds are not following the observed data at 135 deg. It seems that the models predict at this direction a wake-free corridor which cannot be seen in the observed data. The reason for that could be the binning. The models calculate the wakes only at exact 135 deg while the observed data contains 135 ± 2.5 deg as direction.

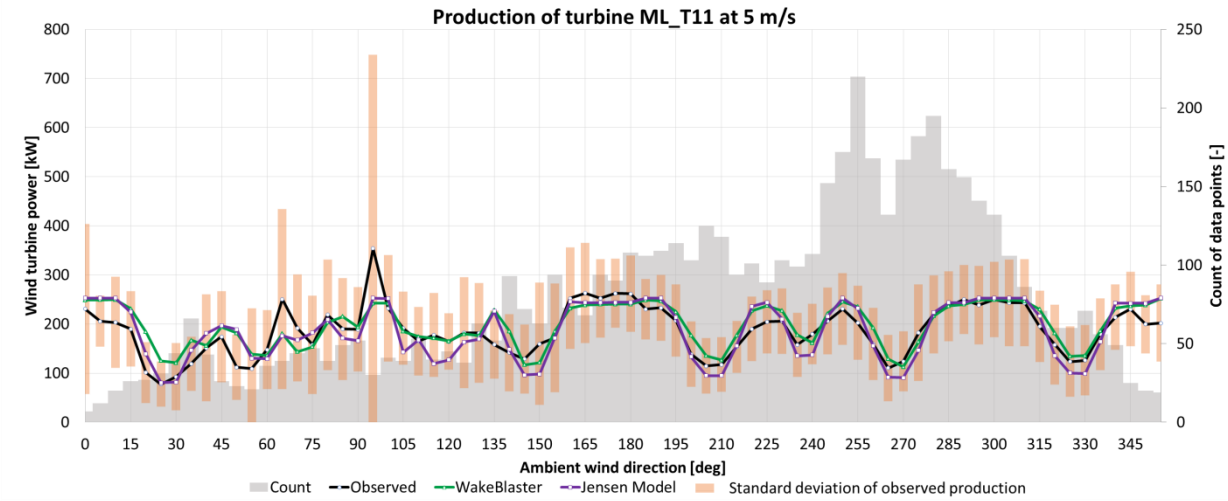

Figure 6-11: Production of ML_T11 of the Mount Lucas wind farm at 5 m/s

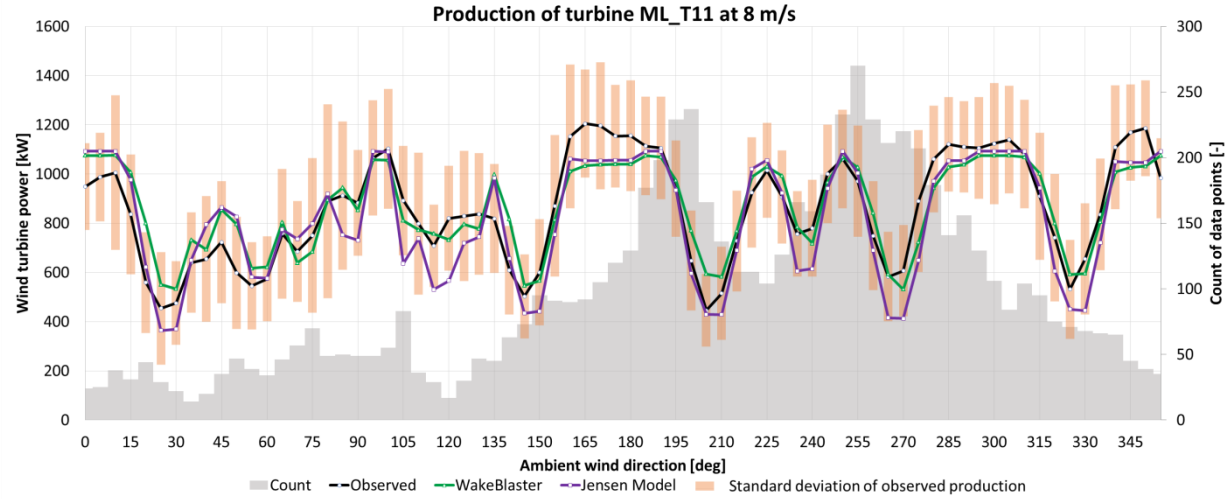

Figure 6-12: Production of ML_T11 of the Mount Lucas wind farm at 8 m/s

The production of turbine ML_T27 is diagrammed in figure 6-13 and influenced by a lot of single (30, 90, 120, 300 and 330 deg) and multiple wakes (150, 180, 210-240, and 270 deg). Also, the same schema like for ML_T11 can be identified. All multiple wakes are better estimated by WakeBlaster. WakeBlaster is also better predicting the single wakes at this turbine. The only exception is the wake from 90 deg.

Both models show a different trend then the observed data from 210 to 225 deg. It seems that for these directions the wake models only take ML_T05 into account. Nevertheless, it seems that also ML_16 and ML_T17 have an effect. A reason for this error could be that the wake models underestimate the dimension of the wakes. To prove this a measurement campaign would be necessary which is out of the limit of the thesis` resources.

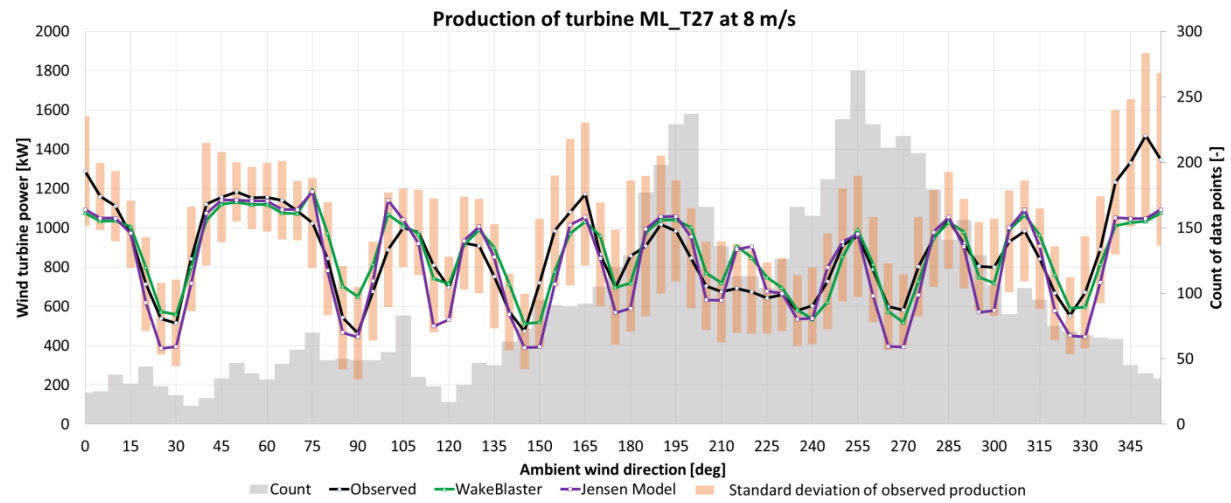

Figure 6-13: Production of ML_T27 of the Mount Lucas wind farm at 8 m/s

6.1.6 Conclusion of the Mount Lucas Wind Farm

This chapter gives a rough conclusion of the results of the Mount Lucas wind farm. In general both models match the trend of the observed data well. Overall is WakeBlaster closer to the observed production. Nevertheless, it tends to overestimate the production, while the Jensen Model changes between over- and underestimation.

The single wakes are predicted well from both models but the multiple wakes are estimated from WakeBlaster much better.

6.2 Gasiri

The results of Gasiri are analysed in the same way as Mount Lucas. The main difference is that the amount of data is limited. This is caused by curtailments and the wind distribution. The data is acceptable from 275 to 0 deg and for low wind speeds also for 90-180 deg.

6.2.1 Wake-Free Sector Analysis

The wake-free sector analysis for Gasiri is more complicated than for Mount Lucas because the wind farm contains two different turbine types and the data is only valid for a small range of wind directions.

For the analysis are the turbines G_T02 (SWT-3.0-101) and G_T04 (SWT-3.0-108) used. Both turbines are for the complete range of valid sectors wake-free. Like for Mount Lucas the production will be shown at different wind speeds. 5, 8 and 15 m/s will be used for the analysis, even when the amount of data decreases at 15 m/s. Additionally, are turbine G_T05 (SWT-3.0-108) and G_T06 (SWT-3.0-101) at 5 m/s analysed because they are wake-free at 90-180 deg

and deliver further information. Both turbine types are analysed to avoid conclusions that apply only to one turbine type.

The production of the G_T01 is diagrammed in figure 6-14, figure 6-15 and figure 6-16. At 5 m/s is the estimation ok. Nevertheless, at the other two wind speeds the production is clearly overestimated. Additionally, the modelled production is nearly constant while the observed changes. This indicates that the ambient wind extrapolation is not very precise at this position. Figure 6-16 shows a feature of the Gasiri wind farm. All turbines are equipped with the Power Boost add-on. The Power Boost allows the turbine to produce more energy than rated power at high wind speeds.

G_T01 is waked for 90-180 deg so these sectors can't be used for the analysis.

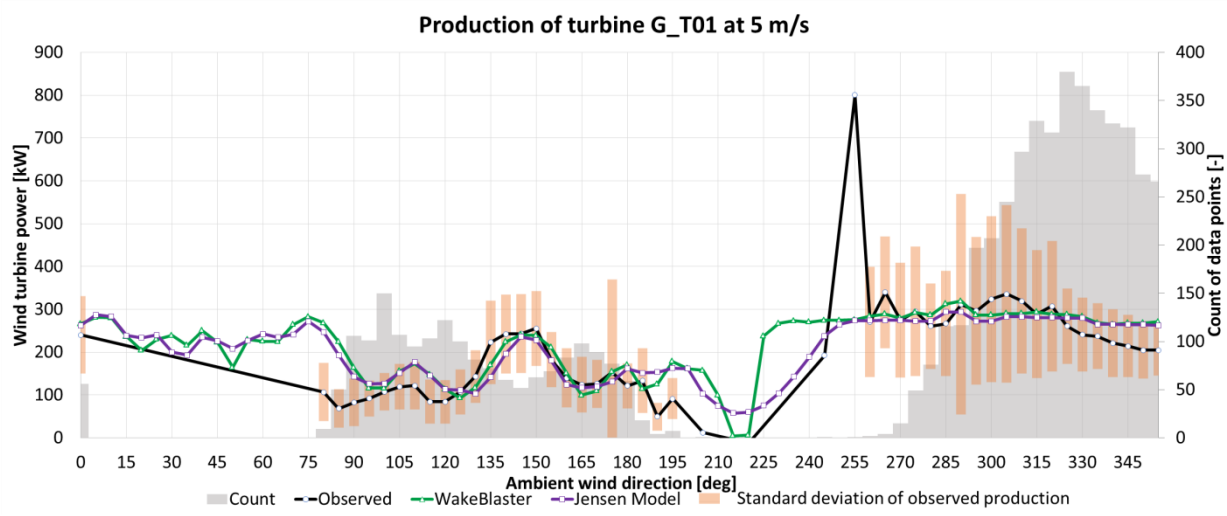

Figure 6-14: Production of turbine G_T01 at 5 m/s

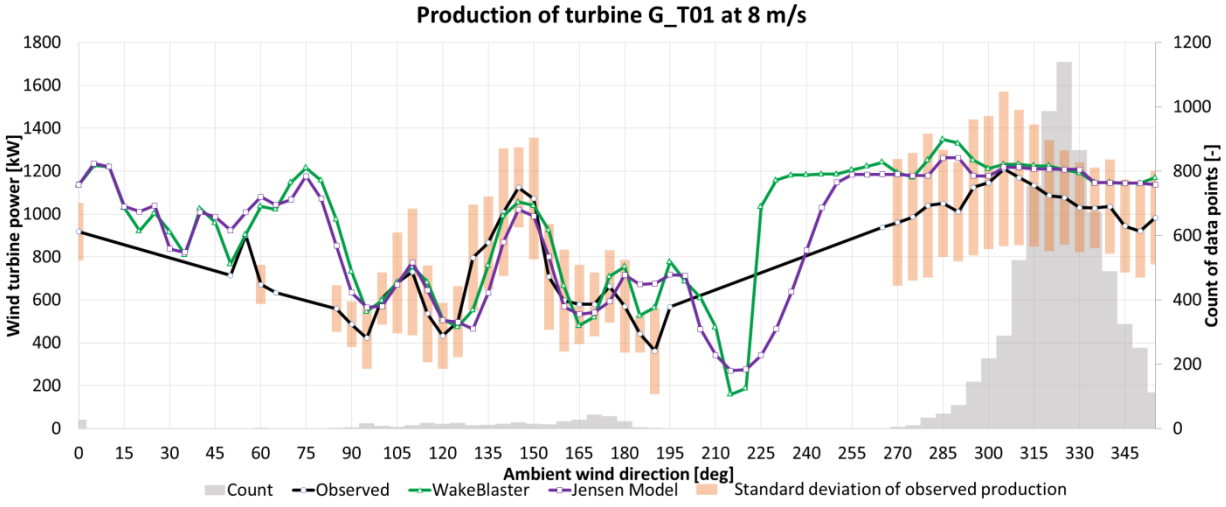

Figure 6-15: Production of turbine G_T01 at 8 m/s

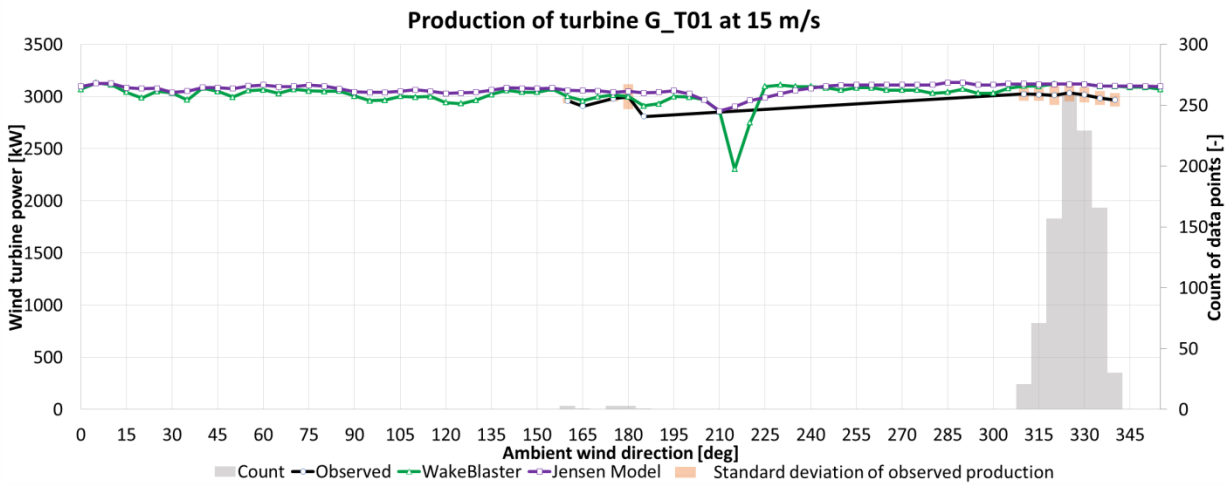

Figure 6-16: Production of turbine G_T01 at 15 m/s

To check other directions the production of turbine G_T06 is shown in figure 6-17. The modelled production fits the observed data for these sectors (90-180 deg) a lot better, even when there is still an overestimation.

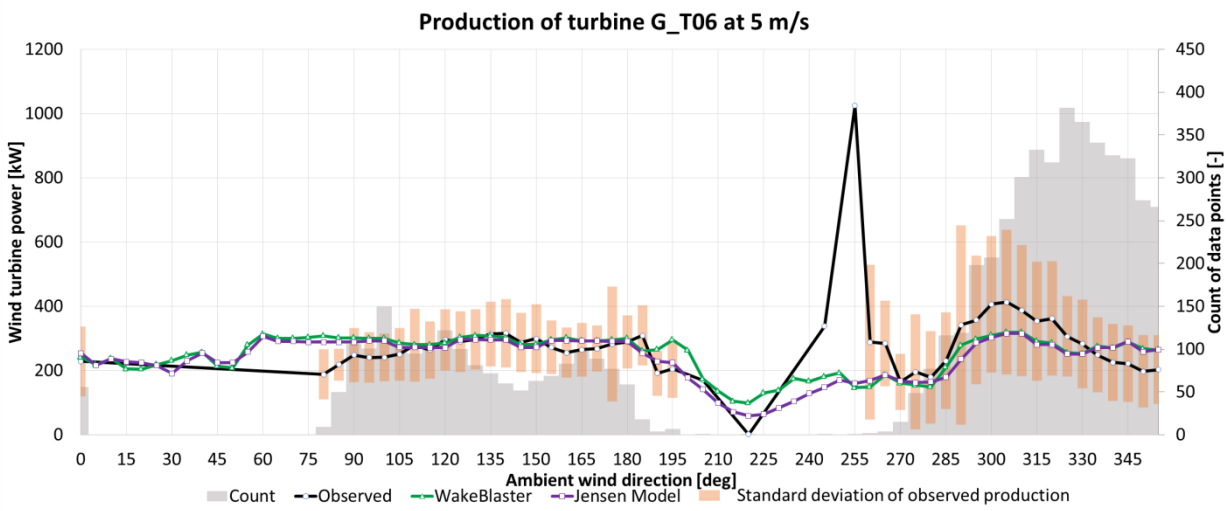

Figure 6-17: Production of turbine G_T06 at 5 m/s

The next turbine type that is analysed is the SWT-3.0-108. The production of turbine G_T04 is shown in figure 6-18, figure 6-19 and figure 6-20. G_T04 is also wake-free from 275 to 0 deg. The production is as well at this position overestimated. Nevertheless, the general trend is better matched then at G_T01.

The sectors from 90 to 180 deg are again waked and not analysed.

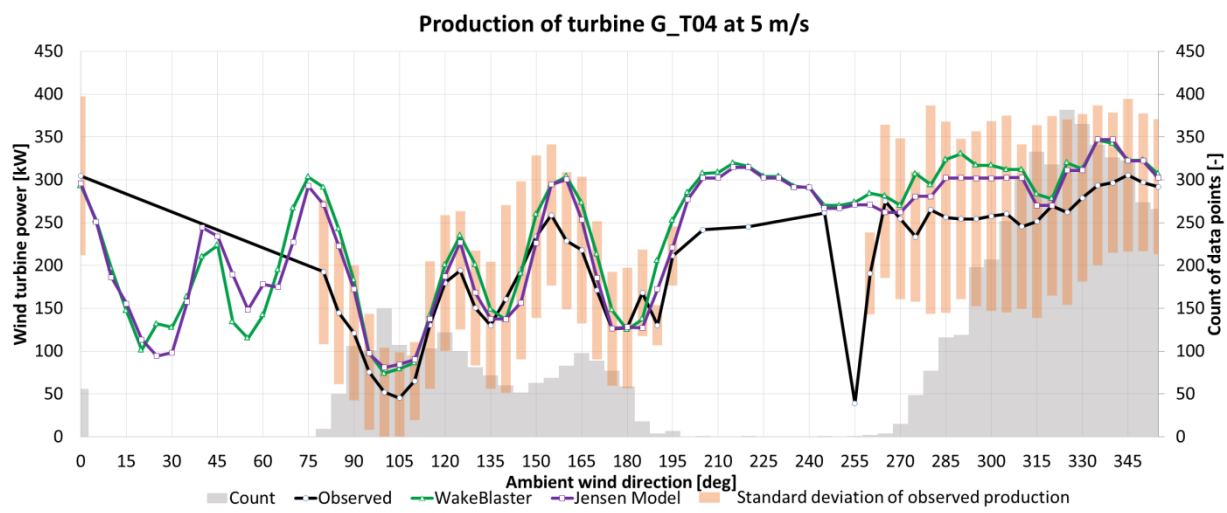

Figure 6-18: Production of turbine G_T04 at 5 m/s

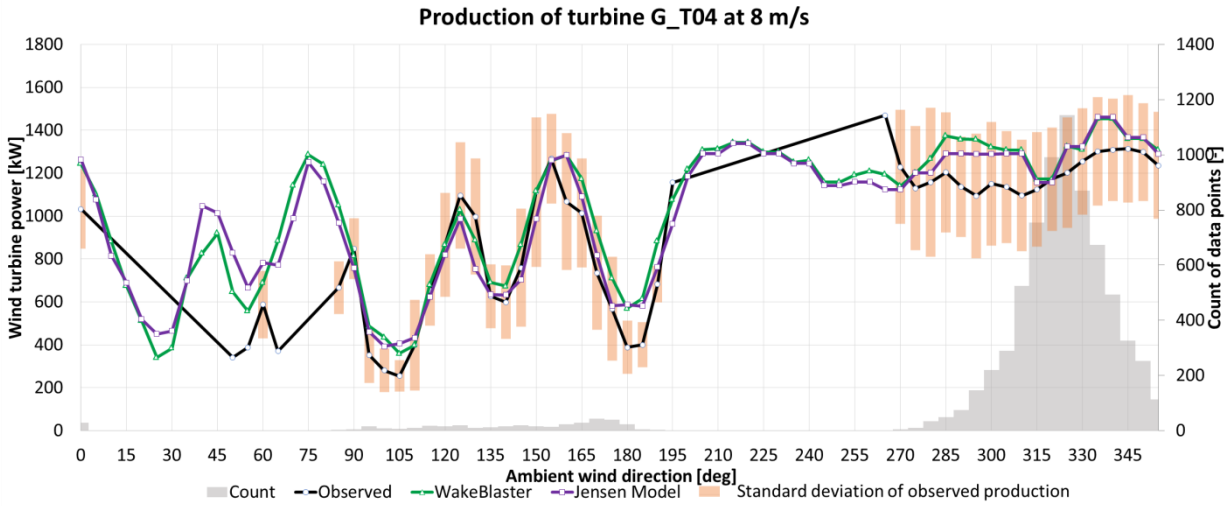

Figure 6-19: Production of turbine G_T04 at 8 m/s

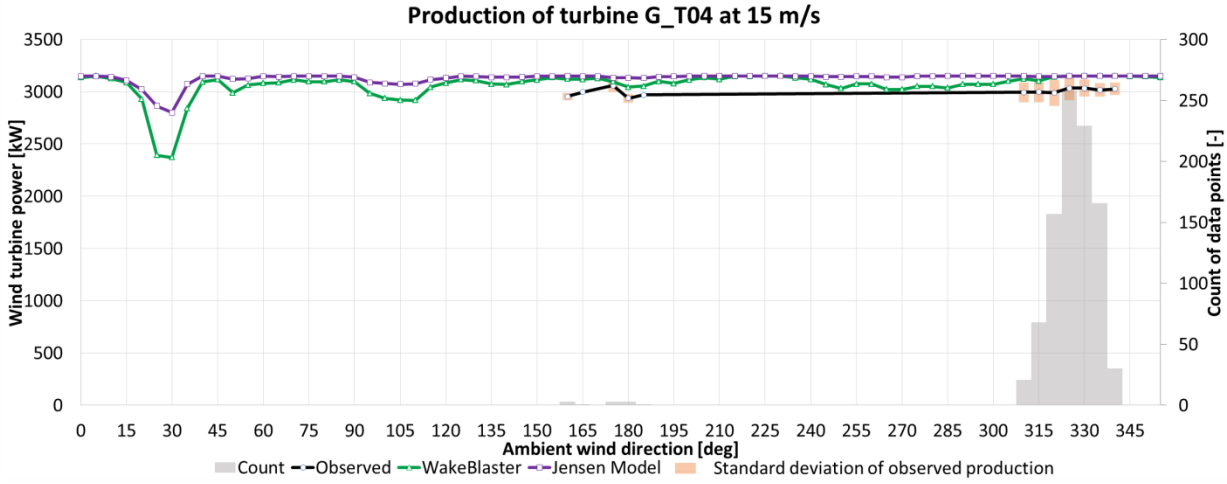

Figure 6-20: Production of turbine G_T04 at 15 m/s

The production of G_T05 in the wake-free sectors (90-180 deg) is again overestimated (figure 6-21). The modelled production follows the observed data well but is still too high.

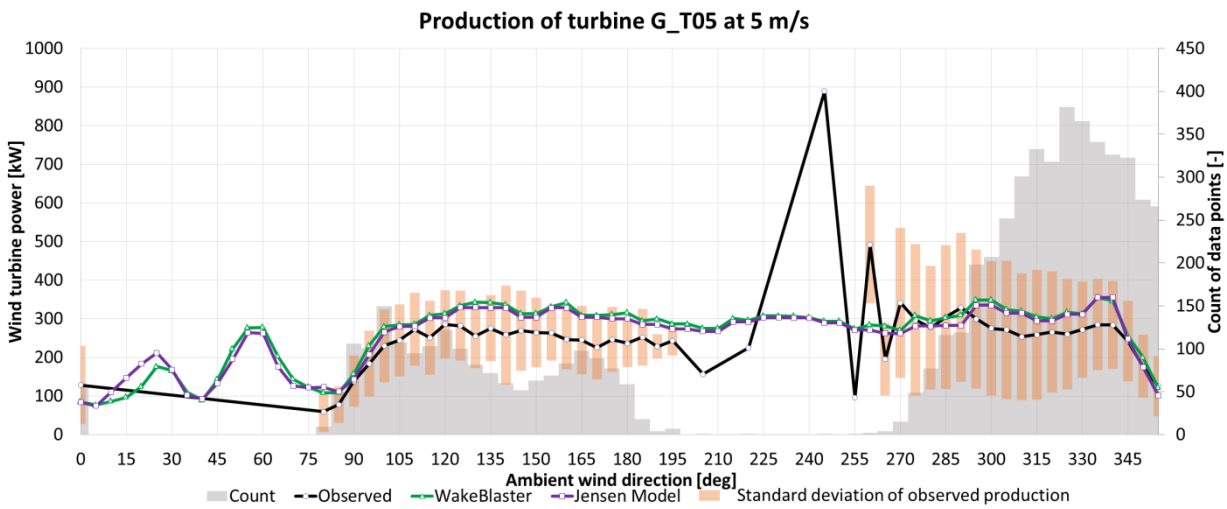

Figure 6-21: Production of turbine G_T05 at 5 m/s

Overall is the observed production overestimated and in some sectors even the general trend of the observed data is not matched. To analyse the wake models a calibration factor is used to lower the ambient wind speed like for Mount Lucas. The calibration factor equals 0.965.

6.2.2 Wind Farm Production and AEP

After analysing the wake-free sectors the next step is to evaluate the production and AEP of the whole wind farm. For the sectors from 90 to 180 deg is the production diagrammed for 5 m/s in figure 6-23. The production for the sectors from 275 to 0 deg is shown for wind speeds of 5, 8, 10 and 12 m/s (figure 6-24, figure 6-25, figure 6-26 and figure 6-27). Additionally is the production for all sectors at 8 m/s diagrammed in figure 6-22. The observed production is at some sectors zero because no data is available at these ones.

The highest wake losses are expected from around 30 deg because all SGRE turbines are then influenced by the neighbouring wind farm and are also directly placed behind each other. High wake losses are also expected by the opposite direction of 210 deg. The turbines are again positioned in a row but now without the influence of the neighbouring turbines. The other directions are nearly constant because the wake situation does not change that much. Most of the time is the half of the turbine just in a single wake of the turbine in front.

Both models show the assumed trend in figure 6-22. It is not possible to assess how well the models estimate the production for all sectors because of missing data but the graphs look reasonable.

The models are for all sectors and wind speeds really close to the observed data. This should be a matter of course because the wake situations that can be investigated are most of the time just simple single wakes. As known from Mount Lucas both models deliver reasonable results for this use case and the differences between them are small.

For the sectors from 90-180 deg (figure 6-23) are the deviations a little bit higher than for 275-0 deg. The wake situation is nearly the same so the additional deviations could be caused by the ambient wind extrapolation or the lower amount of data.

With increasing wind speed get the deviations lower (figure 6-24 to figure 6-27). The highest wake losses occur at 275, 315 and 350 degree, which is in coincidence with the layout. At these directions are nearly all second row turbines in full wakes of the upwind ones.

There are no sectors where the models show a different trend than the observed but at 320 deg the models underestimate the wake losses more than for the other sectors.

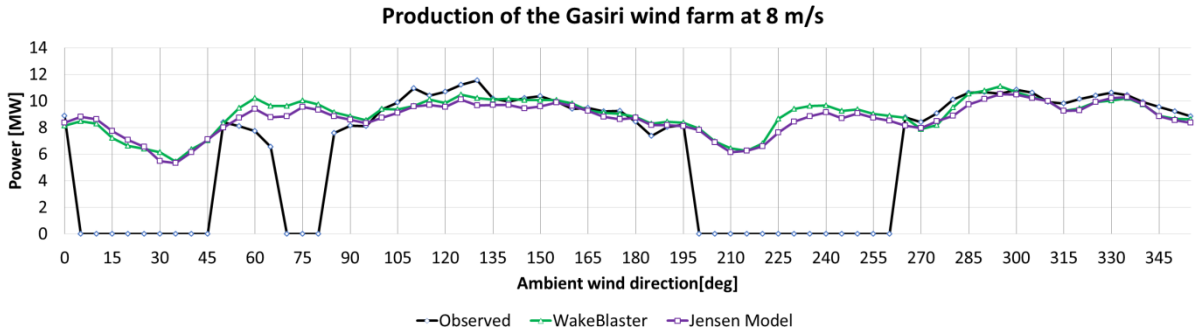

Figure 6-22: Production of the Gasiri wind farm at 8 m/s (0-360 deg)

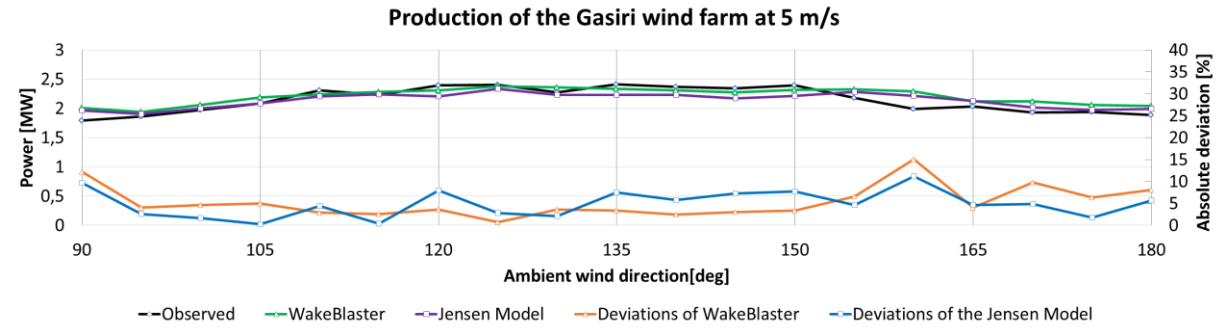

Figure 6-23: Production of the Gasiri wind farm at 5 m/s (90-180 deg)

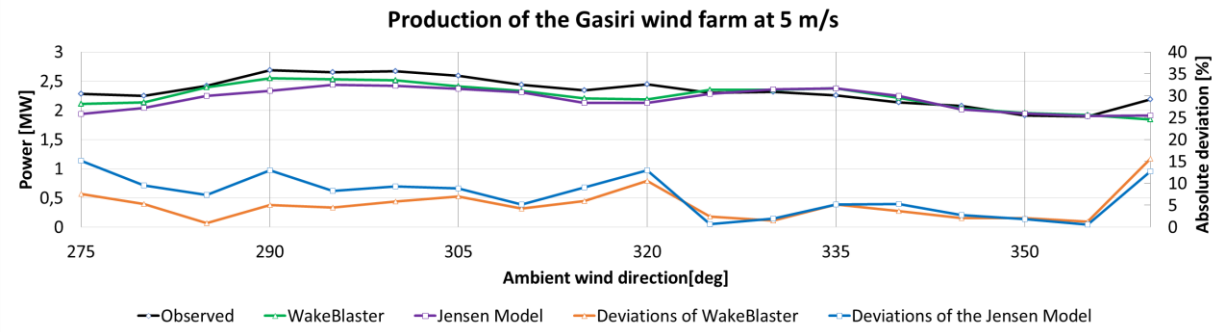

Figure 6-24: Production of the Gasiri wind farm at 5 m/s (275-0 deg)

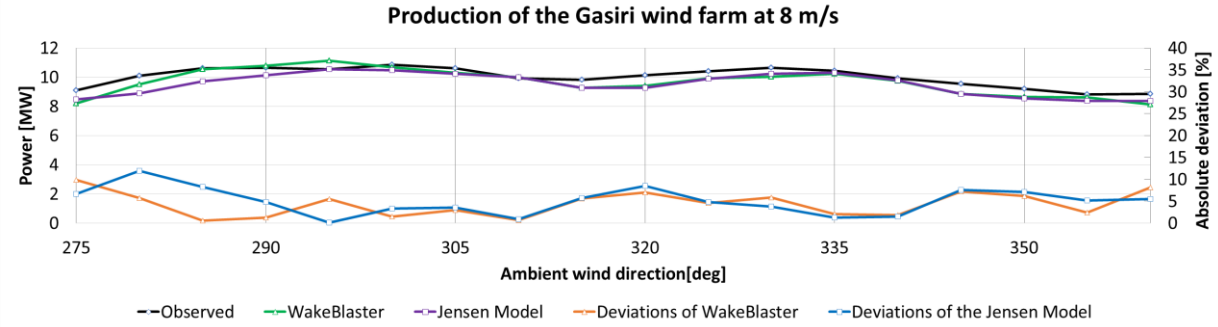

Figure 6-25: Production of the Gasiri wind farm at 8 m/s (275-0 deg)

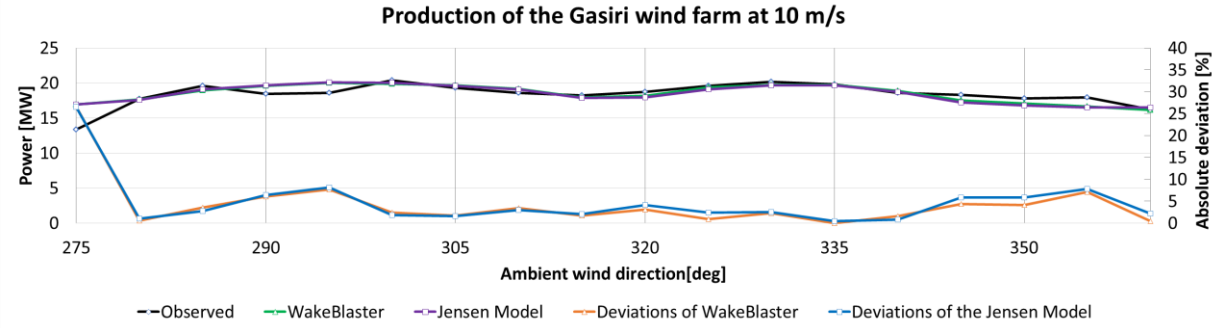

Figure 6-26: Production of the Gasiri wind farm at 10 m/s (275-0 deg)

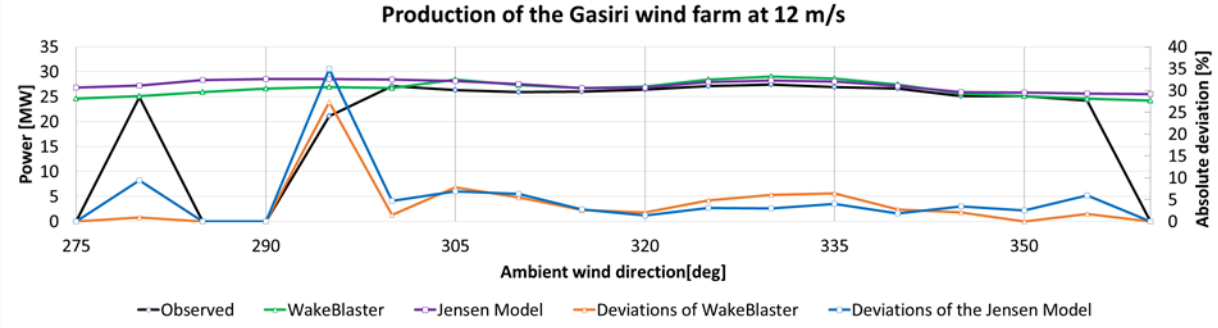

Figure 6-27: Production of the Gasiri wind farm at 12 m/s (275-0 deg)

The AEP is calculated in the same way as for Mount Lucas (chapter 6.1.3). The numbers are shown in table 6-2. All figures above show an overestimation of the production in nearly all sectors and wind speeds so the overestimated AEP is no surprise. The Jensen model is again close to the observed value. So the calibration was correct. Nevertheless, WakeBlaster is also very close to the observed AEP.

More interesting for the assessment of the models is again the absolute error. This time the Jensen Model shows a slightly lower value. However, in comparison to the absolute difference to of the AEP is WakeBlaster again better. This leads to the assumption that without a calibration to the Jensen Model the absolute error would be lower for WakeBlaster.

Table 6-2: AEP of the Gasiri wind farm

	Observed	Jensen Model	WakeBlaster
AEP [GWh]	90.74	90.64	91.33
Deviation [%]	-	0.11	-0.65
Absolute Error [GWh]	-	5.61	5.72

6.2.3 Sectorial Wake Losses

The annual wake losses (figure 6-29) do not show much new content because of the wind rose (figure 6-28). Nearly the whole wind is coming from the North-West. The resulting annual wake losses look corresponding to that very similar.

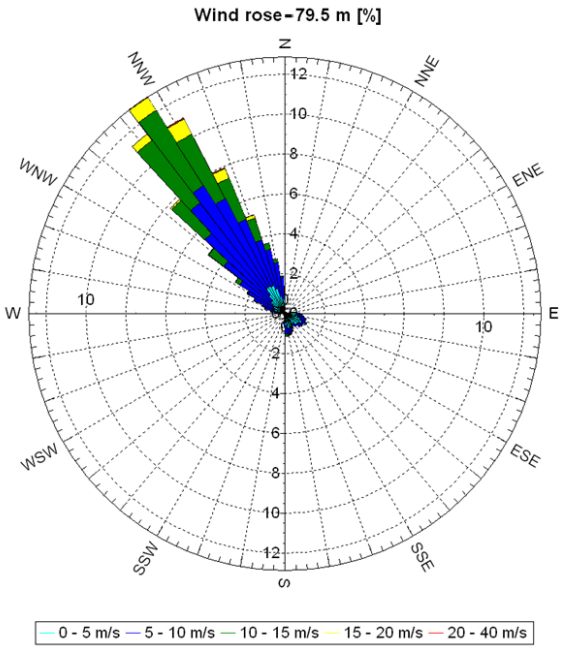

Figure 6-28: Wind rose of the SCADA mast of Gasiri

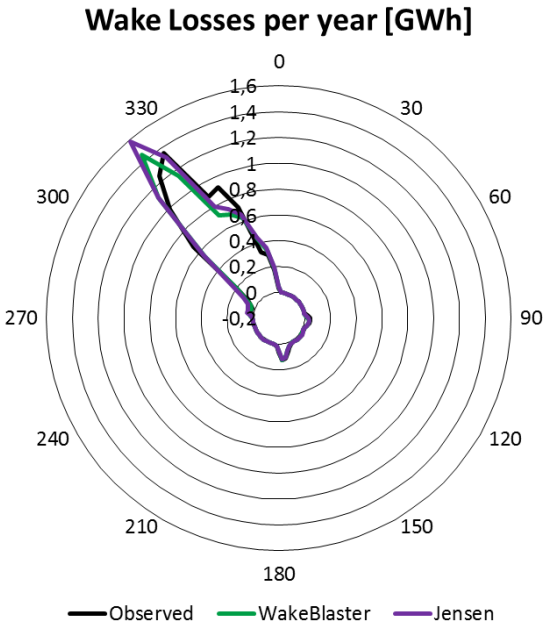

Figure 6-29: Sectorial wake losses per year for Gasiri

The comparison of the efficiency losses reveals more detail (figure 6-30). The models follow the observed trend from 275 to 0 deg well even when they are overestimating the wake losses. For the opposite sectors (90 to 180 deg) are the deviations of the models much bigger. This increase should be a result of the lower amount of data.

The results of the sectors without observed data look also reasonable. The highest efficiency losses appear around 30 and 210 deg. In both cases are the turbines directly located in a row

and these multiple wakes increase the losses. The losses are for 30 deg higher because the neighbouring wind farm is additionally influencing the turbines.

How precise the influence of the neighbouring wind farm is modelled is cannot be measured because of missing data. This is a disappointment because this type of use case cannot be validated.

The observed efficiency losses for different wind speeds are diagrammed in figure 6-31. The scheme of Gasiri differs from the one of Mount Lucas. Higher wind speeds to lower efficiency losses. Only for 10 m/s at 275 deg and 12 m/s at 295 deg the diagram shows something different but this can be explained with low data.

The revealed scheme fits better to the before explained theoretical basics. At higher wind speeds is the thrust coefficient lower which leads to lower wake losses. Even the lower TI values at higher wind speeds and through that a lower recovery rate cannot change that. It seems that through the dense spacing the lower velocity deficit is more important than the recovery rate.

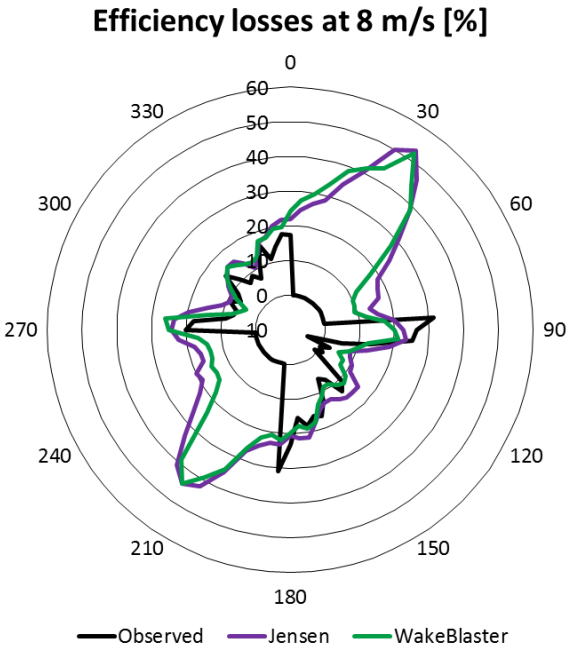

Figure 6-30: Sectorial efficiency losses of the Gasiri wind farm at 8 m/s

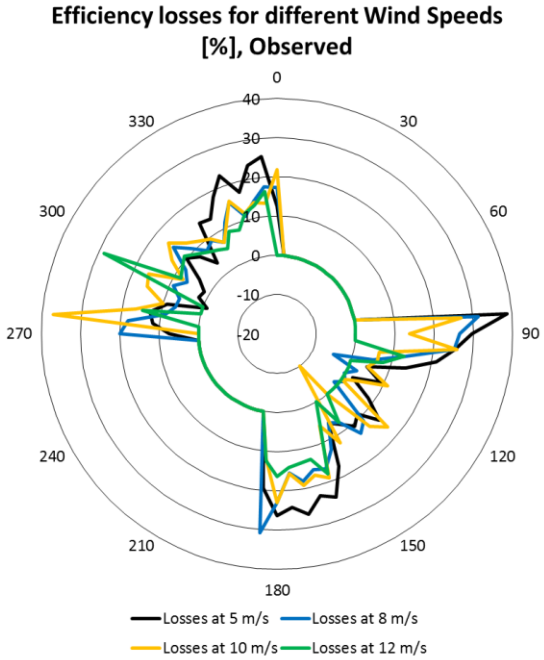

Figure 6-31: Observed sectorial efficiency losses of the Gasiri wind farm

6.2.4 Single Turbine Production

The last step is now to analyse the single turbines. Only the turbines G_T06 to G_T10 can be analysed because of the limitation of the data. The chosen turbines are G_T07, G_T08 and G_T09. These three turbines were chosen because they represent all for Gasiri typical wake cases. All turbines are investigated at 8 m/s.

G_T07 is waked at around 270 deg from G_T02 and around 305 deg from G_T01 (figure 6-32). Between these two directions are the wakes mixing. The mixing is the reason why the production is at 285 deg not as high as for the wake-free sectors like 330 deg. None of the models is estimating this situation really good. Nevertheless, the Jensen Model is estimating the minimum of the wake better than WakeBlaster. This is a surprise because at Mount Lucas WakeBlaster was a lot better at these situations. The peak of the single wake at 305 deg is matched very well by WakeBlaster while the Jensen Model is overestimating the production. The overestimation of the Jensen Model is a surprise because at Mount Lucas it was most of the time underestimating the production at the peaks. This could be explained with a different WDC or the different spacing.

The peak of the wake at 270 deg cannot be analysed because of missing data.

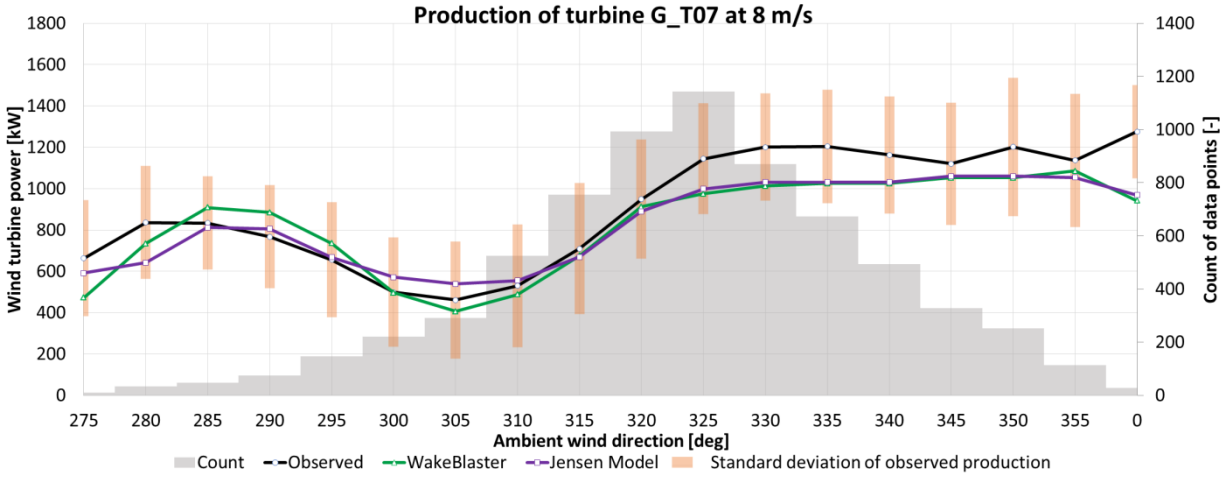

Figure 6-32: Production of turbine G_T07 at 8 m/s

The wake situation is at G_T08 very similar. It is single waked from 270, 315 and 345 deg. The production is shown in figure 6-33. The wakes from 315 and 345 deg are estimated nearly similar from both models, even when WakeBlaster is slightly better. Nevertheless, the wake from 345 deg is from both models clearly overestimated.

The wake at 270 deg cannot be analysed because of missing data.

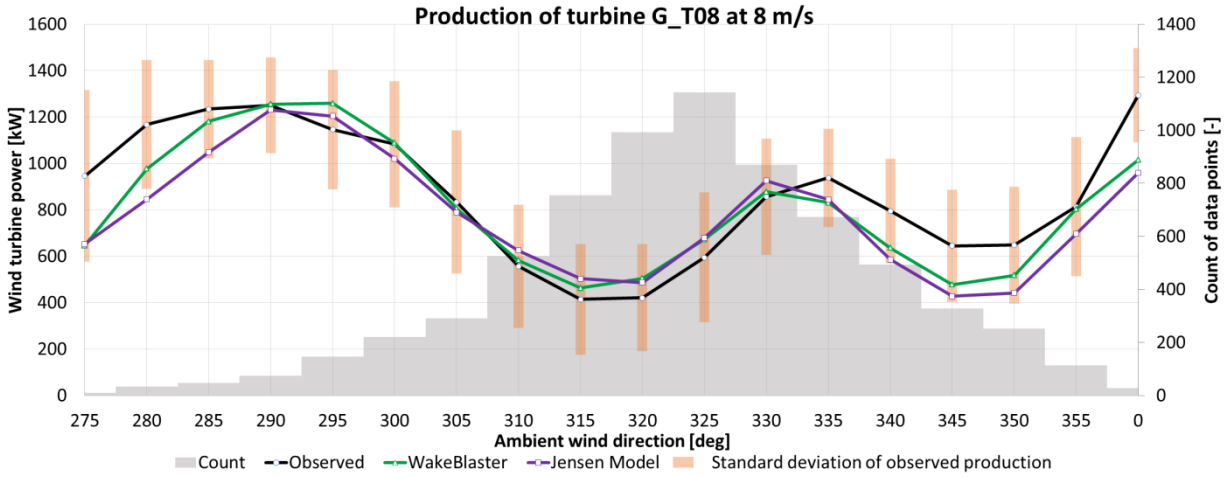

Figure 6-33: Production of turbine G_T08 at 8 m/s

The last analysed turbine is G_T09 (figure 6-34). It is again single waked by three turbines. The wakes arise from 280, 335 and 0 deg.

The wakes from 280 and 335 deg are well matched by the models while the production for the one at 0 deg is underestimated. It seems that the production is in general underestimated around 345-0 deg. This is the case for all three turbines even when G_T07 is not waked from this direction. It could be that the deviations at these sectors do not come from the wake models.

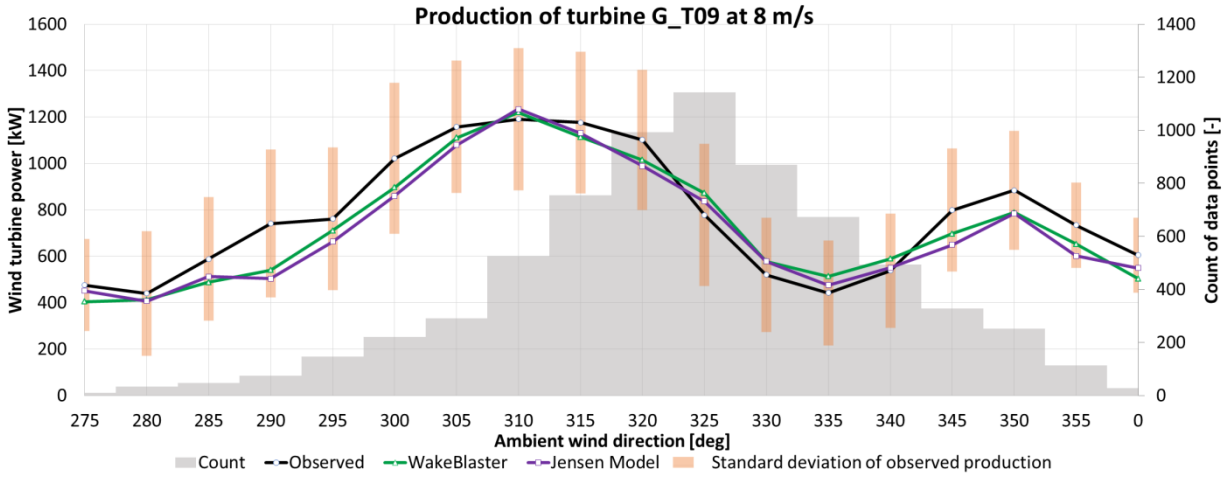

Figure 6-34: Production of turbine G_T09 at 8 m/s

6.2.5 Conclusion of the Gasiri Wind Farm

Gasiri was harder to analyse and the amount of outcome is lower than for Mount Lucas. A positive point is that also for the close layout both models were able to calculate the production of the turbines correctly. The recovery of the wind speed is not so important for this layout. Nevertheless, it seems that the momentum sink is estimated well from both models.

Both wake models delivered nearly identical results for most of the cases. This makes it difficult to analyse the strengths of the model. Also, the fact that the ambient wind speed extrapolation was worse than for Mount Lucas, even with the calibration factor, complicate the investigation.

Another reason for the deviations of the models at certain sectors could be that the TI of the met mast is not representative for the whole wind farm. This TI was used to calculate the WDC and to combine the different WakeBlaster results. It could make a big difference if another source for the TI would be used.

WakeBlaster is again calculation a slightly higher production than the Jensen Model but this time both models are closer together than for Mount Lucas.

7 Additional Work

This chapter contains information that is not directly linked with the observed data. Nevertheless, it shows the importance of wake models for the wind industry and their sensitivity to TI inputs.

7.1 Layout Improvement

This chapter will give attention to the aspect of layout improvements. This part was done only for Mount Lucas because of the low amount of data for Gasiri. The idea is really simple. It should be shown that the AEP can be increased when the layout is improved. To limit the number of variables and make the layouts comparable the only possibility was to rotate the layout. So the spacing is kept constant.

The influence of the topography and orography should be for the rotated layout acceptable small. The main aspect is to reduce the annual wake losses.

The layout was rotated counter clockwise in 5 deg steps. The production was then calculated with the Jensen Model. WakeBlaster would have needed too much time. The layout was only rotated around 90 deg. The additional amount of gained information a further rotation would not justify the additional effort.

The annual wake losses at different points of the rotation are shown in figure 7-1. The wake-free production that was used to calculate the wake losses was the one from the original layout. The minimum annual wake losses are 20.84 GWh at -75 deg rotation (figure 7-2) compared to 32.91 GWh from the original layout. To realise how much this is, the difference between these two values will be calculated and transformed to money. First is the additional gained energy calculated (7-1). Then is the additional gained money per year calculated (7-2). The last formula multiplies the annual gained money with the operational period (7-3). This period is assumed with 20 years even when to trend goes to 25 or 30 years.

The price used for the calculation equals 7.49 ct/kWh. [57]

$$Original\ Wake\ Losses - Minimum\ Wake\ Losses = Gained\ Engery$$
$$32.91\ GWh - 20.84\ GWh = 12.07\ GWh \quad (7\text{-}1)$$

$$Gained\ Energy * Energy\ Price = Gained\ Money$$
$$12.07\ GWh * 7.49\ \frac{ct}{kWh} = \ 904\ 195.44\ € \quad (7\text{-}2)$$

$$Gained\ Money * Operating\ Period = Gained\ Money\ for\ Operating\ Period$$
$$904\ 195.44 * 20\ Years = \ 18.08\ Mio\ \ € \quad (7\text{-}3)$$

Over the whole operating period the additional gain would be 18.08 Mio. €.

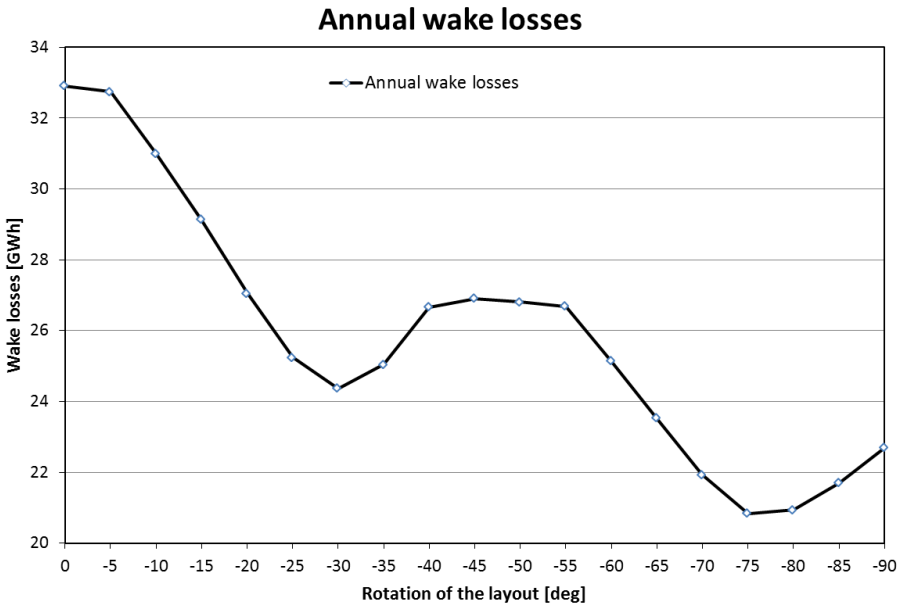

Figure 7-1: Annual wake losses of Mount Lucas with the rotated layout

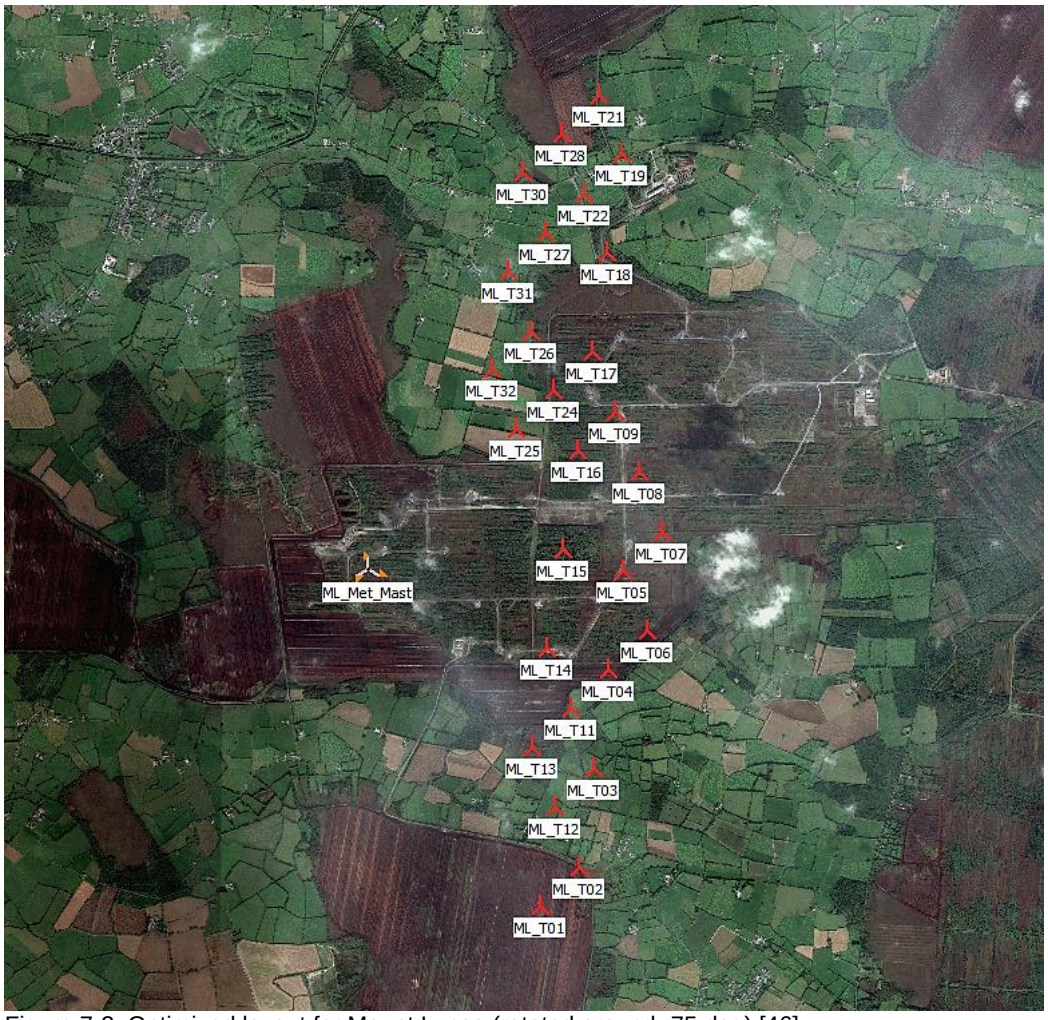

Figure 7-2: Optimized layout for Mount Lucas (rotated around -75 deg) [46]

7.2 Turbulence Sensitivity

The standard approach for energy calculations in the Siting department of SGRE is to use the Jensen Model with a WDC of 0.075 for all sectors. The idea of this chapter is to show the influences of the TI for the models and arouse interest for a more precise TI and WDC approach.

The production at Mount Lucas was calculated for different ambient TI or corresponding WDC values. The values are listed in table F-1. The results are shown for ML_T11 because of it different wake scenarios. The results of the Jensen Model are shown in figure 7-3 and the ones of WakeBlaster in figure 7-4.

Two things that can be clearly seen are that a correct TI input is essential for an acceptable result and that the Jensen Model is more sensitive to the TI. The difference between the two extreme TI graphs is for the Jensen Model twice as big as for WakeBlaster.

With the amount of data it is not possible to conclude which model correlates better to the reality. However, it was shown that the TI has to be treated with care for both models.

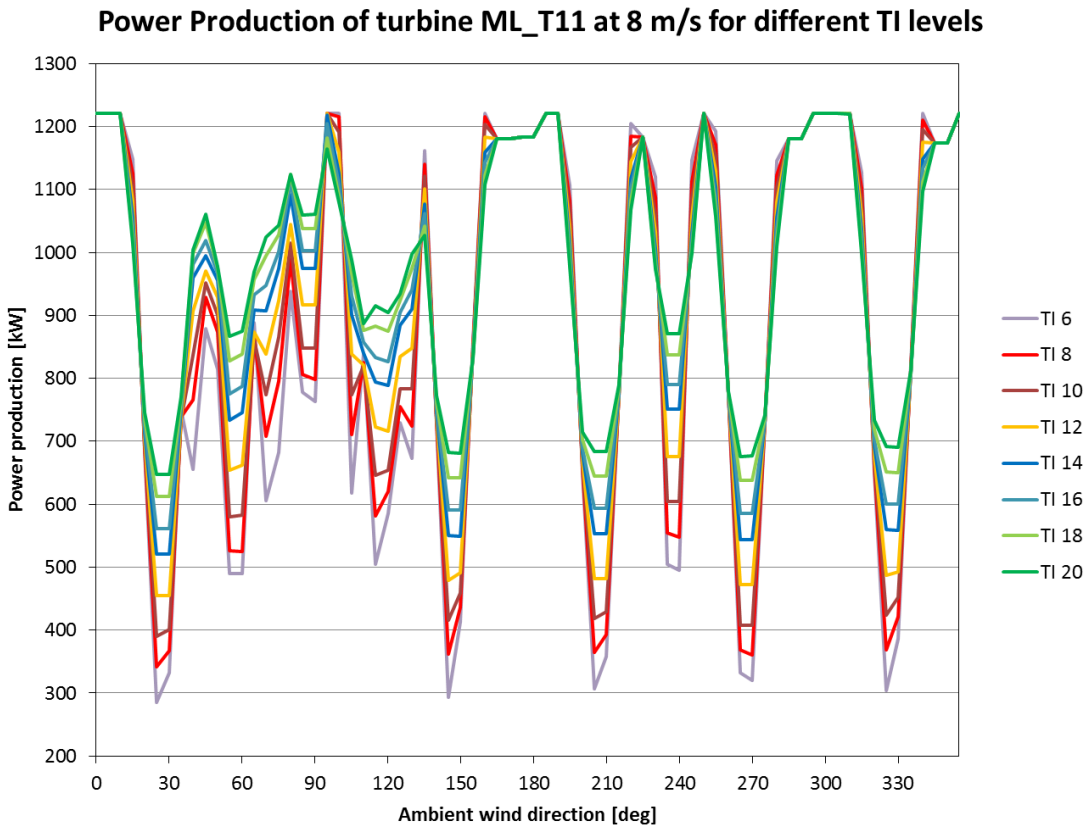

Figure 7-3: Turbulence intensity sensitivity of the Jensen Model

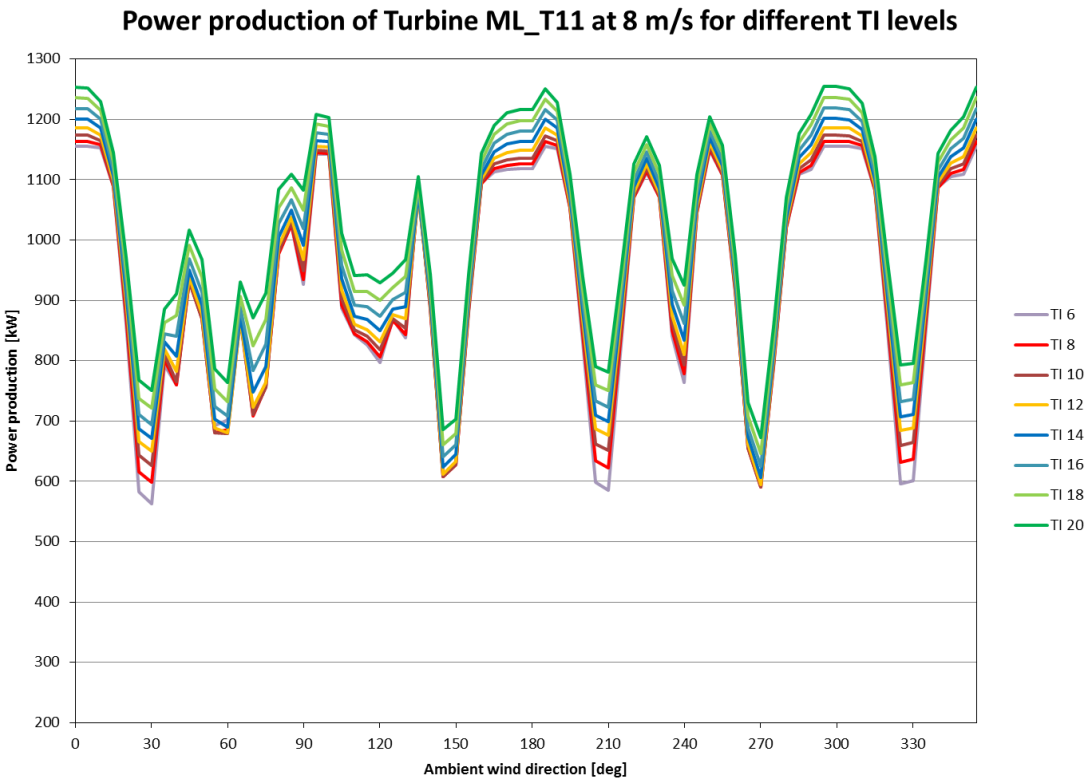

Figure 7-4: Turbulence intensity sensitivity of WakeBlaster

8 Discussion

This chapter is used to reveal the essentials of this thesis. It starts with the limitation of the study and goes on with the implications which include recommendations for the business practice and suggestions for future research.

8.1 Limitation of the Study

Like for all challenging topics not all aspects could be investigated to the full satisfaction of the researcher. The time and budget are limited. Also, the models have limitations.

The budget and time restrictions made it impossible to visit the sites. Through that all assumptions regarding roughness and forestry rely on images from Google Earth and Street. Additionally, the topography map was just in shuttle radar topography mission (SRTM) quality available. This introduces uncertainties for the ambient wind flow extrapolation. A topography map with a higher resolution would have been nice but for the simple sites it is acceptable.

Also that WakeBlaster is at the moment only able to calculate 2000 lines of measurement data at once limited the study. A time series based calculation is without a massive expenditure of time not possible.

Another limitation of WakeBlaster is that its results are only valid after two rotor diameter. This is a problem when the turbines are closer together like for Gasiri (G_T06 and G_T07). Then the production is calculated without a wind speed reduction. In the practice this should not be a problem because the yield from so close turbines should be low for the affected sector. Nevertheless, it has to be taken into account.

The Jensen Model does not calculate the additional TI that is induced through the upwind turbines. Through that the recovery of the wind speed is underestimated which increases with the number of upwind turbines. This phenomenon is visible at Mount Lucas for 90 and 270 deg. The Jensen Model is overestimating the wake losses because it does not take the increased wind speed recovery into account. Additionally, the Jensen Model itself is not usable as a base for load calculation because of the missing TI calculation. WakeBlaster is able to do that. How good WakeBlaster's TI calculation is needs to be verified in the future.

Additionally, the Jensen Model is trimmed for medium sized wind farms like Mount Lucas. Through the over- and underestimation at different positions is the overall AEP most of the time matched well. For much smaller or bigger wind farms this is not valid anymore.

8.2 Implications

8.2.1 Recommendation for Business Practice

It is difficult to conclude that one wake model is superior to the other. Both have their strengths and weaknesses. WakeBlaster delivers in most of the cases better results. Especially, when the production is influenced by multiple wakes WakeBlaster should be used. Nevertheless, the Jensen Model is competitive for the production of the complete wind farm.

An approach could be that the Jensen Model is used for the general layout optimisation and for the detailed part WakeBlaster is used. At the beginning of a site assessment are several configurations taken into account and for now it would take too long to use WakeBlaster for this part. However, for a deep analysis of the turbines is the improved accuracy of WakeBlaster an advantage.

Summarising the results; WakeBlaster is at different wake scenarios always close to the observed production and can be assumed valid.

A recommendation for the practice is to improve the speed of the Excel sheet “02_Matrix”. The calculation time was ok for a research project but not for daily usage.

8.2.2 Suggestions for Future Research

The first thing that should be done and is already planned is to compare the results and conclusions of this thesis with other wind farms. An important point is how WakeBlaster behaves in complex terrain.

Furthermore, the TI values of the preconstruction met mast were assumed as representative for the whole site. The first aspect regarding this topic would be to check if this is true and the second one if other sources like the roughness map would deliver better results.

Once WakeBlaster is updated and able to calculate more measurements in one run the time series approach should be tested to improve the precision of the results. Also periods of curtailment could be included with this approach. Additionally, a comparison regarding the TI and wind speed reduction is possible with a time series based approach.

9 Conclusion

The aim of this thesis was to simulate two wind farms and compare the results of the wake models with several years of observed data and derive a statement about the validity of WakeBlaster. The ambient wind conditions are in the majority of the cases only known at one point. To extrapolate them different models can be used. The basics for these models were explained at the beginning of this thesis. Also, a simple actuator disc model was introduced to describe how a turbine is generating energy from the wind.

The next step was to define why this topic is essential for the wind industry. This was followed by the theory about the wakes. This chapter defined the near and far wake and the main influences on the wake development.

This gained knowledge then was expanded with the basic principles of wake modelling. This includes the representation of the rotor, different wake models and an excursus to the turbulence models.

All these chapters are necessary to understand and interpret the results of the models correctly.

The next stage was to introduce how the observed data from the wind farms were measured and filtered. All periods of curtailment were excluded to decrease the number of simulations and simplify the comparison of the results. Also, the two wind farms and the power matrix method were introduced. The last part before the simulation could start was to set up the models.

The results were compared in three stages. First, the wake-free sectors of the models are compared to the observed data to define a calibration factor for the ambient wind speed that was used as input. This should reduce the deviations of the ambient wind speed extrapolation to a minimum. The deviations of the calibrated results should result mostly from the wake models. The calibrated production is then compared for the whole wind farm at different wind speeds. Also the AEP and absolute error were derived and analysed. The last step is then to investigate the single turbine results.

For Mount Lucas the analysis was impossible at wind speeds above 12 m/s and for Gasiri the only valid directions for all wind speeds are 275-0 deg because of curtailments.

WakeBlaster estimated in general values closer to the observed production of the single turbines. Also, the assumed strength of WakeBlaster at multiple wakes could be validated. The AEP values should be treated with care because they are highly dependent on the calibration factor and say nothing about the quality of the wake model.

More detail about the quality of the models is revealed with the absolute error. WakeBlaster derived a smaller value for Mount Lucas and for Gasiri just a slightly higher one. This underlines that WakeBlaster is better suited for the entity of the researched wake cases.

The most important point for the future is to investigate other and more complex sites. Additionally, the power matrix approach should be replaced with a time series based one to increase the precision of the calculation and allow to analyse also periods with curtailment.

WakeBlaster was assumed valid for these two sites because it predicted always reasonable results with small deviations to the observed values.

References

[1] B. Sanderse, Aerodynamics of wind turbine wakes Literature review, ECN Wind Energy, 2009.

[2] S.-E. Dr. Scient. and PhD Gryning, “Coursera,” Technical University of Denmark, [Online]. Available: https://www.coursera.org/learn/wind-energy/lecture/wpRiT/wind-profiles. [Accessed 5 March 2018].

[3] M. H. Zhang, Wind Ressource Assement And Micro-Siting, John Wiley & Sons Singapore Pte. Ltd., 2015.

[4] International Electrotechnical Commission, IEC 61400-1 Ed. 3 Wind turbines - Part 1: Design requirements., 3 ed., International Electrotechnical Commission, 2010.

[5] Y.-T. Wu and F. Porté-Agel, “Atmospheric Turbulence Effects on Wind-Turbine Wakes: An LES Study,” *energies,* no. 5, pp. 5340-5362, 2012.

[6] B. Cushman-Roisin, Environmental Fluid Mechanics, Hannover, New Hampshire: John Wiley & Sons, Inc., 2014.

[7] M. C. Holtslag, W. A. A. M. Bierbooms and G. J. W. van Bussel, “Estimating atmospheric stability from observations and correcting shear models accordingly,” *Journal of Physics: Conference Series,* no. 555, p. 012052, 9-11 October 2014.

[8] W. Tian, A. Ozbay and H. Hu, “Terrain effects on characteristics of surface wind and wind turbine wakes.,” *Procedia Engineering,* no. 126, pp. 542-548, 2015.

[9] S. Dr. Schmitz, “e-education Pennsylvania State University,” [Online]. Available: https://www.e-education.psu.edu/aersp583/node/470. [Accessed 13 March 2018].

[10] B. McCormick, Aerodynamics of V/STOL flight, Dover Publications Inc., 1999.

[11] J. F. Manwell, J. G. McGowan and A. L. Rogers, Wind Energy Explained: Theory, Design and Application, 2 ed., John Wiley & Sons, 2010.

[12] L. J. Vermeer, J. N. Sørensen and A. Crespo, “Wind turbine wake aerodynamics,” *Progress in Aerospace Sciences,* no. 39, pp. 467-510, 2003.

[13] T. Grayson, “BoundVortex,” 2008. [Online]. Available: http://www.boundvortex.com/ReadArticle.aspx?ArticleID=53. [Accessed 14 March 2018].

[14] “Wikipedia,” 2017. [Online]. Available: https://en.wikipedia.org/wiki/Helmholtz%27s_theorems?old format=true. [Accessed 14 March 2018].

[15] F. Porté-Agel and L. P. Chamorro, “A Wind Tunnel Investigation of Wind-Turbine Wakes: Boundary-Layer Turbulence Effects,” *Boundary-Layer Meteorology,* no. 132, pp. 129-149, 2009.

[16] M. Bastankhah and F. Porté-Agel, “A new analytical model for wind-turbine wakes,” *Renewable Energy,* no. 70, pp. 116-123, 2014.

[17] P. Hashemi Tari, Near-Wake Flow Dynamics of a Horizontal Axis Wind Turbine, London, Ontario: University of Western Ontario, 2012.

[18] H. Schümann, F. Pierella and L. Sætran, “Experimental investigation of wind turbine wakes in the wind tunnel,” *Energy Procedia,* no. 35, pp. 285-296, 2013.

[19] L. E. M. Lignarolo, D. Ragni, C. Krishnaswami, Q. Chen, C. Simão Ferreira and G. J. W. van Bussel, “Experimental analysis of the wake of a horizontal-axis wind-turbine model,” *Renewable Energy,* no. 70, pp. 31-46, 2014.

[20] F. Mühle, M. S. Adaramola and L. Sætran, “The effect of the number of blades on wind turbine wake – a comparison between 2-and 3-bladed rotors,” *Journal of Physics: Conference Series,* no. 753, p. 032017, 2016.

[21] M. Abkar and F. Porté-Agel, “The effect of atmospheric stability on wind-turbine wakes: A large-eddy simulation study,” *Journal of Physics: Conference Series,* no. 524, p. 012138, 2014.

[22] M. Damaschke, C. Illig, F. Stache and F. Prof. Dr. Baumjohan, “Damage Increase by Wind Farm Operation: Measurement versus Simulation,” in *DEWEK 2004*, Wilhelmshaven, 2004.

[23] J. Koutroumpas and K. Koutroumpas, “Optimal wind farm sitting using high-resolution digital elevation models and randomized optimization,” *AIMS Energy,* no. 3, pp. 505-524, 2015.

[24] M. L. Thøgersen, T. Sørensen, P. Nielsen, A. Grötzner and S. Chun, WindPRO / PARK Introduction to Wind Turbine Wake Modelling and Wake Generated Turbulence, 1 ed., Aalborg: EMD International A/S, 2005.

[25] R. Barthelmie, S. Frandsen, O. Rathman, K. Hanse, E. Politis, P. J., J. Schepers, K. Rados, D. Cabezon, W. Schlez, A. Neubert and M. Heath, Flow and wakes in large wind farms: Final report for UPWIND WP8. Technical Report Risø-R-1765 (EN), Roskilde: Danmarks Tekniske Universitet, Risø Nationallaboratoriet for Bæredygtig Energi, 2011.

[26] B. Hu, Design of a Simple Wake Model for the Wind Farm Layout Optimization Considering the Wake Meandering Effect, Delft: Delft University of Technology, 2016.

[27] D. Medice, Experimental Studies of Wind Turbine Wakes - Power Optimisation and Meandering, Stockholm: KTH Mechanics, Royal Institute of Technology, 2005.

[28] G. C. Larsen, H. Aagaard Madsen, F. Bingöl, J. Mann, S. Ott, J. Sørensen, V. Okulov, N. Troldborg, M. Nielsen, K. Thomsen, T. Larsen and R. Mikkelsen, Dynamic wake meandering modeling, Roskilde: Risø National Laboratory, 2007.

[29] M. T. van Dijk, J.-W. van Wingerden, T. Ashuri, Y. Li and M. A. Rotea, “Yaw-Misalignment and its Impact on Wind Turbine Loads and Wind Farm Power Output,” *Journal of Physics: Conference Series,* no. 753, p. 062013, 2016.

[30] F. Porté-Agel, H. Lu and Y.-T. Wu, “Interaction between large wind farms and the atmospheric boundary layer,” *Procedia IUTAM,* no. 10, pp. 307-318, 2014.

[31] F. Porté-Angel, Y.-T. Wu, H. Lu and R. J. Conzemius, “Large-eddy simulation of atmospheric boundary layer flow through wind turbines and wind farms,” *Journal of Wind Engineering and Industrial Aerodynamics,* no. 99, pp. 154-168, 2011.

[32] Smilesgiles89, “Wikipedia,” 23 January 2013. [Online]. Available: https://en.wikipedia.org/wiki/Blade_element_momentum_theory. [Accessed 27 March 2018].

[33] M. O. Hansen, Aerodynamics of Wind Turbines Second Edition, Padstow, United Kingdom: Earthscan, 2008.

[34] Deparment of Wind Energy, Technical University of Denmark, WAsP 11 Help Facility and On-line Documentation, 2014.

[35] I. &. L. P. E. Troen, European Wind Atlas, Roskilde: Risø National Laboratory, 1989.

[36] D. Prof. Dr.-Ing. Schulze, Computational Fluid Dynamics, Sommer 2017 ed., Hamburg: HAW Hamburg, 2017.

[37] A. Bengt, R. Andersson, L. Håkansson, M. Mortensen, R. Sudiyo and B. van Wachen, Computational Fluid Dynamics for Enginners, Cambridge: Cambridge University Press, 2012.

[38] ProPlanEn Ltd., *Product Presentation - What is WakeBlaster? - How can WakeBlaster help you?,* 2017.

[39] R. T. Bayo and G. Parro, “Site suitability asessment with dynamic wake meandering model. A certification point of view,” *Energy Procedia,* no. 76, pp. 177-186, 2015.

[40] D. J. Renkema, Validation of wind turbine wake models using wind farm data and wind tunnel measurements, Delft University of Technology, 2007.

[41] J. Ainslie, “Calculating the flowfield in the wake of the wind turbines,” *Journal of Wind Engineering and Industrial Aerodynamics,* no. 27, pp. 213-224, 1988.

[42] P. E. J. Vermeulen, “An experimental analysis of wind turbine wakes,” in *International Symposium on Wind Energy Systems*, Lyngby, 1980.

[43] P. Bradstock, W. Schlez, M. Tinning and S. Lindahl, *Working With WakeBlaster,* ProPlanEn, 2018.

[44] W. Schlez and P. Bradstock, Interviewees, *Theoretical Background of WakeBlaster.* [Interview]. June 2018.

[45] ProPlanEn Ltd., WakeBlaster Getting Started Guide, ProPlanEn, 2018.

[46] N. Stergiannis, J. van Beeck and M. C. Runacres, “Full HAWT rotor CFD simulations using different RANS turbulence models compared with actuator disk and experimental measurements,” Wind Energi Science Discussions, https://doi.org/10.5194/wes-2017-6, 2017.

[47] M. Laegdsmand, “Get SCADA met mast data,” Siemens Gamesa Renewable Energy, 26 October 2017. [Online]. Available: http://dkbdkb7app004x.ww007.siemens.net:3838/ParkMetDataTo WindPRO/. [Accessed 7 May 2018].

[48] W. Schlez and S. Lindahl, Due Diligence Process and Post Construction Analysis (Internal Document), ProPlanEn, 2018.

[49] W. Schlez and S. Lindahl, Methodology Review (Internal Document), ProPlanEn, 2017.

[50] N. Burillo, “Mount Lucas Climatic Conditions Review,” Siemens Gamesa Renewable Energy, 2012.

[51] Google Inc., Digital Globe, *Background map of Mount Lucas wind farm,* 2018.

[52] West wind, Mountlucas Mast Installation Report - May 2006, West wind, 2006.

[53] Bord Na Mona Energy Limited, “Mountlucas & Bruckana Wind Farms Specification for:ELECTRICAL BALANCE OF PLANT,” Bord Na Mona Energy Limited, 2010.

[54] N. Shen, “Turbine Suitability Review Gasiri,” Siemens Gamesa Renewable Energy, 2013.

[55] Google Inc., DigitalGlobe, SK Energy, *Background map of Gasiri wind farm,* 2018.

[56] N. Shen, “WindPRO Project Gasiri,” Siemens Gamesa Renewable Energy, 2014.

[57] N. Shen, “Technical Note Gasiri,” Siemens Gamesa Renewable Energy, 2016.

[58] P. Nielsen, P. Madsen, T. Sørensen, K. Bredelle, T. Sørensen, L. Svenningsen and P. Møller Nielsen, windPRO 3.1 User guide, Aalborg: EMD International A/S, 2016.

[59] A. Albers, T. Jakobi, R. Rohden and J. Stoltenjohannes, “Influence of meteorological variables on measured wind turbine power curves,” *European Wind Energy Conference and Exhibition 2007, EWEC 2007,* no. 3, 2007.

[60] D.-I. E. Hau, Windkraftanlagen, Vol. 4, Springer Verlag, 2008.

[61] ProPlanEn Ltd., “WakeBlaster API and SDK Documentation,” 29 May 2018. [Online]. Available: http://beta.docs.wakeblaster.net/#api-_. [Accessed 4 June 2018].

[62] “Windbranche,” 4 September 2017. [Online]. Available: https://www.windbranche.de/news/politik/artikel-34383-neue-eeg-verguetungssaetze-fuer-windenergie-zum-jahreswechsel-. [Accessed 24 September 2018].

Appendix

Appendix A: Configuration of Mount Lucas and Gasiri

Table A-1: Mount Lucas wind farm configuration [45]

Turbine Id	Easting	Northing	Turbine Type	Rotor diameter [m]	Hub height [m]	Rated power [kW]
ML_T01	248838	224540	SWT-3.0-101	101	99.5	3000
ML_T02	249108	224119	SWT-3.0-101	101	99.5	3000
ML_T03	249607	224133	SWT-3.0-101	101	99.5	3000
ML_T04	250107	224148	SWT-3.0-101	101	99.5	3000
ML_T05	250605	224162	SWT-3.0-101	101	99.5	3000
ML_T06	250376	223727	SWT-3.0-101	101	99.5	3000
ML_T07	250875	223741	SWT-3.0-101	101	99.5	3000
ML_T08	251105	224176	SWT-3.0-101	101	99.5	3000
ML_T09	251335	224611	SWT-3.0-101	101	99.5	3000
ML_T11	249837	224568	SWT-3.0-101	101	99.5	3000
ML_T12	249337	224554	SWT-3.0-101	101	99.5	3000
ML_T13	249567	224989	SWT-3.0-101	101	99.5	3000
ML_T14	250067	225004	SWT-3.0-101	101	99.5	3000
ML_T15	250565	225018	SWT-3.0-101	101	99.5	3000
ML_T16	251065	225032	SWT-3.0-101	101	99.5	3000
ML_T17	251565	225046	SWT-3.0-101	101	99.5	3000
ML_T18	252063	225060	SWT-3.0-101	101	99.5	3000
ML_T19	252563	225075	SWT-3.0-101	101	99.5	3000
ML_T21	252792	225510	SWT-3.0-101	101	99.5	3000
ML_T22	252293	225495	SWT-3.0-101	101	99.5	3000
ML_T24	251295	225467	SWT-3.0-101	101	99.5	3000
ML_T25	251025	225888	SWT-3.0-101	101	99.5	3000
ML_T26	251524	225901	SWT-3.0-101	101	99.5	3000
ML_T27	252023	225916	SWT-3.0-101	101	99.5	3000
ML_T28	252523	225930	SWT-3.0-101	101	99.5	3000
ML_T30	252252	226351	SWT-3.0-101	101	99.5	3000
ML_T31	251754	226337	SWT-3.0-101	101	99.5	3000
ML_T32	251255	226323	SWT-3.0-101	101	99.5	3000

Table A-2: Gasiri wind farm configuration [49]

Turbine Id	Easting	Northing	Turbine Type	Rotor diameter [m]	Hub height [m]	Rated power [kW]
G_T01	288843	3696069	SWT-3.0-101	101	74.5	3000
G_T02	288713	3695907	SWT-3.0-101	101	79.5	3000
G_T03	288572	3695668	SWT-3.0-101	101	79.5	3000
G_T04	288457	3695399	SWT-3.0-108	108	79.5	3000
G_T05	288453	3695011	SWT-3.0-108	108	79.5	3000
G_T06	289222	3696023	SWT-3.0-101	101	79.5	3000
G_T07	289101	3695890	SWT-3.0-101	101	79.5	3000
G_T08	288937	3695676	SWT-3.0-108	108	79.5	3000
G_T09	288724	3695336	SWT-3.0-108	108	79.5	3000
G_T10	288758	3695065	SWT-3.0-108	108	79.5	3000

Table A-3: Existing turbines close to the Gasiri wind farm [49]

Turbine Id	Easting	Northing	Turbine Type	Rotor diameter [m]	Hub height [m]	Rated power [kW]
G_ET01	289464	3697538	Unison U50-750kW	50	50	750
G_ET02	289332	3697367	Unison U50-750kW	50	50	750
G_ET03	289202	3697137	Unison U50-750kW	50	50	750
G_ET04	289111	3696928	Unison U50-750kW	50	50	750
G_ET05	289714	3697376	Unison U50-750kW	50	50	750
G_ET06	289929	3697232	Unison U50-750kW	50	50	750
G_ET07	290183	3697069	FUHRLÄNDER 1500-77	77	70	1500
G_ET08	289542	3697089	FUHRLÄNDER 1500-77	77	70	1500
G_ET09	289820	3696952	FUHRLÄNDER 1500-77	77	70	1500
G_ET10	290036	3696805	FUHRLÄNDER 1500-77	77	70	1500
G_ET11	289309	3696767	FUHRLÄNDER 1500-77	77	70	1500
G_ET12	289565	3696653	FUHRLÄNDER 1500-77	77	70	1500
G_ET13	289806	3696529	FUHRLÄNDER 1500-77	77	70	1500

Appendix B: Spacing of Mount Lucas and Gasiri

Table B-1: Minimum spacing of the Mount Lucas wind farm (red values are below SGRE's recommendation)

Turbine Id	Prevailing wind directions		Non-prevailing wind directions	
	Distance [D]	Sector [°]	Distance [D]	Direction [°]
MLT01	≥10	180, 210, 240, 270	4.9	60, 90
MLT02	≥10	180, 210, 240, 270	4.9	0, 30
MLT03	4.9	240, 270	4.9	0, 30
MLT04	4.9	240, 270	4.9	60, 90, 300, 330
MLT05	4.9	180, 210	4.9	60, 90, 120, 150
MLT06	≥10	180, 210, 240, 270	4.9	0, 30
MLT07	4.9	240, 270	4.9	0, 30
MLT08	4.9	180, 210	4.9	0, 30
MLT09	4.9	180, 210	4.9	0, 30
MLT11	4.9	180, 210	4.9	0, 30
MLT12	4.9	180, 210	4.9	0, 30
MLT13	4.9	180, 210	4.9	60, 90
MLT14	4.9	180, 210	4.9	60, 90
MLT15	4.9	240, 270	4.9	60, 90
MLT16	4.9	240, 270	4.9	0, 30
MLT17	4.9	180, 210	4.9	60, 90, 300, 330
MLT18	4.9	240, 270	4.9	0, 30
MLT19	4.9	240, 270	4.9	0, 30
MLT21	4.9	180, 210	4.9	300, 330
MLT22	4.9	180, 210	4.9	0, 30
MLT24	4.9	180, 210	4.9	0, 30
MLT25	8.5	180	4.9	0, 30
MLT26	4.9	180, 210	4.9	0, 30
MLT27	5.0	240, 270	4.9	0, 30
MLT28	4.9	180, 210	4.9	120, 150
MLT30	4.9	180, 210	5.0	120, 150
MLT31	4.9	180, 210	4.9	60, 90
MLT32	4.9	180, 210	4.9	60, 90

Table B-2: Minimum spacing for the Gasiri windfarm (red values are below SGRE's recommendation)

Turbine Id	Minimum spacing in prevailing wind directions		Minimum spacing in non-prevailing wind directions	
	Distance [D]	Sector [°]	Distance [D]	Direction [°]
G_T01	≥10	330	2.06	180, 210, 240
G_T02	≥10	330	2.06	0, 30, 60
G_T03	≥10	330	2.71	180, 210, 240
G_T04	≥10	330	2.54	90, 120
G_T05	3.59	330	2.87	60, 90
G_T06	≥10	330	1.78	180, 210, 240, 270
G_T07	3.11	330	1.78	0, 30, 60, 90
G_T08	3.19	330	2.67	0, 30, 60
G_T09	3.62	330	2.53	150, 180, 210
G_T10	2.53	330	2.53	0, 30

Appendix C: Matlab Code

Table C-1: Matlab parameters

Matlab variable	Explanation
CF	Calibration factor for the ambient wind speed
design_id_turbine	Links WTG file and turbine positions (could be several times in code), has to be the same as in the json farm layout file.
design_id	Links the met mast design file to the mast position (could be several times in code), has to be the same as in the json farm layout file.
farm_id	Defines the farm .json file with the simulation
ext_turbines	Defines number of existing turbines.
pressure	Defines the air pressure (is used for the calculation of the air density).
temperature	Defines the air temperature (is used for the calculation of the air density).
start_shear/end_shear	Defines the start and end values of the shear. Recommended value from representative time series from WindPRO. At the moment only one shear value is used for the complete process to reduce the amount of data.
_nr_shear	Number of shear values that will be calculated.
height_ini	Defines the height were the simulation start, has to be the same height as in the rsf file that is used for calculation at the reference point.
height_shear	Can be chosen free but not the same as height_ini. Is used to calculate a second wind speed for the shear calculation.
start_TI/end_TI	Defines the start and end value of the turbulence intensity in percent
nr_TI	Number of TI values that will be calculated
start_WS/end_WS	Defines start and end values for wind speeds in m/s
nr_WS	Number of wind speed values
start_WD/end_WD	Defines start and end values for the wind direction in deg
nr_WD	Number of wind direction values
upload_turbine_design	The path of the WTG file has to be adapted to the one step before created one (maybe several times in the code).
met_mast_design	The path of the met mast design file has to be adapted.
wind_farm_def	The path of the farm definition file has to be adapted.
upload_asset	The path of the rsf file has to be adapted.
simulation_config	The path of the configuration file has to be adapted.

Appendix D: Calibrated Production of Single Turbines at Munt Lucas

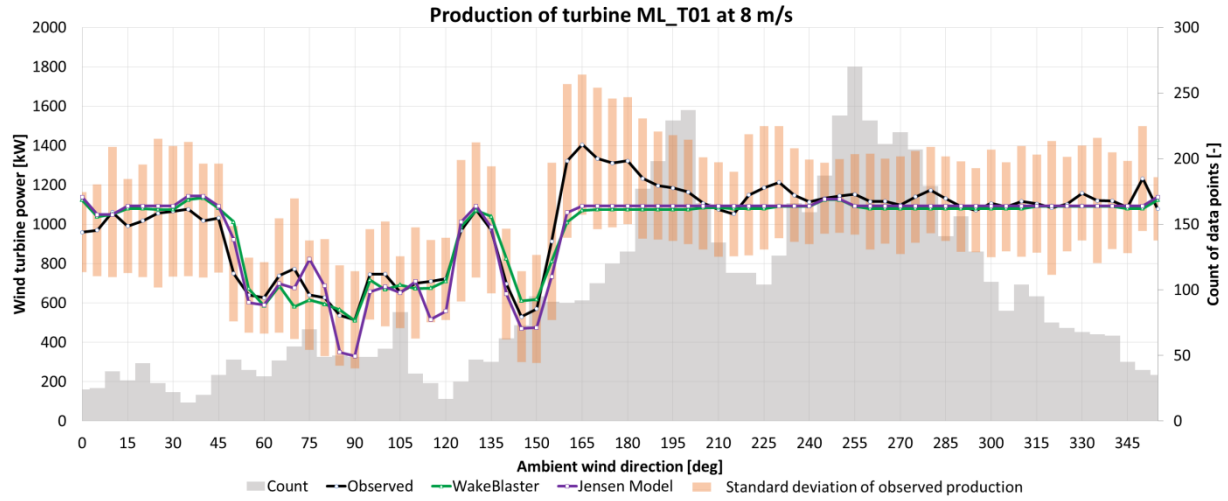

Figure D-1: Production of turbine ML_T01 at 8 m/s

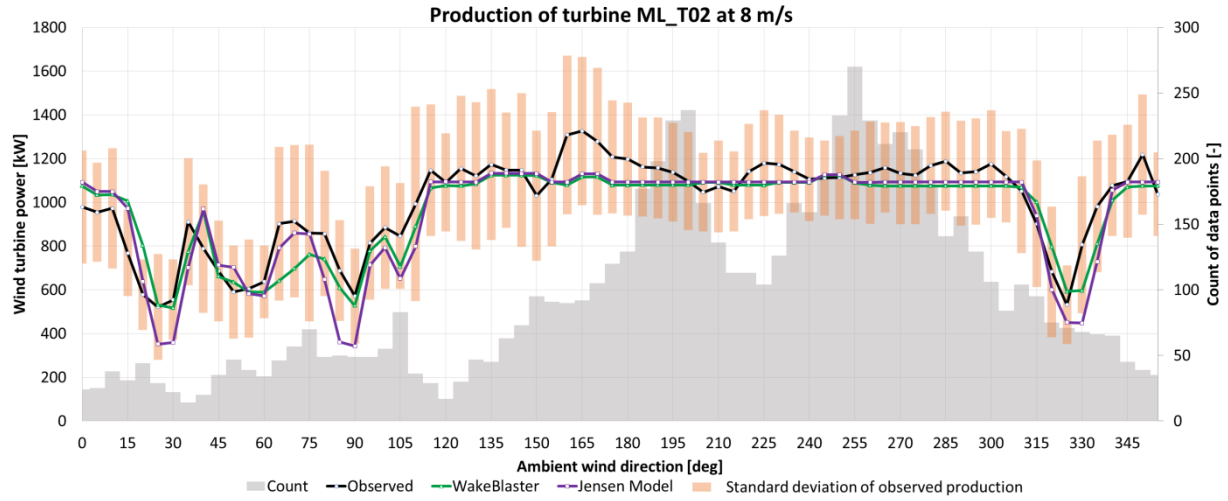

Figure D-2: Production of turbine ML_T02 at 8 m/s

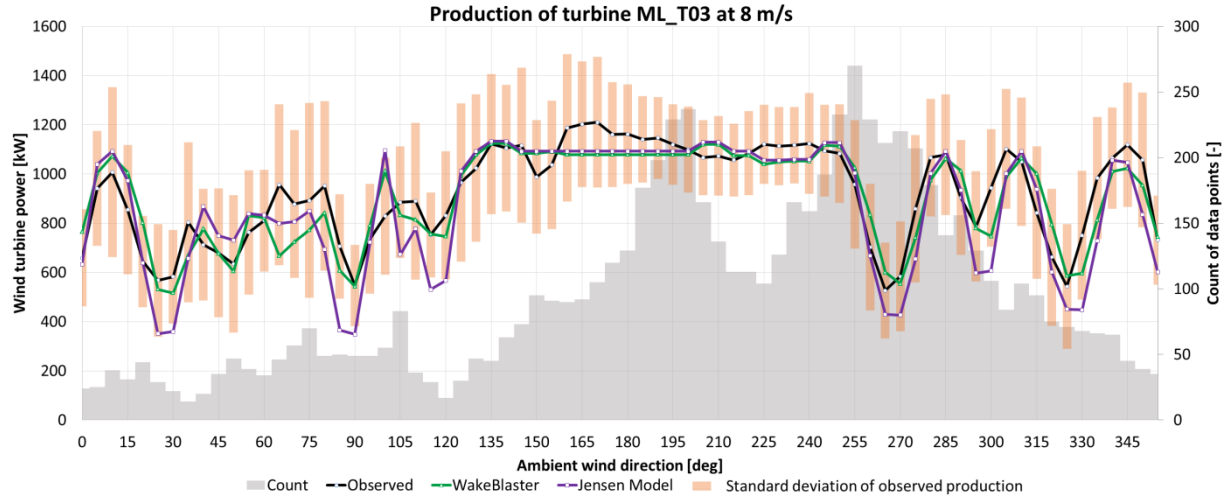

Figure D-3: Production of turbine ML_T03 at 8 m/s

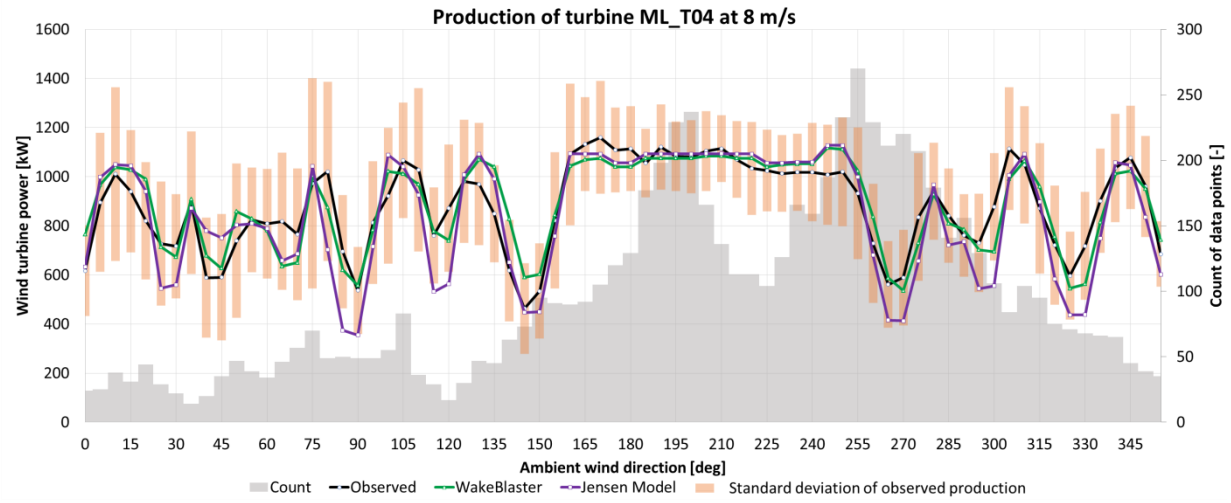

Figure D-4: Production of turbine ML_T04 at 8 m/s

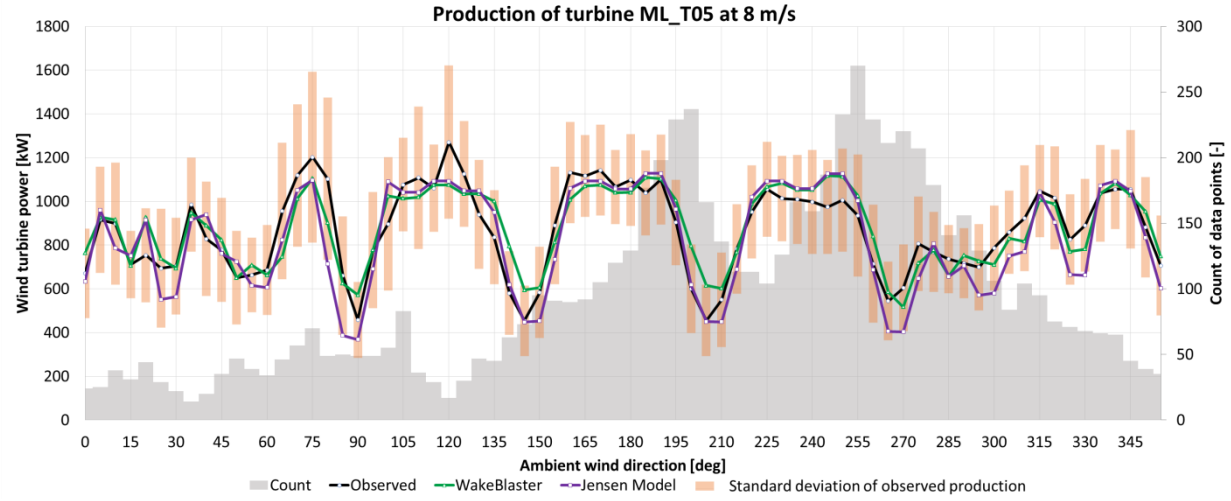

Figure D-5: Production of turbine ML_T05 at 8 m/s

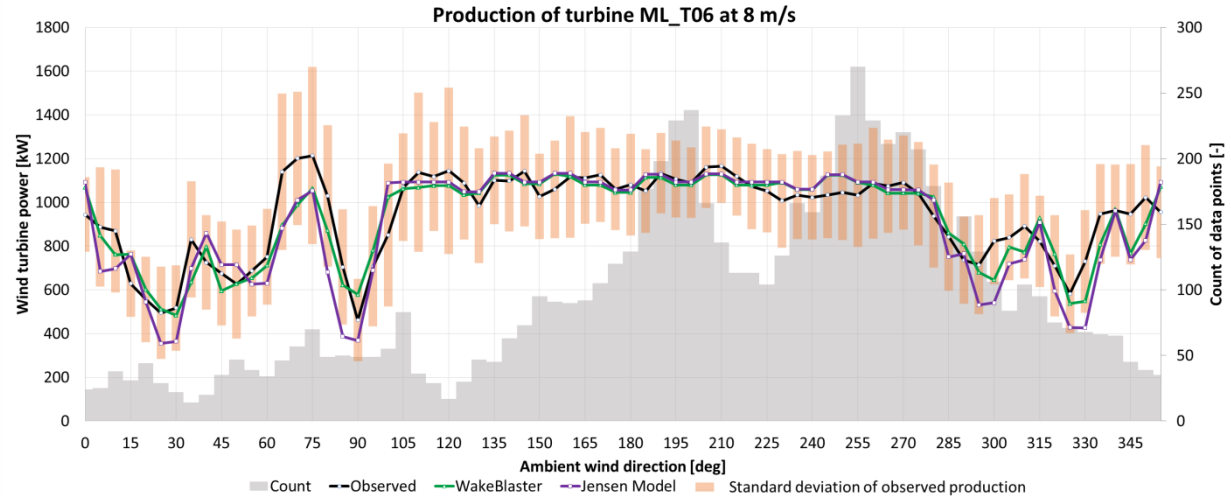

Figure D-6: Production of turbine ML_T06 at 8 m/s

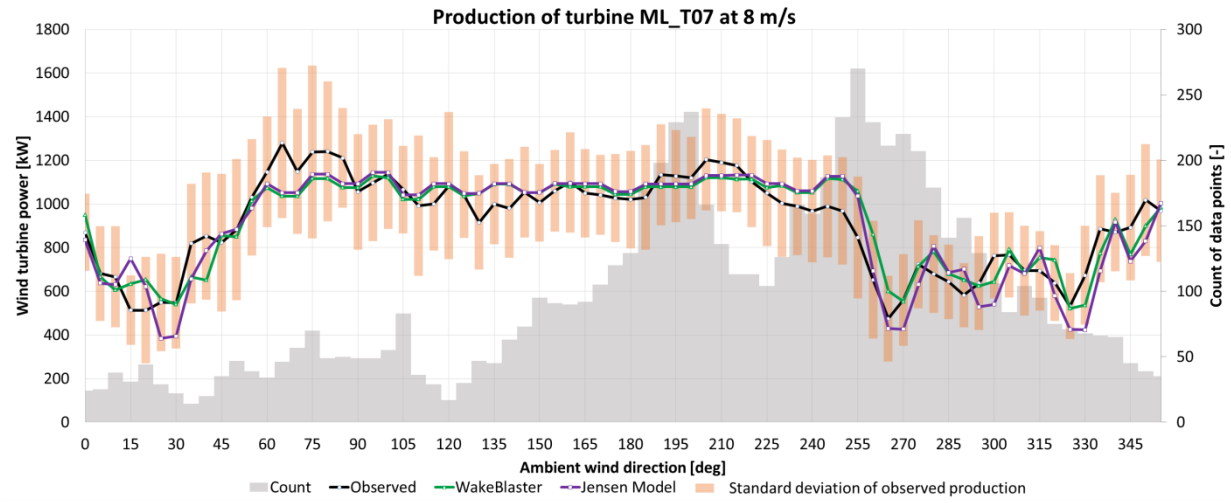

Figure D-7: Production of turbine ML_T07 at 8 m/s

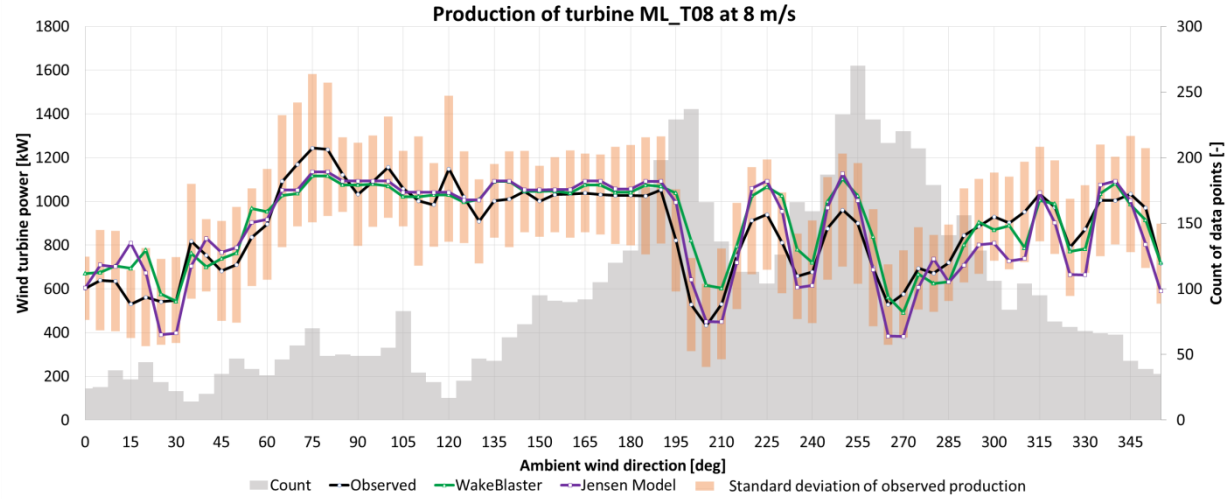

Figure D-8: Production of turbine ML_T08 at 8 m/s

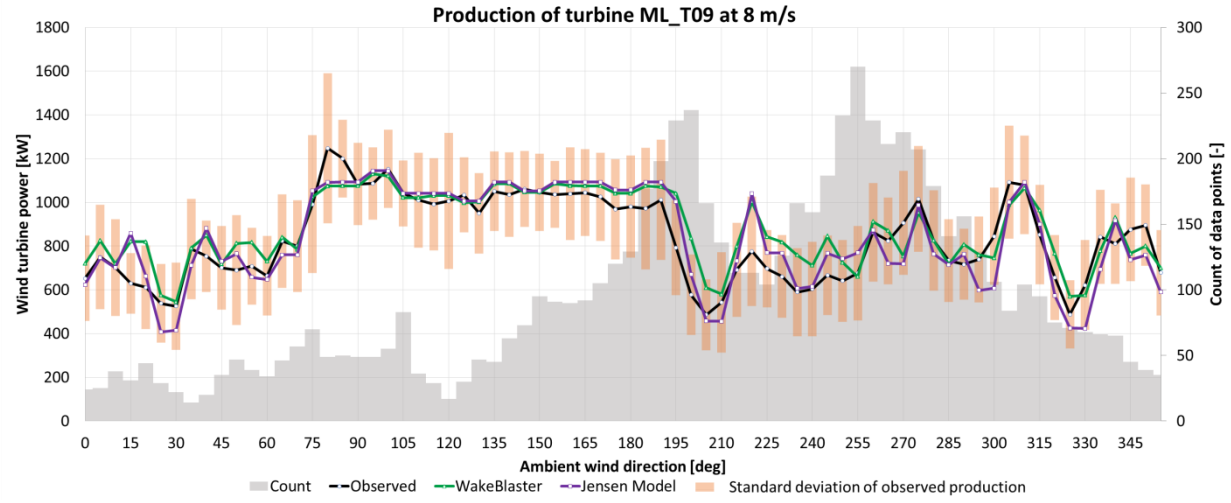

Figure D-9: Production of turbine ML_T09 at 8 m/s

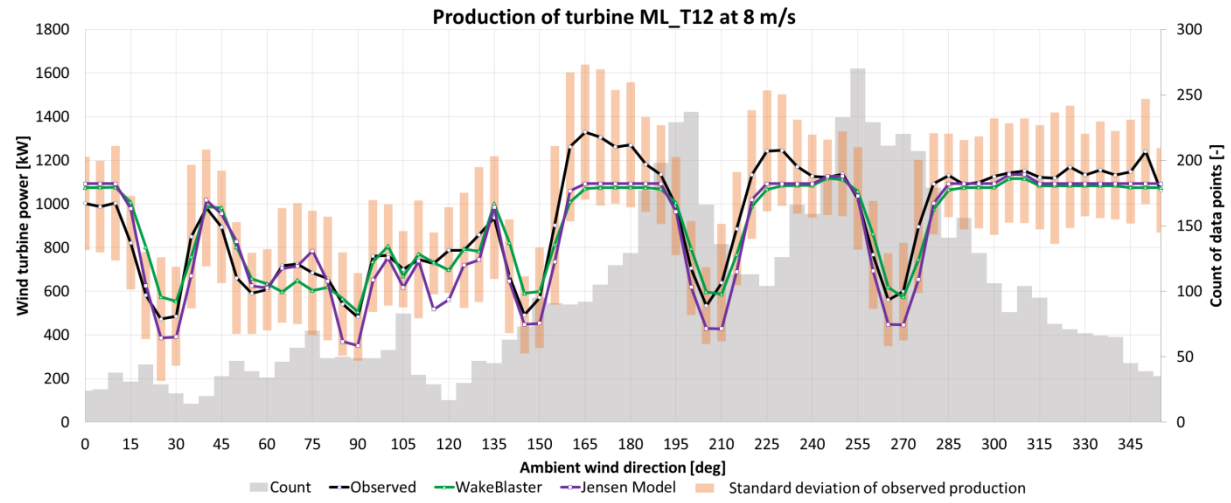

Figure D-10: Production of turbine ML_T12 at 8 m/s

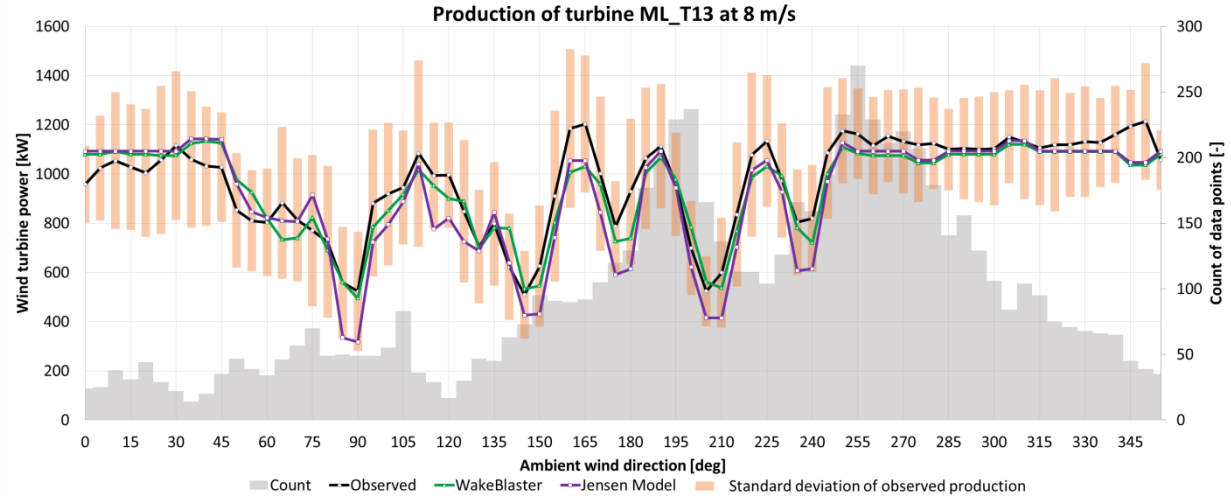

Figure D-11: Production of turbine ML_T13 at 8 m/s

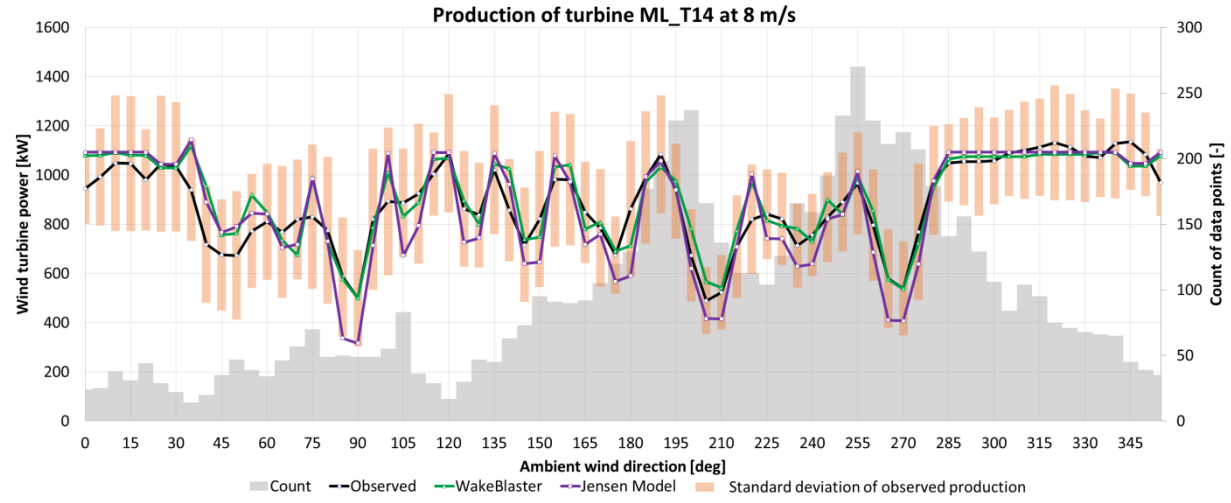

Figure D-12: Production of turbine ML_T14 at 8 m/s

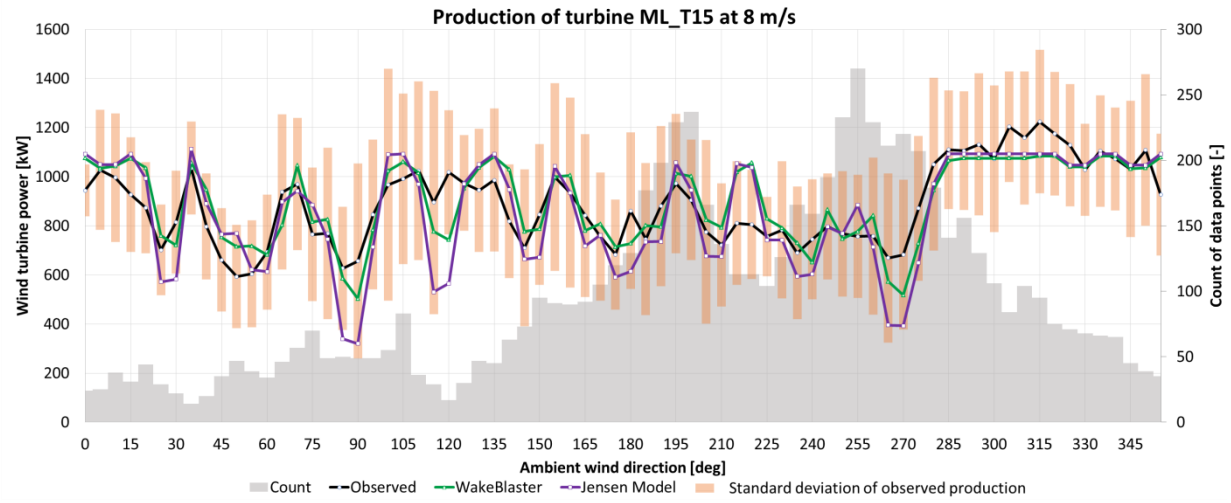

Figure D-13: Production of turbine ML_T15 at 8 m/s

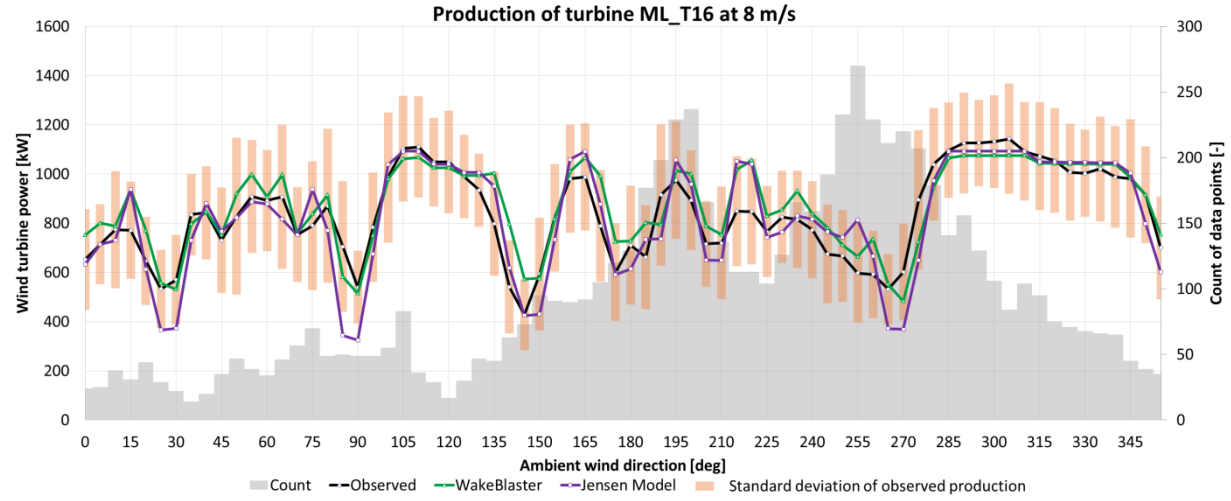

Figure D-14: Production of turbine ML_T16 at 8 m/s

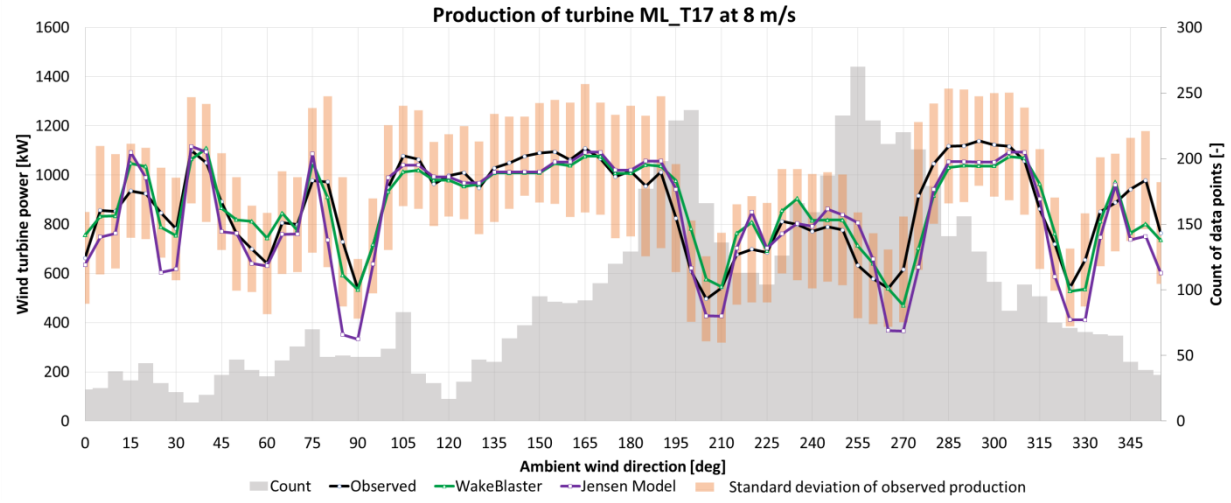

Figure D-15: Production of turbine ML_T17 at 8 m/s

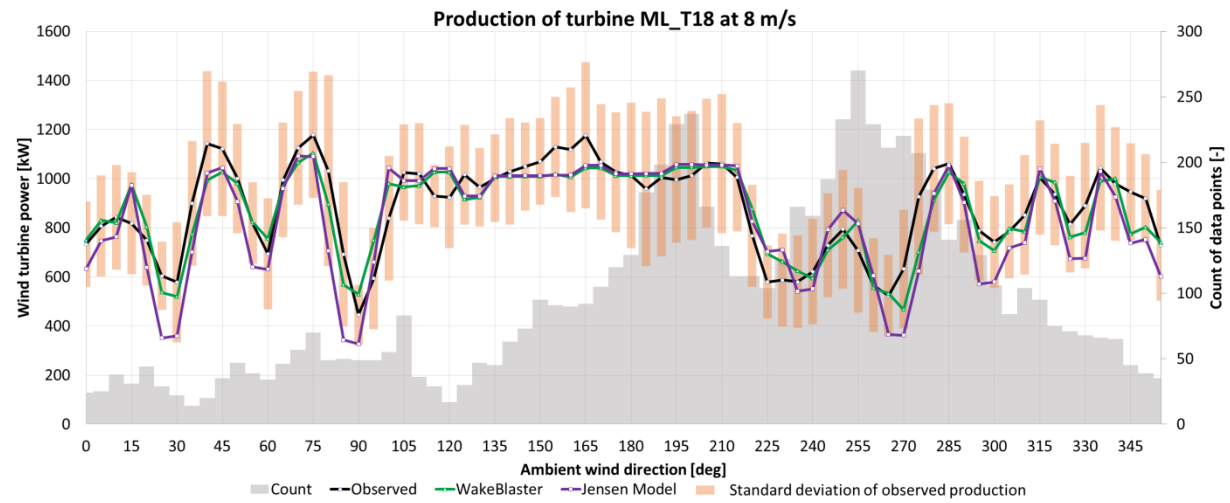

Figure D-16: Production of turbine ML_T18 at 8 m/s

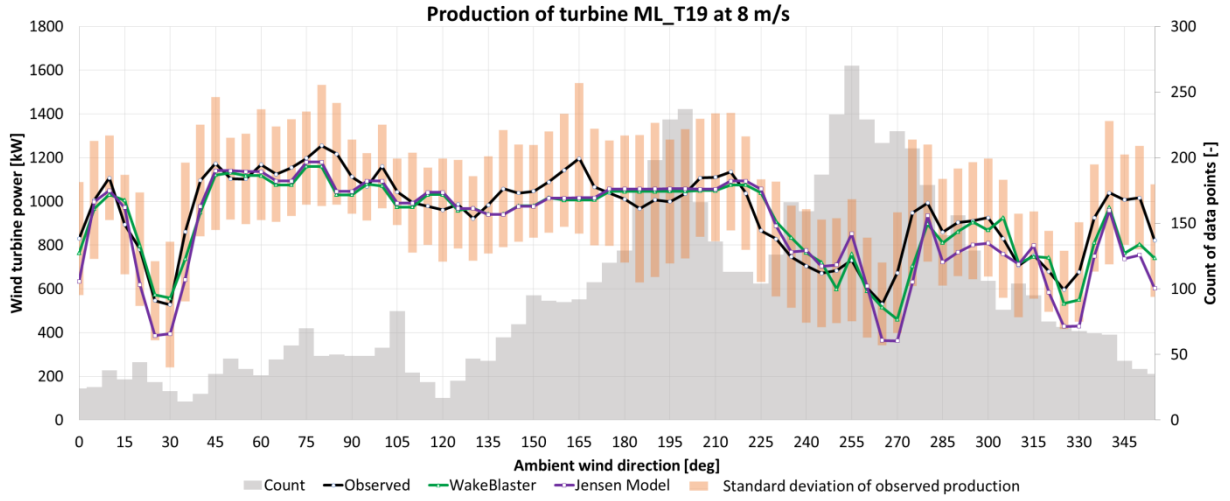

Figure D-17: Production of turbine ML_T19 at 8 m/s

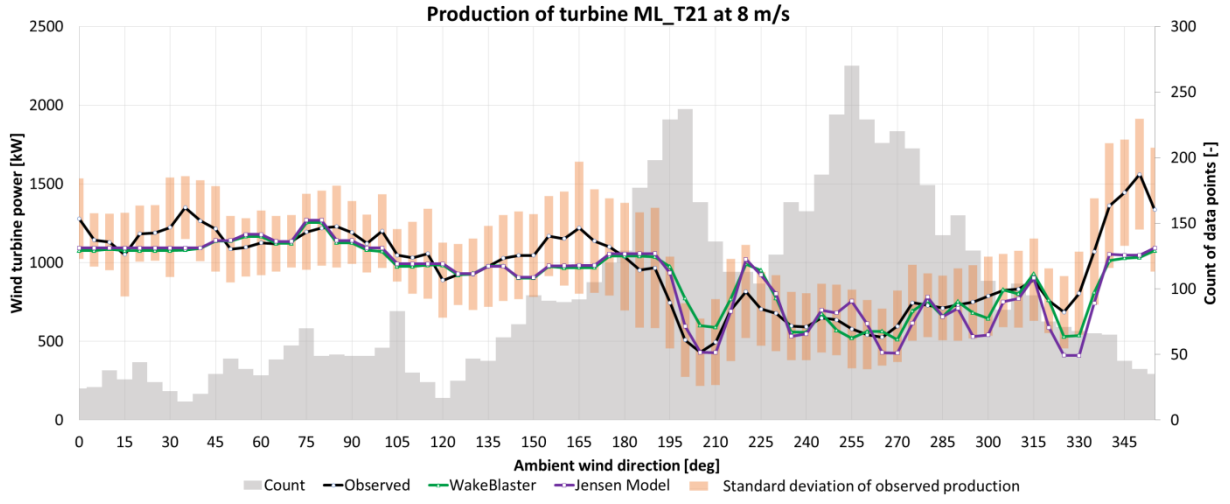

Figure D-18: Production of turbine ML_T21 at 8 m/s

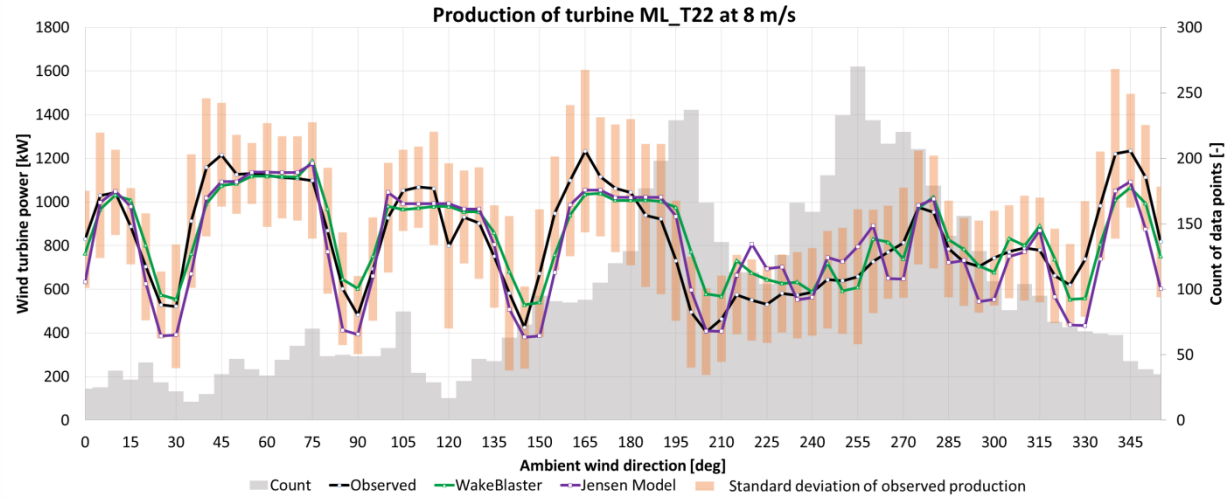

Figure D-19: Production of turbine ML_T22 at 8 m/s

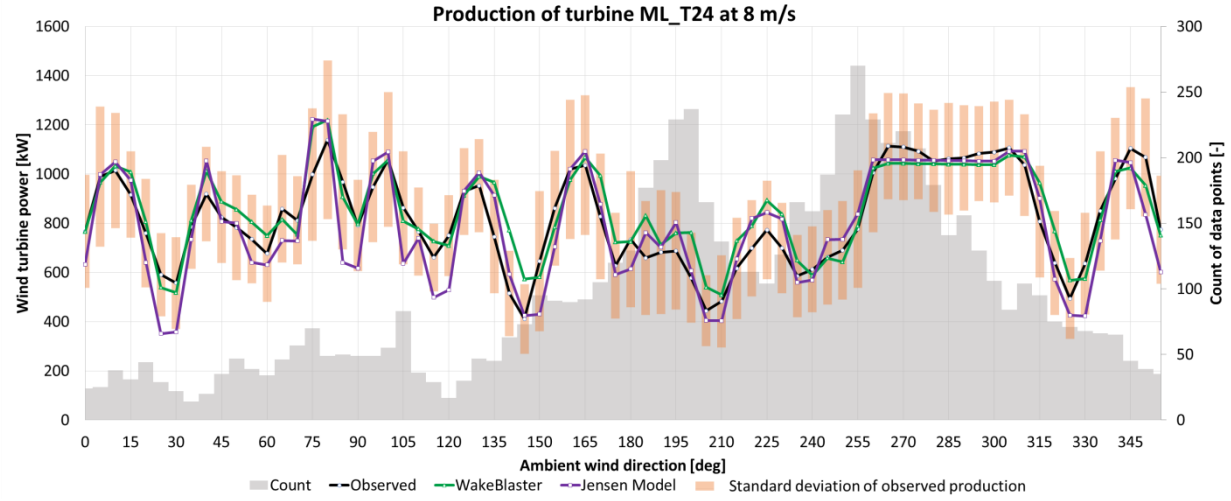

Figure D-20: Production of turbine ML_T24 at 8 m/s

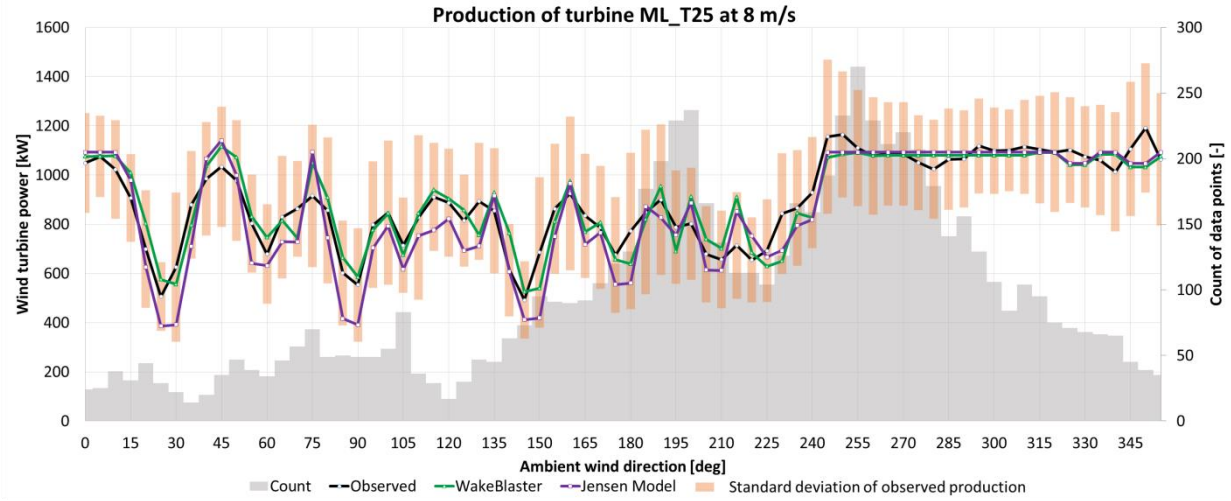

Figure D-21: Production of turbine ML_T25 at 8 m/s

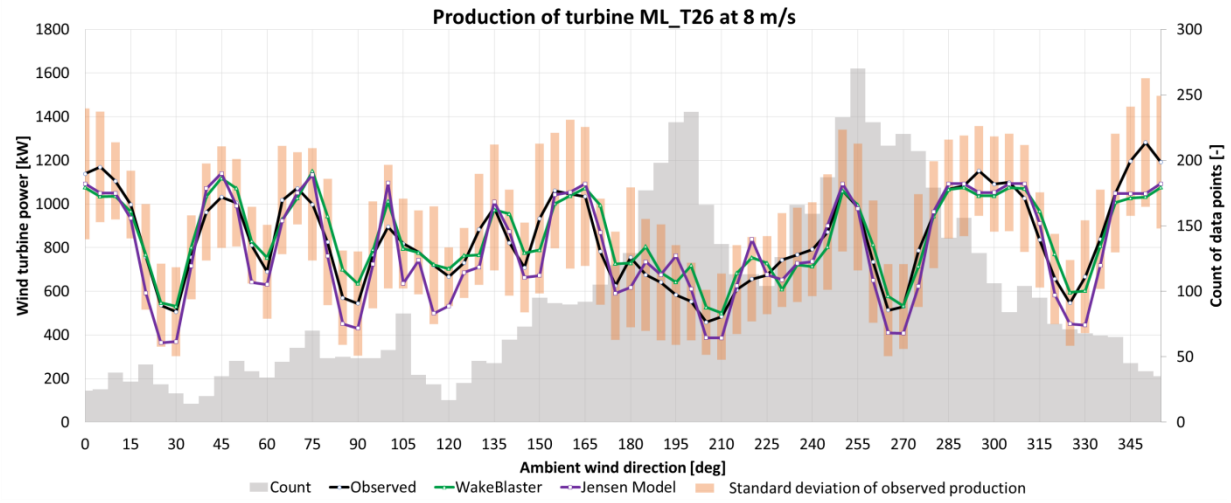

Figure D-22: Production of turbine ML_T26 at 8 m/s

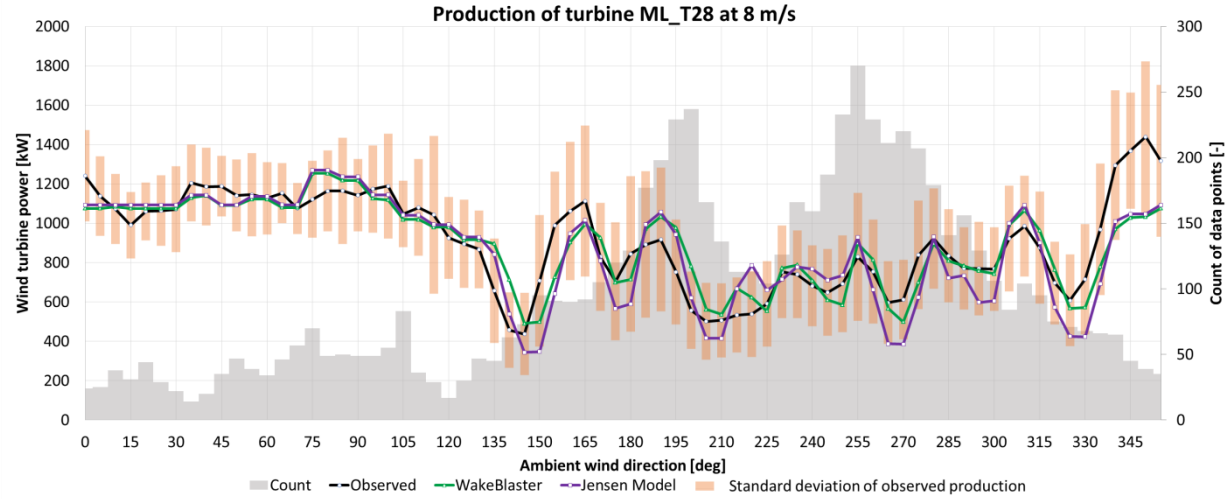

Figure D-23: Production of turbine ML_T28 at 8 m/s

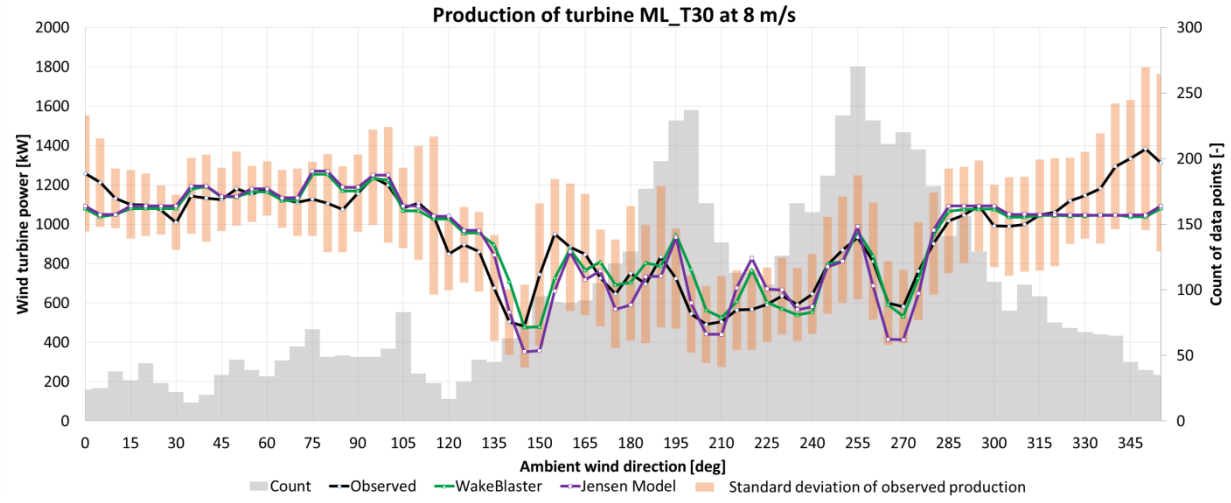

Figure D-24: Production of turbine ML_T30 at 8 m/s

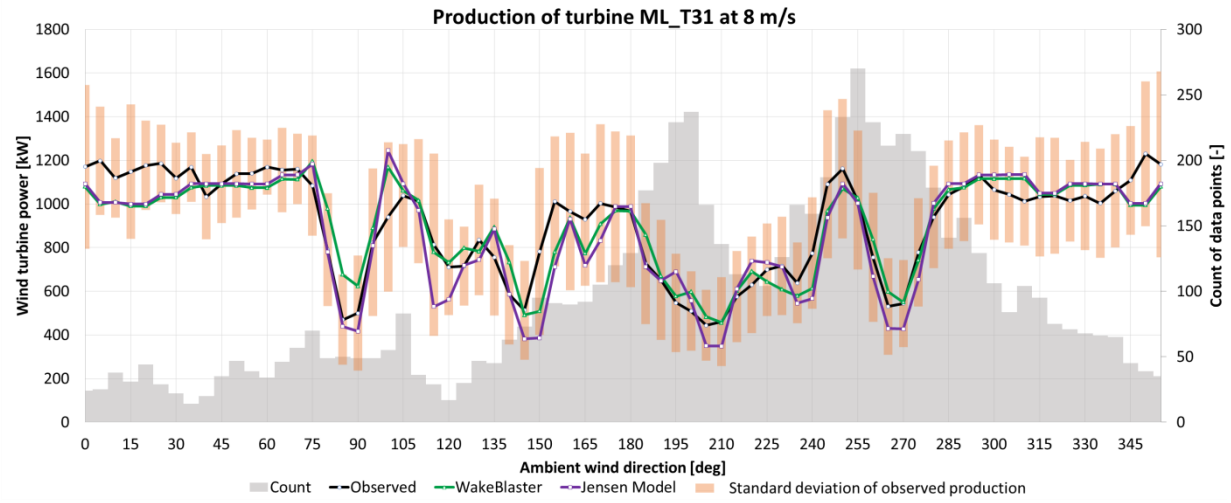

Figure D-25: Production of turbine ML_T31 at 8 m/s

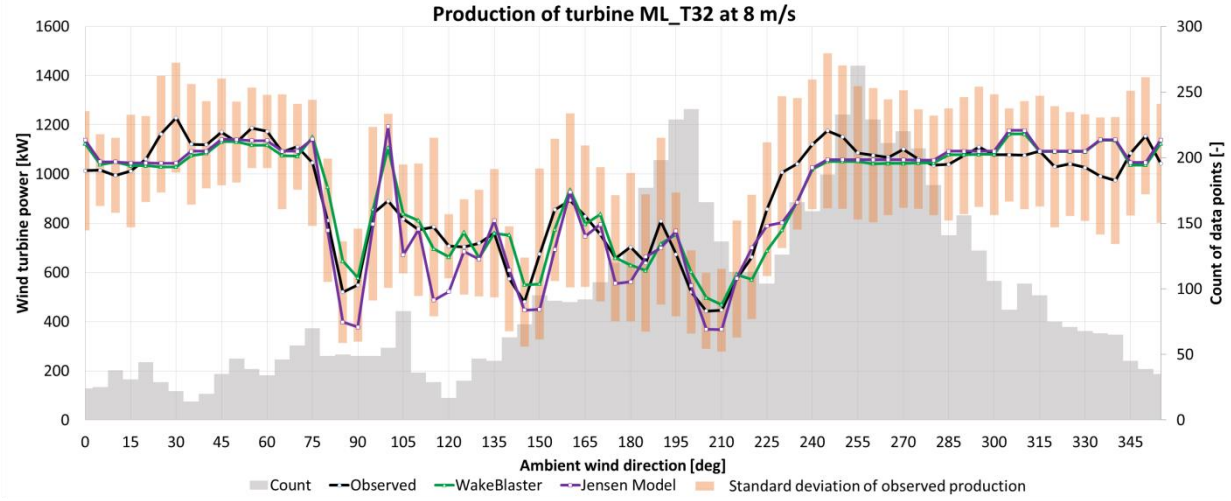

Figure D-26: Production of turbine ML_T32 at 8 m/s

Appendix E: Calibrated Production of Single Turbines at Gasiri

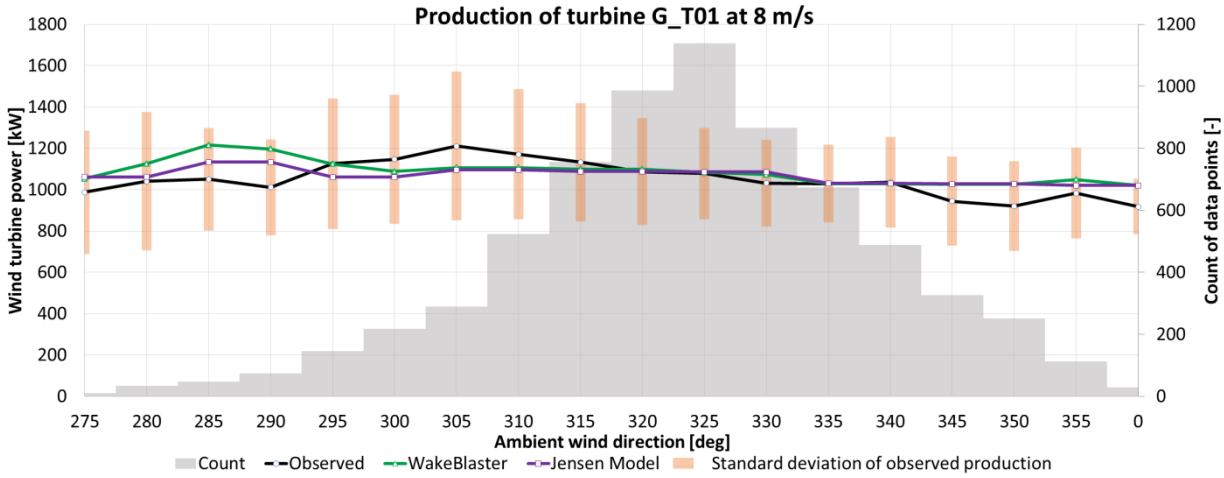

Figure E-1: Production of turbine G_T01 at 8 m/s (275-0 deg)

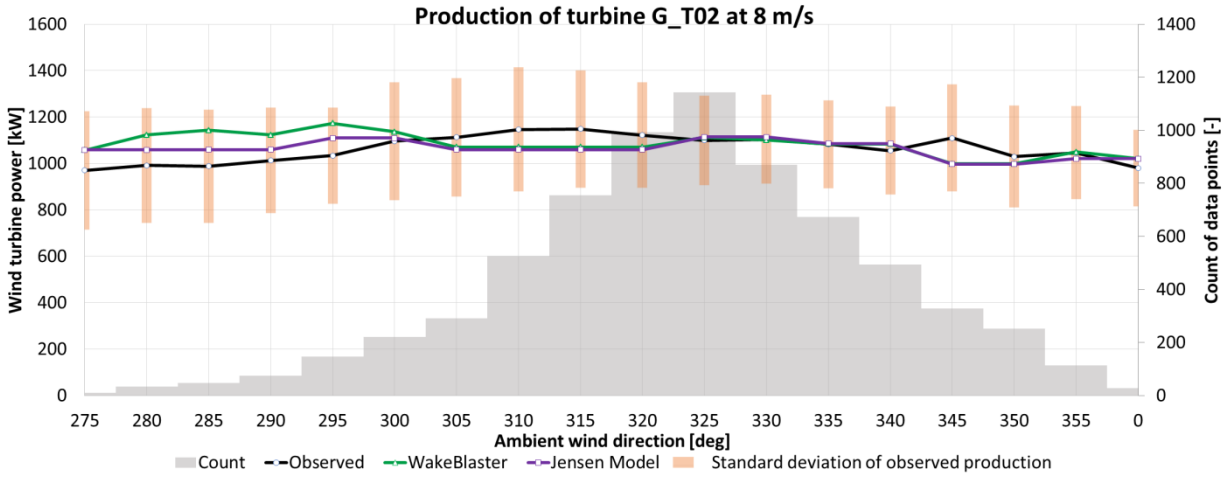

Figure E-2: Production of turbine G_T02 at 8 m/s (275-0 deg)

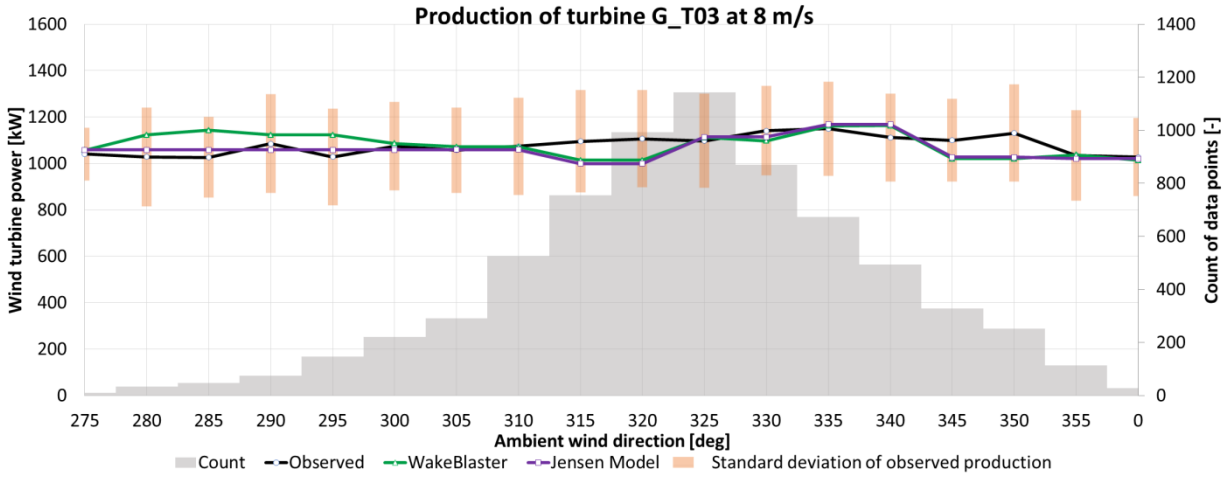

Figure E-3: Production of turbine G_T03 at 8 m/s (275-0 deg)

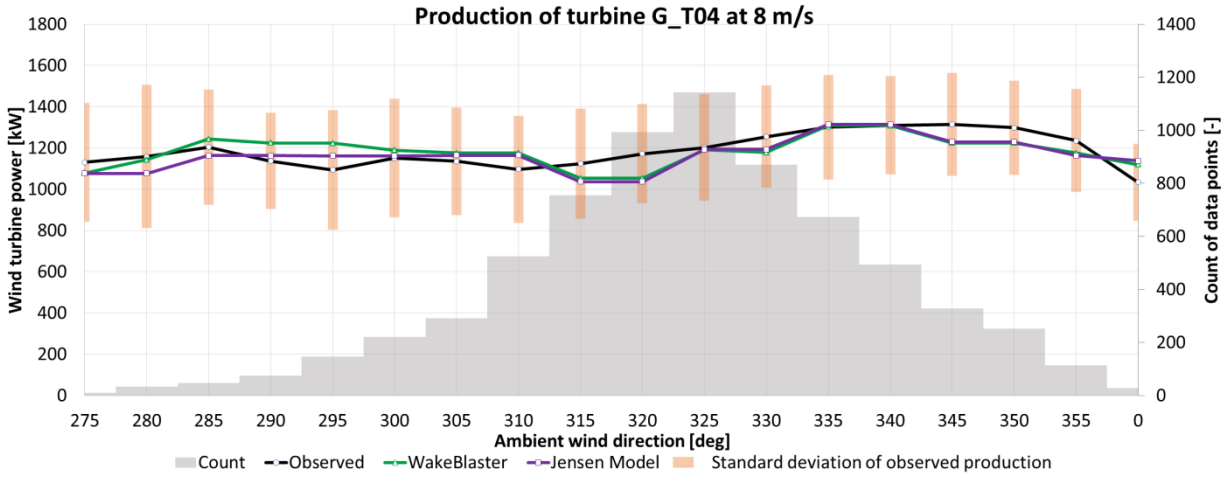

Figure E-4: Production of turbine G_T04 at 8 m/s (275-0 deg)

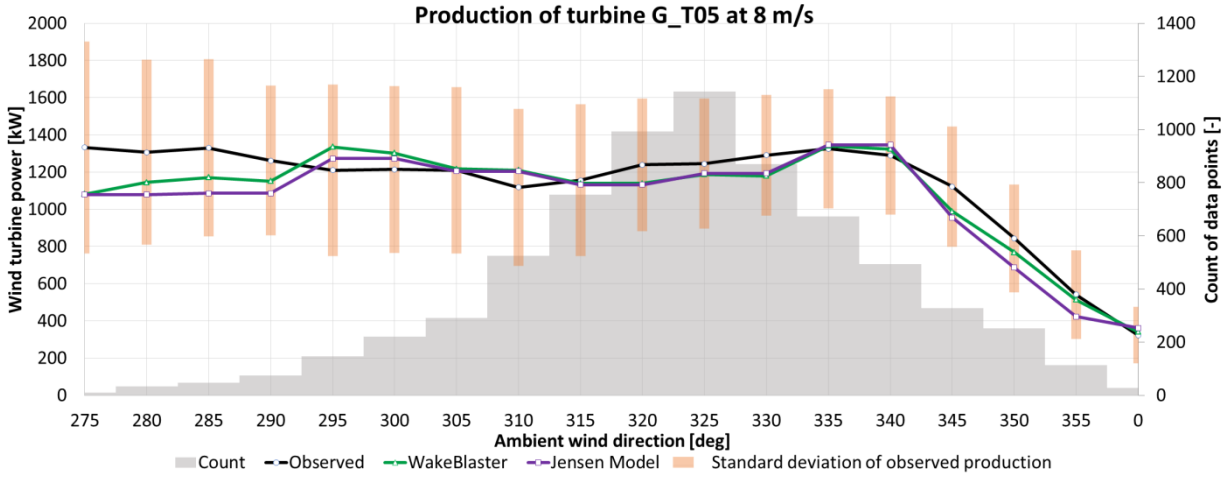

Figure E-5: Production of turbine G_T05 at 8 m/s (275-0 deg)

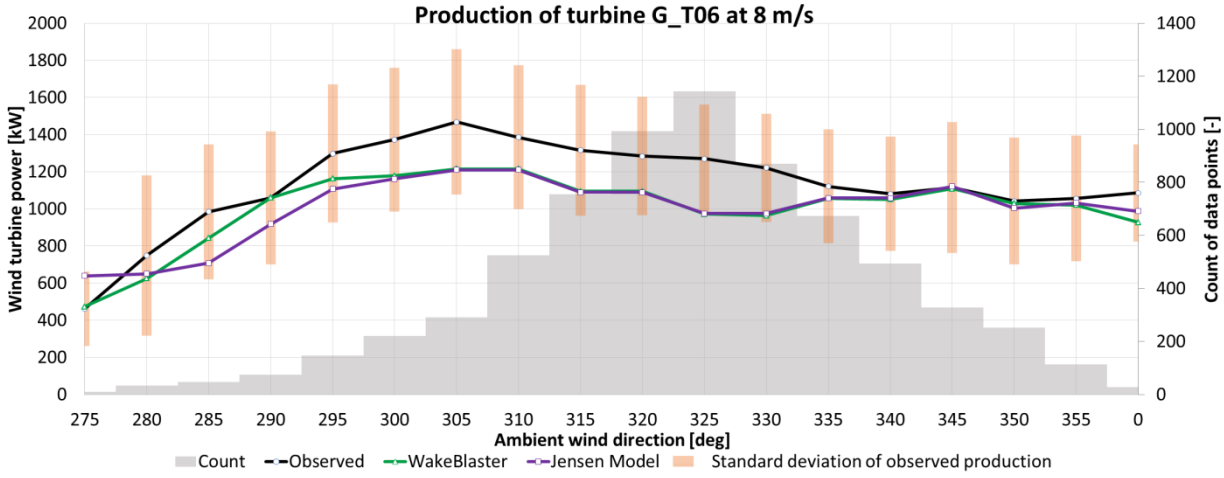

Figure E-6: Production of turbine G_T06 at 8 m/s (275-0 deg)

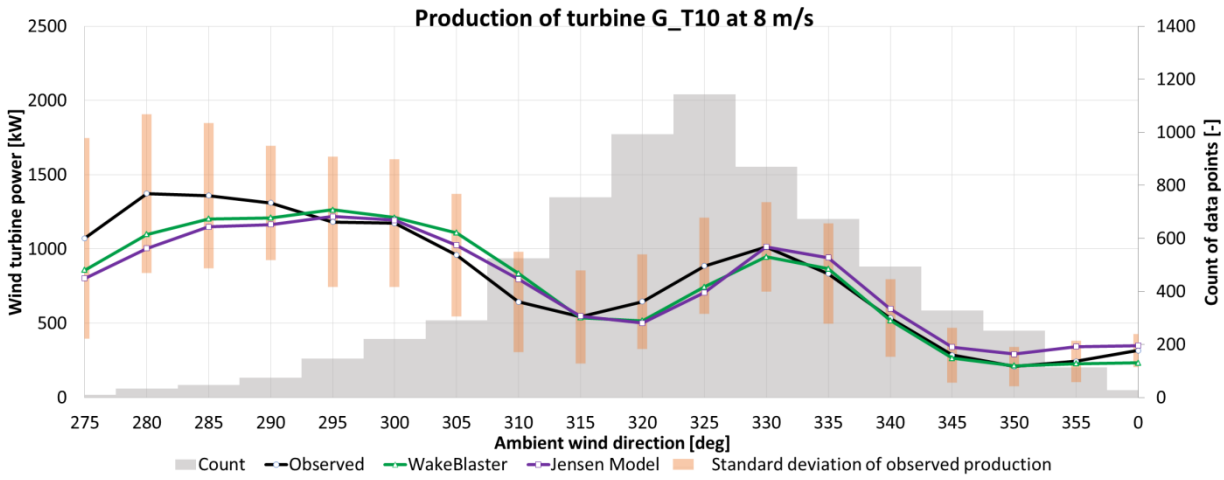

Figure E-7: Production of turbine G_T10 at 8 m/s (275-0 deg)

Appendix F: Turbulence Intensity and Corresponding Wake Decay Constant

Table F-1: Turbulence intensity and corresponding wake decay constant values

Turbulence intensity [%]	Wake decay constant
6	0.030
8	0.038
10	0.045
12	0.054
14	0.065
16	0.072
18	0.082
20	0.090

Appendix G: List of Figures

Appendix H: List of Tables